unclassified

SECURITY CLASSIFICATION OF THIS PAGE

REPORT DOCUMENTATION PAGE

Form Approved OMB No. 0704-0188

1a REPORT SECURITY CLASSIFICATION: UNCLASSIFIED	1b RESTRICTIVE MARKINGS
2a SECURITY CLASSIFICATION AUTHORITY	3 DISTRIBUTION/AVAILABILITY OF REPORT: Approved for public release; distribution is unlimited.
2b DECLASSIFICATION/DOWNGRADING SCHEDULE	
4 PERFORMING ORGANIZATION REPORT NUMBER(S)	5 MONITORING ORGANIZATION REPORT NUMBER(S)
6a NAME OF PERFORMING ORGANIZATION: Naval Postgraduate School; 6b OFFICE SYMBOL (If applicable): MR	7a NAME OF MONITORING ORGANIZATION
6c ADDRESS (City, State, and ZIP Code): Monterey, CA 93943-5000	7b ADDRESS (City, State, and ZIP Code)
8a NAME OF FUNDING/SPONSORING ORGANIZATION; 8b OFFICE SYMBOL (If applicable)	9 PROCUREMENT INSTRUMENT IDENTIFICATION NUMBER
8c ADDRESS (City, State, and ZIP Code)	10 SOURCE OF FUNDING NUMBERS: PROGRAM ELEMENT NO; PROJECT NO; TASK NO; WORK UNIT ACCESSION NO

11 TITLE (Include Security Classification)

A NUMERICAL, ANALYTICAL AND OBSERVATIONAL STUDY OF THE EFFECT OF CLOUDS ON SURFACE WIND AND WIND STRESS DURING THE CENTRAL ARCTIC WINTER

12 PERSONAL AUTHOR(S): Guest, Peter Staples

13a TYPE OF REPORT	13b TIME COVERED	14 DATE OF REPORT (Year, Month, Day)	15 PAGE COUNT
Ph.D. Thesis	FROM _____ TO _____	1992 March 13	188

16 SUPPLEMENTARY NOTATION: The views expressed in this thesis are those of the author and do not reflect the official policy or position of the Department of Defense or the U.S. Government.

17 COSATI CODES		
FIELD	GROUP	SUB GROUP

18 SUBJECT TERMS (Continue on reverse if necessary and identify by block number)

Arctic clouds, Arctic wind stress, Arctic longwave radiation, Arctic winter, CEAREX, Arctic boundary layer, Arctic surface layer, ice movement, pack ice

19 ABSTRACT (Continue on reverse if necessary and identify by block number)

Results of measurements from several Arctic field programs and numerical models show that clouds affect wind stress during the central Arctic winter by changing the longwave cooling of the surface and cloud layers. The longwave cooling alters the thermodynamic structure of the lower atmosphere which in turn affects the efficiency of momentum transfer to the surface. For typical Arctic conditions, wind stress is changed by about 40% one hour after a cloud condition change, due to changes in both the surface layer stability and surface layer wind speed. The actual wind stress effect due to clouds during this time is a function of wind speed, thermal wind, atmospheric boundary layer depth, magnitude of radiation change, snow age and, sometimes, snow depth. After several hours, surface heat fluxes are no longer important, but the structure of the atmosphere has been permanently altered. This affects the wind stress by about 10% to 20% during certain situations, but can vary depending on the initial atmospheric structure. Measurements of these effects show variations in wind stress associated with clouds. Operational and research studies of ice and ocean dynamics will benefit from consideration of cloud effects on wind stress.

20 DISTRIBUTION/AVAILABILITY OF ABSTRACT: ☒ UNCLASSIFIED/UNLIMITED ☐ SAME AS RPT ☐ DTIC USERS	21 ABSTRACT SECURITY CLASSIFICATION: Unclassified
22a NAME OF RESPONSIBLE INDIVIDUAL: K.L. Davidson	22b TELEPHONE (Include Area Code): 408-646-2309; 22c OFFICE SYMBOL: MR/Ds

DD Form 1473, JUN 86 — Previous editions are obsolete — S/N 0102-LF-014-6603

SECURITY CLASSIFICATION OF THIS PAGE: Unclassified

Approved for public release; distribution is unlimited.

A Numerical, Analytical and Observational Study of the Effect of Clouds on Surface Wind and Wind Stress during the Central Arctic Winter

by

Peter S. Guest
Meteorologist, Naval Postgraduate School
B.A., Middlebury College, 1977
M.S., The Florida State University, 1982

Submitted in partial fulfillment of the requirements for the degree of

DOCTOR OF PHILOSOPHY IN METEOROLOGY

from the

NAVAL POSTGRADUATE SCHOOL
March 14, 1992

ABSTRACT

Results of measurements from several Arctic field programs and numerical models show that clouds affect wind stress during the central Arctic winter by changing the longwave cooling of the surface and cloud layers. The longwave cooling alters the thermodynamic structure of the lower atmosphere which in turn affects the efficiency of momentum transfer to the surface. For typical Arctic conditions, wind stress is changed by about 40% one hour after a cloud condition change, due to changes in both the surface layer stability and surface layer wind speed. The actual wind stress effect due to clouds during this time is a function of wind speed, thermal wind, atmospheric boundary layer depth, magnitude of radiation change, snow age and, sometimes, snow depth. After several hours, surface heat fluxes are no longer important, but the structure of the atmosphere has been permanently altered. This affects the wind stress by about 10% to 20% during certain situations, but can vary depending on the initial atmospheric structure. Measurements of these effects show variations in wind stress associated with clouds. Operational and research studies of ice and ocean dynamics will benefit from consideration of cloud effects on wind stress.

TABLE OF CONTENTS

I. INTRODUCTION....1

A. BACKGROUND....1

B. MOMENTUM FLUX AT THE AIR/ICE/SEA INTERFACE....2

C. ATMOSPHERIC FACTORS WHICH AFFECT MOMENTUM FLUXES....3

D. CLOUDS AND LONGWAVE RADIATION....4

II. PREVIOUS RESEARCH....7

A. WIND STRESS MEASUREMENTS AND MODELS BEFORE MIZEX....7

1. Early Studies....7

2. AIDJEX....8

3. Other Studies....8

4. Wind Drag Coefficient Models....10

B. CLOUD STUDIES....10

1. Early Studies....11

2. AIDJEX....11

3. Arctic Stratus Cloud Experiment....12

4. Other Cloud Studies....13

C. WIND STRESS AND CLOUDS: MEASUREMENTS AND MODELS SINCE MIZEX....13

1. Surface Wind Stress Measurements....13

2. Observations of Clouds during MIZEX and CEAREX....16

3. Boundary Layer Models....19

4. Wind Stress in the MIZ....21

III. AN EXAMINATION OF THE RELATION BETWEEN CLOUDS AND ATMOSPHERIC BOUNDARY LAYER THERMODYNAMIC STRUCTURE....23

A. CEAREX DRIFT MEASUREMENTS....26

B. THERMODYNAMIC COUPLING OF THE SURFACE, CLOUD LAYER AND ISOTHERMAL LAYER....27

C. CLOUDS AND BOUNDARY LAYER THERMAL STRUCTURE...34

1. Inversion Height - Average Values....34

2. Inversion Height and u. Scaling....36

3. Types of Atmospheric Boundary Layers....44

D. CLOUDS AND SURFACE FLUXES....48

E. FACTORS INFLUENCING SURFACE HEAT FLUX....52

1. General Classification Scheme....54

2. Scale Analysis....56

3. Graphical Representation of ABL Temperature and Surface Heat Flux Events....58

F. EXAMPLES FROM CEAREX DRIFT....62

G. CONCLUSIONS ON CLOUD EFFECTS ON ATMOSPHERIC THERMODYNAMIC STRUCTURE....66

IV. THE EFFECT OF CLOUDS ON SURFACE LAYER STABILITY, THE SNOW/ICE LAYER AND WIND STRESS....68

A. DEFINING SURFACE LAYER STABILITY EFFECTS....68

B. PURPOSE OF SURFACE LAYER STABILITY STUDIES....68

C. CONDUCTION OF HEAT THROUGH SNOW/ICE (ANALYTICAL MODEL)....69

D. CONDUCTION OF HEAT THROUGH SNOW/ICE (NUMERICAL MODEL)....75

1. Model Description....75

2. Model Time Scales....75

3. Snow/Ice Model Predictions of Surface Layer Stability Effects on Wind Stress....80

a. Standard (Reference) Case....80

b. Initial Radiation Imbalance, Wind Speed and ABL Depth Effects....88

c. Snow Characteristics Effects....91

d. Physical Time Scales....103

4. Ice Model Conclusions....109

V. CASE STUDIES OF THE EFFECT OF CLOUDS ON WIND STRESS....112

A. NUMERICAL ABL MODEL....113

1. Basic ABL Model....113

2. Cloud Model....114

3. Radiation Model....114

4. Boundary Conditions and External Forcing....117

5. Model Initialization....118

B. OCT 22 CASE STUDY - CLEARING EVENT....123

C. OCT 30 CASE STUDY - CLOUD FORMS ABOVE ABL....132

D. OCT 21 CASE STUDY - CLOUD FORMATION AND DISSIPATION IN THE ABL....137

E. OTHER MODEL SIMULATION RESULTS....142

F. CASE STUDY CONCLUSIONS....143

VI. STATISTICAL RELATIONSHIPS BETWEEN CLOUDS AND WIND STRESS....145

A. WIND STRESS AND ABL STRUCTURE....145
B. WIND STRESS AND CLOUDS AND MOISTURE....148
C. CONCLUSIONS ON STATISTICAL RELATIONSHIPS....156
VII. CONCLUSIONS....160
A. SUMMARY OF FINDINGS....160
B. SIGNIFICANCE OF RESULTS....162
C. APPLICATIONS OF RESULTS....163
LIST OF REFERENCES....165
INITIAL DISTRIBUTION LIST....176

LIST OF ACRONYMS

ABL	Atmospheric planetary Boundary Layer
AMA	Arctic Marine Atmosphere
AIDJEX	Arctic Ice Dynamics Joint EXperiment
ASC	Arctic Stratus Cloud Experiment
CCN	Cloud Condensation Nuclei
CEAREX	Coordinated Eastern Arctic Regional EXperiment
CTEI	Cloud Top Entrainment Instability
EPG	Environmental Physics Group
FIRE	First ISCCP Regional Experiment
ISCCP	International Satellite Cloud Climatology Program
MO	Monin-Obukhov surface layer similarity theory
MIZ	Marginal Ice Zone
MIZEX	Marginal Ice Zone EXperiment
NCAR	National Center for Atmospheric Research
NOAA	National Oceanographic and Atmospheric Administration
OD	Overland and Davidson (1992)
OG	Overland and Guest (1991)
OBL	upper Ocean planetary Boundary Layer
SODAR	SOund Detection And Ranging
TKE	Turbulent Kinetic Energy

ACKNOWLEDGMENTS

The support, advice and encouragement of my advisor, Ken Davidson, was greatly appreciated. I thank the committee members and Jim Overland for their useful comments and discussions. Steve Burk provided numerical model computer code. This study would not have been possible without the contributions from the many people who were involved in the organization, data collection and logistics for the projects described here. Arlene proofread this dissertation, kept me fed and entertained Brian, which are all large tasks, while I was working on this study. This dissertation is dedicated to Arlene and Brian Guest.

Support for this research came from the Office of Naval Research Arctic Program (Tom Curtin), the former Naval Oceanographic and Atmospheric Research Lab in Monterey, CA (presently, National Research Lab) and the Direct Research Funding Program at the Naval Postgraduate School.

This page has been intentionally left blank.

I. INTRODUCTION

A. BACKGROUND

This doctoral dissertation is the result of an investigation of the effect of clouds on surface wind stress in the Arctic. The two physical phenomena which are the focus of this research, clouds and surface wind stress, represent very different physical processes, but both play important roles in the Arctic marine atmosphere (AMA) and their interactions are poorly understood.

Clouds affect the AMA in many different ways. The focus of this research is on those aspects of Arctic clouds which are most relevant to modeling and physical understanding of surface momentum flux or wind stress. Wind stress has special importance in the Arctic because it is the primary force driving ice movement (Thorndike and Colony, 1982).

The goal of this research is to answer the following questions, which were originally posed in the doctoral dissertation research proposal:

(1) Are clouds important to wind stress in the Arctic?
(2) What are the situations when clouds are the most important?
(3) What is the quantified effect of clouds on wind stress?

Cloud particles do not directly affect wind stress. Latent heat and radiation processes within and outside of clouds cause diabatic heating/cooling of the atmosphere and surface. The resulting temperature changes affect surface heat fluxes and stability in the lower atmosphere, which are crucial factors in determining the geostrophic drag coefficient in the Arctic (Overland, 1985; Overland and

Davidson, 1992). Therefore, the answers to the above questions are closely related to the thermal structure of the atmosphere and snow/ice surface.

The very stable atmospheric boundary layer (ABL), which often is present during clear weather in the central Arctic, tends to suppress turbulence and dynamically de-couple the surface from the rest of the AMA. The surface temperature is free to drop until a balance is reached between the upward and downward longwave radiation, with a small contribution from conductive heat transfer to the surface. If ABL clouds exist, the longwave surface cooling is mostly counteracted by radiation from the cloud base. The heat originating from the ice surface will be turbulently transported to the top of the clouds where it will be lost from cloud top longwave radiation. By changing the location of the major heat loss from the surface to the top of the ABL, the clouds have fundamentally altered the ABL.

After a change in cloud conditions, the surface of the snow is subjected to an energy imbalance. This will cause the snow surface temperature, hereafter referred to as surface temperature, to change and generate turbulent heat fluxes which affect both surface layer stability and overall ABL stability. After this initial phase, which lasts a few hours, surface layer stability is no longer important, but clouds will continue to affect wind stress by changing the overall thermodynamic structure of the ABL.

B. MOMENTUM FLUX AT THE AIR/ICE/SEA INTERFACE

The transfer of momentum between the atmosphere and the ocean directly affects both the atmospheric and oceanic boundary layers (OBL). Momentum transfer and the associated shear generate turbulent kinetic energy (TKE) in the ABL and the OBL. An increase in TKE can enhance mixing and entrainment, thus

thickening the ABL and OBL. The mean currents in the upper ocean are also driven primarily by the momentum flux from the atmosphere.

The formation, destruction and movement of sea ice is controlled by heat and momentum fluxes. Campbell *et al.* (1987) showed that Fram Strait ice movement and deformation were primarily controlled by the atmospheric momentum flux when surface wind speeds are greater than 6 m/s. Ocean currents, internal stresses and surface tilt, which also drive ice motion, are related to wind stress fields.

Formation of sea ice is a direct result of atmospheric factors such as high winds and low temperatures. Melting also can be directly caused by the atmosphere, but in the Greenland Sea Marginal Ice Zone (MIZ) most melting occurs when the ice is forced over warmer water (McPhee *et al.*, 1987). In this case, the atmosphere causes ice melting indirectly by moving the ice.

C. ATMOSPHERIC FACTORS WHICH AFFECT MOMENTUM FLUXES

Momentum flux is controlled by the surface wind speed, surface topography and atmospheric stability. The relation between wind speed and momentum flux can be parameterized by the equation

$$\tau = \rho C_d U^2, \qquad (1)$$

where τ is the surface wind stress, ρ is air density, U is a surface wind speed and C_d is a drag coefficient which is a function of surface roughness, atmospheric stability and height of U. Considerable progress has been made in recent years in developing schemes for estimating the value of C_d.

Although C_d as a function of ice conditions is now well known, estimates of wind stress in the Arctic are only as accurate as the specification of U. The

dependence of stress on the square of U makes wind stress estimates particularly sensitive to U. Although surface wind data are typically not available in the Arctic, there are enough buoys with pressure measurements to enable the estimation of the geostrophic wind speed, U_G, and direction with as much accuracy as mid-latitude locations (Moritz, 1985).

The scalar relation between surface wind stress and geostrophic wind can be parameterized by use of a geostrophic drag coefficient, C_G, which is defined as

$$C_G \equiv \frac{u_*}{U_G}, \qquad (2)$$

where u_*, the friction velocity, is defined as

$$u_* \equiv \left(\frac{\tau}{\rho}\right)^{\frac{1}{2}}. \qquad (3)$$

This is similar to $C_d^{1/2}$, except that the geostrophic wind rather than the surface wind is used. Unlike C_d, C_G is not easy to determine accurately. Many boundary layer effects such as stability, baroclinicity, isobar curvature, depth of the boundary layer and horizontal changes of these quantities, as well as surface conditions influence C_G. Therefore, virtually any phenomenon which affects the boundary layer will also affect the value of C_G.

D. CLOUDS AND LONGWAVE RADIATION

One phenomenon which affects the ABL and C_G is clouds. Clouds affect the atmosphere in three ways. (1) They release or store latent heat associated with

water phase changes; (2) they strongly influence long and short wave radiation processes; and (3) they may create hydrometeors (liquid or ice particles large enough to be affected by gravity). In the Arctic, liquid and/or ice clouds can exist in the boundary layer. This study will analyze only dark season situations with no shortwave radiation effects considered. Latent heat effects are minor in the cold Arctic winters. Hydrometeors and suspended particulate matter affect radiation and surface energy balance, but we do not have good measurements of these particles. Therefore, the focus of this study will be on how the longwave radiation characteristics of clouds affect wind stress.

Longwave radiation is affected primarily by (1) water vapor, (2) clouds, (3) CO_2 and other trace gases and (4) aerosol. The amount of water vapor in the Arctic atmosphere is limited by the cold temperatures. The other gases are constant, except on climatic time scales. Therefore, the effect of changing cloud cover on longwave radiation is particularly important in the Arctic. The longwave radiation emitted from particles near the top of clouds is greater than the amount absorbed, particularly when the air above the cloud is clear. Usually the bottom of a cloud will have radiation flux convergence, since the radiation sources below the cloud are usually warmer than the cloud base. Both these effects will tend to destabilize the cloud layer and lead to larger TKE and entrainment.

The net effect of the longwave radiation from low clouds is to cool the lower atmosphere. Cooling of the lower atmosphere can also occur indirectly due to turbulent heat fluxes from a surface cooled by radiation. This is common on clear nights over land or non-moist ice. Open ocean and moist ice or snow surfaces have mixing (open ocean) or liquid/solid phase changes (moist ice or snow) which prevent radiation processes from causing large temperature changes of the surface

material. Therefore, in the ABL of the AMA, the major loss of heat due to longwave radiation is caused directly by clouds and indirectly by surface cooling. The latter is only important when the surface is dry (below freezing) and no clouds are present in the ABL.

This dissertation is arranged as follows. After this introduction, the current state of knowledge concerning wind stress and clouds in the Arctic is reviewed. The discussion of results begins with an analysis of the effect of clouds on the thermal structure of the AMA using experimental data. Next, the short term effects of clouds on surface layer stability are analyzed. Following, longer term and complete ABL physics are modeled in order to determine the effect of clouds on wind stress for realistic situations. Then, statistical relationships between clouds and wind stress are examined. The conclusion will summarize the significance of the results and potential applications.

II. PREVIOUS RESEARCH

This chapter will examine the state of knowledge concerning wind stress and clouds in the Arctic previous to this dissertation. This chapter is divided into three sections (1) Results from wind stress studies before the Marginal Ice Zone Experiment (MIZEX) programs, (2) Cloud studies based on programs before MIZEX and (3) Wind stress and cloud studies from MIZEX and later programs. Data from the MIZEX program and later studies were obtained by the investigators at the Naval Postgraduate School.

A. WIND STRESS MEASUREMENTS AND MODELS BEFORE MIZEX

A summary of results from all wind stress measurements over sea ice reported in Western literature before 1983 is available from Overland (1985). Some of these results will be mentioned, but the reader is referred to this source for references to all studies of C_d and summaries of specific values obtained as a result of these studies.

1. Early Studies

Since the earliest explorations of the Arctic, there has been interest in the effect of wind on ice movement (Nansen, 1902; Sverdrup, 1933; Shuleikin, 1938). These earlier studies estimated magnitude ratios and angles between wind velocity and ice drift.

The recent emphasis has been on measurement and modeling of the ratio between wind speed and momentum transfer. The first estimates of surface drag coefficients over sea ice were based on measurements of surface wind speed profiles from towers (Untersteiner and Badgley, 1965, Doronin, 1969, Ling and

Untersteiner, 1974). Smith *et al.* (1970) is the first publication reporting C_d estimates based on direct eddy-correlation measurements using a sonic anemometer.

2. AIDJEX

The first extensive program to relate wind stress to surface and atmospheric factors in the Arctic occurred during the Arctic Ice Dynamics Joint Experiment (AIDJEX), which took place in the Beaufort Sea in 1971-1976. Results of surface eddy correlation measurements during AIDJEX were reported by Banke and Smith (1973) and Banke *et al.* (1976, 1980), while results from dissipation measurements were reported by Leavitt (1980). The value of C_d from these studies ranged from 1.14×10^{-3} to 1.90×10^{-3}. The locations for these measurements were chosen to avoid any wake effects from ice ridges. Therefore, the C_d values were too low to be used for area averaged wind stress estimates.

AIDJEX aircraft eddy correlation and momentum integral measurements reported by Brown (1977), Katz (1979,1980) and Carsey (1980) range from 1.7×10^{-3} to 2.8×10^{-3}. The higher values obtained by the latter methods are in good agreement with hindcast estimates of C_d from floe trajectories in Coon (1980), Hibler (1979) and Neralla *et al.* (1980).

3. Other Studies

In the late 1970's and early 1980's more surface and aircraft based measurements of wind stress over sea ice were obtained using a variety of methods. These are reviewed by Overland (1985) and will not be discussed individually here. Overland's summary of surface drag coefficients is shown in Table 1. Higher drag

TABLE 1
COMPOSITE SURFACE DRAG COEFFICIENTS AS A FUNCTION OF ICE AND METEOROLOGICAL REGIME

Ice Regime	Characteristics	$T_a \sim 0°$	$T_a < -5°$, $Z_i < 300$ m	$T_a < -5°$, $Z_i > 400$ m
Smooth ice	large, flat floes	1.5[a]	1.5[b]	
Arctic pack	large range of floe sizes, large pressure ridges, $C_i > 0.9$	1.7[c]	2.6[d,e]	
Marginal seas	broken, first-year ice, C_i = 0.9, occasional big floes	2.2[f]	2.7[g]	3.0[h]
Inner MIZ	small floes, rafted, C_i = 0.8–0.9	2.6[i]	3.0[j]	3.7[k]
Outer MIZ	C_i = 0.4	2.2[l]		
	C_i = 0.3, rubble field	2.8[m]		

Footnotes refer to the data sets that form the basis for the coefficient. Numbers represent a subjective median for a range of values. Error estimates are not possible.

coefficients were obtained over sea ice in the marginal seas than in the central Arctic. The highest values were found in the MIZs.

4. Wind Drag Coefficient Models

Arya (1973,1975) partitioned the surface momentum stress into a skin drag and a form drag. The skin drag was caused by the regular floe surface while the form drag was due to pressure ridges. The surface measurements from AIDJEX were considered to be measurements of skin drag only. Guest and Davidson (1984b) extended this model to include the effect of floe edges, which are usually the dominant roughness elements in the MIZ.

Banke *et al.* (1980) related C_d to surface roughness elements after filtering wavelengths greater than 13 cm. Brown (1981) modeled the geostrophic drag coefficient using a two layer ABL model containing a surface layer and a modified Ekman layer. His model included the effect of secondary circulations and thermal wind. Above a classic surface layer, the wind profile was calculated by using similarity functions which were empirically determined from AIDJEX measurements. The value of C_G was sensitive to stability at near-neutral conditions. The effect of clouds was not considered.

B. CLOUD STUDIES

The effect of clouds on the ABL has been the object of a considerable research in recent years. Stull (1988) provides a good review of our basic knowledge concerning clouds and the ABL. Almost all observational cloud studies have occurred in the mid-latitudes and tropics. Many of the observed effects of clouds on the dynamics of the ABL can be applied to the Arctic, although differences in temperature, cloud condensation nuclei (CCN) size spectra and other factors must

be considered. The most common type of clouds in the Arctic are stratus, stratocumulus and fog (fog will be considered to be a type of cloud). These types of clouds are the focus of this dissertation.

1. Early Studies

Vowinckel and Orvig (1970) compiled cloud statistics for the marine Arctic which showed a high percentage of stratus in the summer. Jayaweera and Ohtake (1973) observed that Arctic stratus usually occurred in several layers, unlike mid-latitude stratus. This layering was modeled by Herman and Goody (1976). They show that the layering can be caused by shortwave radiation which is trapped inside a cloud that is opaque to longwave radiation. They propose that diurnal effects prevent similar layering in mid-latitude clouds.

2. AIDJEX

The stratus cloud coverage during AIDJEX was anomalously low in 1975, due to unusual northerly winds (Jayaweera, 1977). Jayaweera also describes results from May 1976 *Cessna 180* aircraft missions which found that the inversion would lower to the center of the stratus clouds after a few days.

AIDJEX included two radiation missions by the NCAR *Electra* aircraft described by Herman (1977). He estimated Arctic stratus shortwave radiation parameters such as bulk values for reflectance, transmittance and absorbance, and other parameters such as single scattering albedo, absorption optical depth and multiple scattering parameters.

Using data from the same flights, Herman (1980) determined various longwave parameters for the Arctic stratus, including mass absorption coefficients for selected liquid water distributions. He concluded that the longwave radiative properties of Arctic stratus are similar to mid-latitude stratus.

3. Arctic Stratus Cloud Experiment

During June 1980, six NCAR *Electra* missions were flown over the Beaufort Sea as part of the Arctic Stratus Cloud experiment (ASC). This was the most comprehensive program to specifically study Arctic clouds. The first direct measurements of cloud liquid water and droplet spectra were made. There were no surface based measurements during ASC.

Tsay and Jayaweera (1984) described the cloud morphology and drop size spectra in the clouds. Tsay and Jayaweera (1983) emphasized the different radiative properties resulting from wide variations in droplet spectra. Herman and Curry (1984) analyzed the effect of the clouds on shortwave radiation with the aid of a theoretical model. Curry and Herman (1985a) analyzed the longwave radiation properties. These papers contain detailed tables and figures of cloud characteristics and radiation measurements. There was a large variability observed in the cloud characteristics on different days so that a "typical" summer Arctic stratus cloud could not be described. Large-scale factors which affect the occurrence of Arctic stratus were examined by Curry and Herman (1985b).

Curry (1986) examined the interactions between turbulence, radiation and microphysics in Arctic stratus by examining four case studies of the ASC flights. She has several conclusions which are important to understanding how Arctic clouds might affect surface wind stress. (1) The cloud layer is often de-coupled from the surface, and several cloud and/or fog layers may exist. Therefore the entire ABL cannot be modeled as a mixed layer. (2) The clouds themselves are well mixed due to cloud top radiative cooling and latent heat but not due to surface fluxes. (3) The longwave cooling in the clouds always exceeds the warming from shortwave absorption. The magnitude and vertical distribution of cooling is sensitive to size

spectra and liquid water amount at the top of the clouds. (4) The direct effects of entrainment on temperature and liquid water are not obvious lower than 50 meters below the cloud top. (5) There is no evidence of inhomogeneous mixing as described by Baker and Latham (1979). (6) Surface fluxes of moisture do not contribute significantly to maintaining the clouds. Gravitational settling has a strong effect on the particle size spectra in different regions of the clouds. (7) The spectral dispersions of droplet radii are very large due to a variety of mechanisms. (8) Only 10% of the cloud-top cooling is balanced by turbulent sensible and latent fluxes from below. The rest of the heat comes from entrainment and droplet growth. Curry does not mention subsidence.

4. Other Cloud Studies

A major current program to study marine stratocumulus clouds is called the First ISCCP Regional Experiment (FIRE; ISCCP = International Satellite Cloud Climatology Project). Much of the research related to this program is based on a field program which occurred off the coast of southern California during the summer of 1987 (Kloessel *et al.*, 1988).

Borisenkov *et al.* (1985) numerically modeled the influence of Arctic clouds on large scale meteorology. They found Arctic stratus clouds would increase precipitation in Europe and other places far from the Arctic.

C. WIND STRESS AND CLOUDS: MEASUREMENTS AND MODELS SINCE MIZEX

1. Surface Wind Stress Measurements

Monin-Obukhov surface layer similarity theory (reviewed by Dyer, 1974) applies to surfaces that are horizontally homogeneous. But recent evidence (see

Stull, 1988) shows that the theory can also be used when some horizontal variability is present. Therefore, more recent Arctic surface measurements were obtained with ridges, ice floe edges, or other roughness elements upwind, instead of in the center of large flat floes as in earlier studies.

During the Marginal Ice Zone Experiments of 1983 and 1984, (MIZEX-83 and MIZEX-84) many geophysical studies were carried out (MIZEX Group, 1986). Results from wind stress measurements were reported by Guest and Davidson (1984a, b, c, d, 1985, 1987a), Davidson and Guest (1986,1987), Davidson and Geernaert (1984a, b, 1985), Fairall and Markson, (1987) and Anderson, (1987). All the studies show that C_d increased with ice concentration in the MIZ. Guest and Davidson (1987a) and Anderson (1987) measured higher drag coefficients over rough ice than had been previously reported. The highest MIZ values of C_d, 5-6 x 10^{-3}, were measured in regions of very rough ice that had been broken up and rafted due to swell action.

During the MIZEX-87 spring field program (MIZEX '87 Group, 1989) the air temperature was well below freezing and new ice was forming. Many stages of ice formation were encountered. Guest *et al.* (1988), Davidson and Guest (1988) and Guest and Davidson (1991a) determined values of C_d as a function of all ice types (Table 2).

The highest values of C_d ever measured over sea ice occurred during the Coordinated Eastern Arctic Experiment (CEAREX) drift phase. Multi-year ice had undergone extensive deformation as it was pushed, along with the vessel *Polarbjoern*, toward Kvitoya island. Pressure ridges as high as 4 m were common around the ship. An average C_d value of 8 x 10^{-3} was obtained during a two-day

TABLE 2
THE ROUGHNESS LENGTH, z_0, AND NEUTRAL DRAG COEFFICIENT, C_{dn}
FOR VARIOUS ICE AND SEA SURFACES

Ice Type	$z_0 \times 10^3$ m, Median	$C_{dn} \times 10^3$		
		Median	Minimum	Maximum
Grease	0.0027	0.7	0.6	1.1
Nilas	0.45	1.6	1.4	1.9
Pancake				
Diameter <0.75 m	0.016	0.9	0.7	1.3
Diameter 0.75–1.5 m	0.45	1.6	1.1	2.2
Diameter >1.5 m	2.8	2.4	1.9	2.9
Fused	1.0	1.9	1.5	2.6
Young				
Smooth	2.4	2.3	1.9	2.7
Rough	7.5	3.1	2.6	3.6
First year				
Very smooth*	0.33	1.5	1.2	1.9
Smooth	1.3	2.0	1.6	2.4
Rough	7.5	3.1	2.2	4.0
Very rough	21.0	4.2	3.1	5.0
Multiyear				
Very smooth*	0.33	1.5	1.2	1.9
Smooth	2.0	2.2	1.9	2.5
Rough	10.0	3.4	2.5	4.1
Very rough	27.0	4.6	3.6	5.5
Extremely rough	110.0	8.0	6.7	9.1
Ice-free water				
(Steady state open ocean)†				
$U = 10\ ms^{-1}$	0.15	1.3	na	na
$U = 25\ ms^{-1}$	1.3	2.0	na	na
East Greenland Sea ($U < 12\ m\ s^{-1}$)				
All wind directions	0.80	1.8	0.7	3.0
Ice upwind 2–10 km	0.23	1.4	1.1	1.8

Values are based on author's measurements unless otherwise noted and are only from periods when lowest inversion was higher than 150 m. At least 85% of the stated ice type was upwind.

*Includes studies summarized by *Overland* [1985].

†From *Smith* [1988]. No ranges given.

period. These recent measurements show that C_d can have higher values than reported by Overland (1985) in certain regions.

As a result of these studies, the value of the surface drag coefficient can be accurately estimated for variations in ice condition. For this to be useful, methods must be developed to identify types and concentrations of ice in the Arctic. The ice maps currently produced by NOAA give only general descriptions of ice types and concentrations.

2. Observations of Clouds During MIZEX and CEAREX

During the MIZEX or CEAREX programs continuous surface measurements, observations and rawinsonde profiles provide a large data base to study many aspects of clouds in the Arctic (Davidson *et al.*, 1984; Lindsay, 1985; Guest and Davidson, 1988). During certain periods, there were SODAR measurements, aerosol measurements and aircraft missions with cloud physics instrumentation.

Guest (1985) developed techniques for forecasting fog in the MIZ. Stratus or low fog is virtually always present during on-ice winds in the MIZ and fog forms from stratus lowering. With parallel wind flow, boundary layer fronts are common, and the onset of fog or stratus will be abrupt.

Statistical studies by Guest and Davidson (1987b, 1988) show that the presence and thickness of clouds were correlated with the height of the inversion base, Z_i. When stratus clouds were present, Z_i was higher and was less correlated with wind speed than clear sky cases (Figure 1).

Guest *et al.* (1988) compared median Z_i values for on-ice and off-ice winds in the MIZ (Figure 2). At all relative locations, Z_i medians were higher for on-ice winds than off-ice winds. The difference in Z_i becomes greatest over the

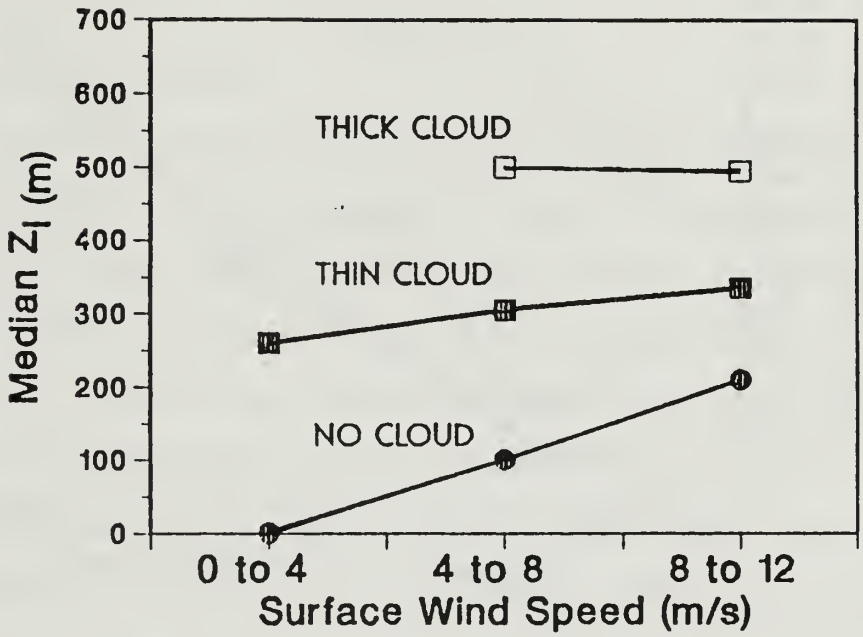

Figure 1 Composite Median Inversion Base Heights, Z_i, from MIZEX-84 Divided into Wind Speed and Cloud Thickness Categories. Note that during clear (no cloud) conditions the inversion was lower and more greatly affected by wind speed than during cloudy conditions.

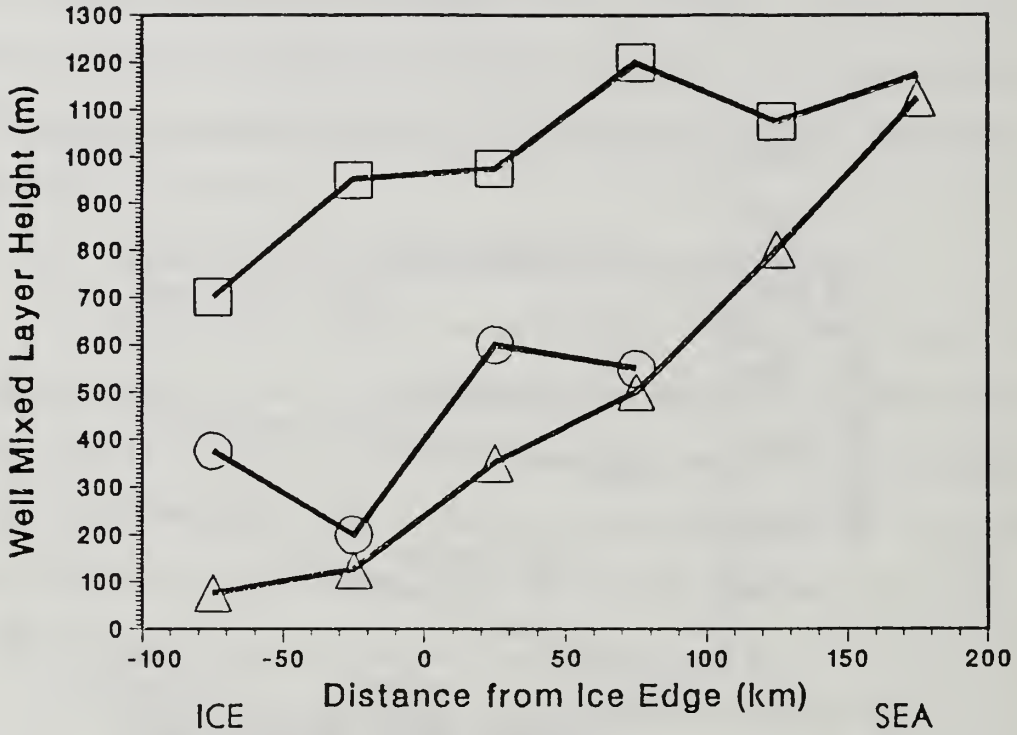

Figure 2 Composite Median Z_i Values Across the MIZ for Different Wind Directions during MIZEX-87. Triangles, circles and squares represent off-ice (left-to-right), parallel-right (out-of-paper) and on-ice wind conditions, respectively.

pack ice. During on-ice winds, fog or stratus inevitably would exist over the ice. The destabilizing effect of the clouds may be a major reason for the observed difference in Z_i between wind regimes. (There are also influences due to advection and subsidence.) If the clouds affect Z_i, they will also affect surface momentum flux, because a higher Z_i is associated with more efficient transport of momentum to the surface.

3. Boundary Layer Models

Although surface drag coefficients are well known and straightforward to use, their use requires measurements of surface wind speed. Estimating wind stress from a pressure field is much more complicated. This involves the specification of the geostrophic drag coefficient, C_G, which requires some type of ABL model.

Overland (1985) used a steady-state one-dimensional ABL model to determine C_G and the turning angle between the geostrophic and surface wind, α, as a function of a mechanical mixing stability parameter. He found that when the atmosphere became very stable, the surface wind tends to de-couple from the upper winds, and C_G is no longer affected by surface roughness. These results are applicable in the Arctic pack ice away from the MIZs. Clouds effects were not considered.

In the 1980's, the focus of Arctic studies was on MIZs. The few ABL models for the MIZ that have been published will be reviewed. Overland *et al.* (1983) used a primitive equation slab model to explain observations of the Bering sea MIZ in March during off-ice winds. Reynolds (1984) examined the same case with a similar model, but included radiative cooling from clouds. He attributed the observed variations in temperature, wind and ABL height to drag variation over the

ice and heat flux over the open ocean. Clouds and heat flux through the ice were not important.

Andreas *et al.* (1984) described a MIZ ABL based on a rawinsonde cross-section of the Antarctic MIZ during off-ice winds in the Weddell sea. Bennett and Hunkins (1986) simulated this case with a two-dimensional, multi-level model which includes radiation. They concluded that adiabatic lifting due to convergence and longwave cooling from clouds dominate the cooling in the ABL. Although there was some discussion concerning model details (Andreas, 1987; Bennett and Hunkins, 1987), all authors agreed that there were large changes in the wind stress across the MIZ due to roughness and cloud effects.

Chu (1986a, b, c, 1988a, b, c) has modeled several mechanisms by which air-ice-sea interactions may cause ice features in the MIZ. Chu *et al.* (1990) and Chu and Garwood (1990, 1991) investigated feedback mechanisms between clouds and surface fluxes over ice-free oceans.

Brown (1986) applied his one-dimensional, two-level ABL model to an off-ice wind case in the Fram Strait MIZ. A realistic surface roughness and temperature field was used. The greater roughness in the outer MIZ slows and backs the surface wind. A greater upward heat flux at the surface has the opposite effect.

Recent results of two dimensional multi-level MIZ ABL models by Glendening (1992) and Kantha and Mellor (1989) show the same general results for off-ice winds. Kantha and Mellor also examined the MIZ ABL during on-ice, parallel-left and parallel-right wind regimes. The above studies show the surface stress field is very complicated in the MIZ because of the changes in the ABL due to

surface roughness and horizontal temperature variations. Cloud effects have not been modeled by these researchers.

Glendening's model of the MIZ ABL during off-ice winds shows that Z_i is controlled by surface wind stress over the ice regions and surface temperatures (heat fluxes) over open ocean regions. He has not examined very stable cases when surface conditions become de-coupled from the upper ABL.

Modeling stable ABL situations is more difficult because of the intermittent nature of the mixing events. Overland (1988) approaches the problem with a one-dimensional, multi-level, TKE-mixing length model which simulates the ABL over ice in the winter. When cloud radiation effects are introduced, the boundary layer becomes unstable and surface stress increases by approximately 20%.

4. Wind Stress in the MIZ

The above models, as well as observations (Davidson and Guest, 1988) show that the surface wind stress field does not match the surface drag coefficient field because there are changes in the surface wind speed across the MIZ. The wind speed at the surface is affected by changes in stability and surface roughness. By using observations and Overland's (1985), Brown and Liu's (1982) and Brown's (1986) ABL models, Campbell *et al.* (1987) and Guest (1988) showed that the combined effects of horizontally varying surface wind speeds and roughness result in a wind stress field which is complicated and dependent on the wind direction relative to the ice. Typically, the wind stress is greater over the open ocean than the pack ice, even though C_d has an opposite distribution. This fact has been neglected by several MIZ ice movement models (Roed, 1983; Roed and O'Brien, 1983; Hakkinen, 1986a,b; Smith *et al.* 1988). These models use an unrealistic constant

surface wind speed and direction across the MIZ, which results in greater stress over the ice regions.

Guest (1988) also shows that clouds can have a large effect on surface wind stress if they change the stability of the surface layer from stable to unstable. This effect of clouds will be further examined.

III. AN EXAMINATION OF THE RELATION BETWEEN CLOUDS AND ATMOSPHERIC BOUNDARY LAYER THERMODYNAMIC STRUCTURE

Clouds influence wind stress by their thermodynamic effects on the atmosphere. This chapter will examine the thermodynamic effects of clouds, which form the basis for understanding the effect of clouds on wind stress.

Divergence of longwave radiation at cloud tops and/or at the snow surface has a significant effect on the thermodynamic structure of the lower atmosphere over pack ice during the Arctic winter. Overland and Guest (1991), hereafter OG, showed how the temperature at the surface was primarily controlled by longwave radiation. Heat conduction through the ice and leads are less important but do prevent extremely cold temperatures (< -40 C) from existing over sea ice. The layer of air just above the inversion, or isothermal layer, contains the warmest temperatures in the atmosphere (Figure 3). It will tend to experience more radiational cooling than the rest of the atmosphere. Warm horizontal advection must counteract the longwave cooling in the isothermal layer, on the average.

The actual location of the maximum longwave cooling in the lower atmosphere depends on the cloud conditions. The location of the cooling affects the stability and therefore the dynamics of the lower AMA. When conditions are clear, the maximum longwave cooling occurs in a thin layer at the top of the snow/ice. When clouds exist, the maximum radiational cooling occurs at the top of the upper cloud layer. There is a strong correlation between amount of cloud cover and downward longwave radiation (Figure 4). When low overcast is present, all of our Arctic data indicate a clear trend: the downward longwave radiation at the surface is within ± 10 Wm^{-2} of the blackbody radiation at cloud bottom. Therefore, it can be

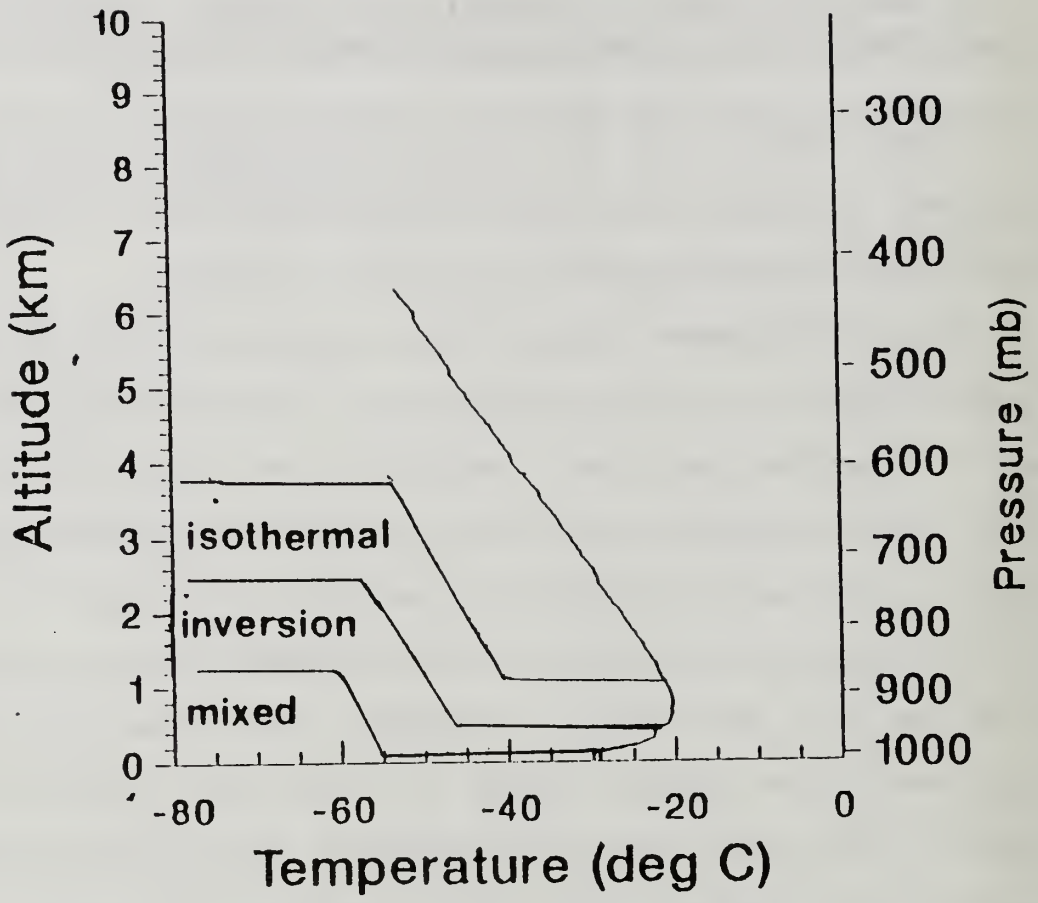

Figure 3 A Typical Temperature Sounding From the CEAREX Drift. The mixed layer, lower 200 m, inversion layer, 200 to 500 m, and the isothermal layer (500 to 1200 m) are shown.

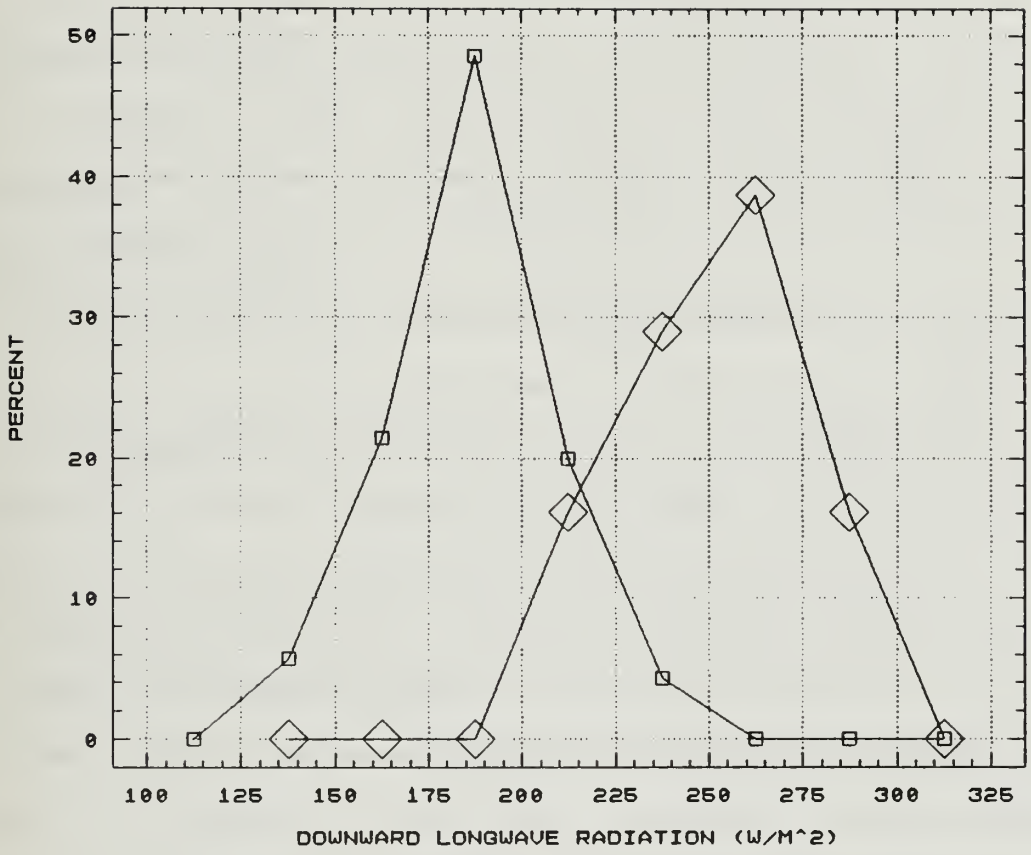

Figure 4 Frequency Distribution of Downward Longwave Radiation during the CEAREX Drift for Clear (small squares) and Low Overcast (large diamonds) Conditions. Note that the peak frequency for cloudy conditions is about 75 Wm^{-2} higher than for clear conditions.

assumed that all but the thin (less than 100 m) low level cloud layers that exist in the Arctic are essentially black to longwave radiation. The examination will be based on data obtained during the MIZEX and CEAREX programs.

A. CEAREX DRIFT MEASUREMENTS

Most of the observational data used for this study were from measurements from the *Polarbjoern* during the CEAREX drift phase, 15 September to 12 December, 1988. During the drift phase, the *Polarbjoern* was moored to a large ice floe which drifted in the region North and East of Svalbard. Instrumentation was located both on a large ice floe (alpha floe) to which the *Polarbjoern* was moored, and on board.

A meteorological station was located on a platform extending forward of the *Polarbjoern*'s bow mast at a height of 14 meters above sea level. This station measured wind speed and direction, temperature, and relative humidity. Temperature data were accurate to within 1.0 C. The humidity measurement was not reliable. Wind speeds were accurate to within 0.3 m/s and direction to within 10 degrees, although during periods of unfavorable wind direction, errors may have been larger.

The radiation system measured both downward infrared and downward solar irradiance, and was located on the ice until the floe was crushed on November 15. At this time the system was relocated aboard the *Polarbjoern*. The system remained operational until December 12. The sensors would often frost quickly; therefore hourly cleanings were performed. Radio transmissions would interfere with the measurements. The data were manually edited to eliminate poor measurement periods. The instruments were modified so that errors due to temperature

differences within the sensor could be identified and corrected. The resulting irradiances were generally accurate to within 5 watts/m^2.

Rawinsondes provided vertical profiles of temperature, humidity, and wind speed and direction twice daily throughout the experiment, with additional soundings during periods of extreme or unusual weather. The sondes were equipped with thermistors that measure temperatures to within 0.2 C. The humidity sensor consisted of a specially coated glass plate, the resistance across which varies with humidity. It was accurate to about 5%. Sonde wind directions were generally accurate to within 20 degrees.

A 6 meter profile mast, located on an adjacent floe, measured temperature and wind speed at 4 levels. This was used to provide wind stress and heat flux measuirements when the wind direction was favorable. The heat flux was estimated to be accurate to 5 Wm^{-2} and the wind stress to 20%. Surface temperature was measured with a thermistor placed on the snow surface and was accurate to 1.0 C..

B. THERMODYNAMIC COUPLING OF THE SURFACE, CLOUD LAYER AND ISOTHERMAL LAYER

This section will use the results of measurements from the CEAREX drift to examine the relationship between surface temperature, air temperature, ABL temperature and isothermal layer temperature over ice in the Arctic winter. (In a strict sense, the term "air temperature" refers to the temperature at 10 m above the surface. In practice, the temperature at the top of the ice profile mast, 5.2 m, and at the ship mast, 14 m, were used to determine air temperature.) The differences between these temperatures determine the stratification of the lower atmosphere which in turn affects momentum transfer to the surface. The effect of clouds on the stratification will be examined.

The surface temperature and the air temperature are closely linked (Figure 5) because surface sensible heat flux quickly counteracts any temperature difference between the snow and near-surface air. The one period when there was a difference of greater than 2 C, 2-6 November 1988, occurred during very low or zero winds, when turbulent surface fluxes were suppressed. Usually, enough turbulence exists to support surface layer heat fluxes and therefore the difference between surface temperature and ABL potential temperature is usually very small.

OG showed how surface temperature, and therefore air temperature, is thermally coupled to a radiational boundary layer (RBL). The RBL is characterized by an isothermal temperature layer above an inversion layer. The isothermal layer extends to approximately 1.5 km elevation. The surface is prevented from becoming extremely cold because the heat that is lost by upward longwave radiation is replaced by downward radiation from the isothermal layer, plus a small amount of heat conduction upward through the ice/snow.

OG did not consider the effect of clouds, which, in the isothermal layer or ABL, would greatly increase the downward radiation at the surface compared to clear sky conditions. This causes a very close thermodynamic coupling between the clouds and the surface. This coupling is illustrated in Figure 6, a time series plot of surface air temperature vs. sky temperature. Sky temperature, T_{sky}, is defined as the temperature of a blackbody corresponding to the measured downward radiation at the surface, $R_{downsfc}$

$$T_{sky} \equiv \left(\frac{R_{downsfc}}{\sigma} \right)^{\frac{1}{4}}, \qquad (4)$$

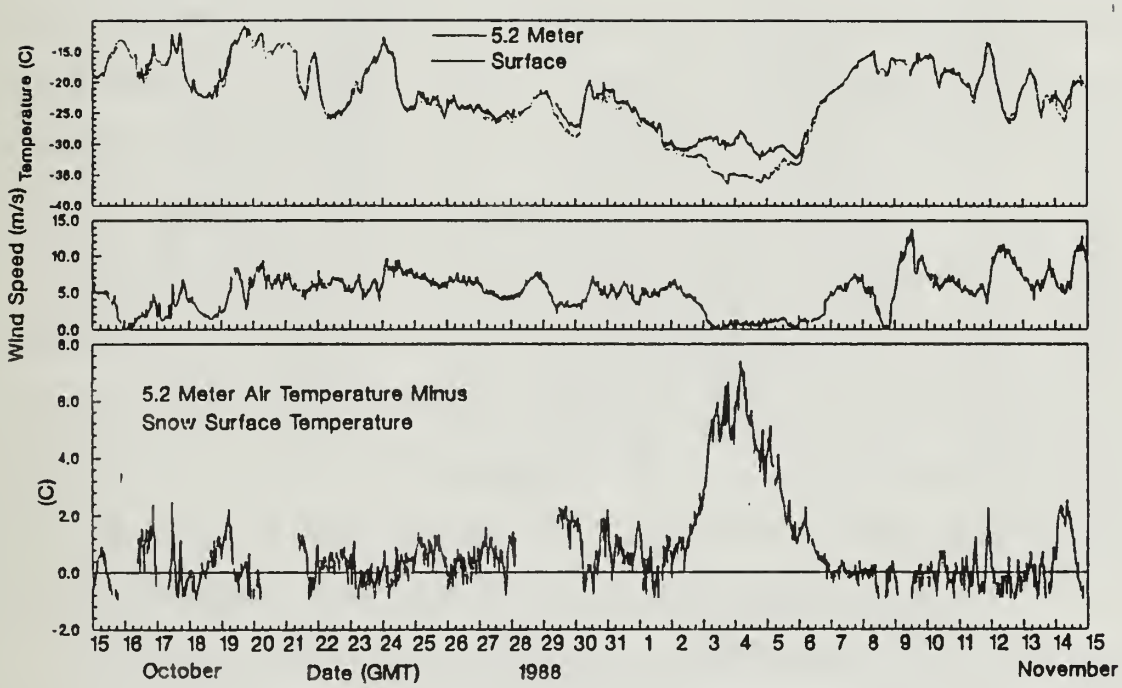

Figure 5 Time Series of Surface Temperature, 5.2 Meter Air Temperature, Wind Speed and Air-Snow Temperature Difference during the CEAREX Drift.

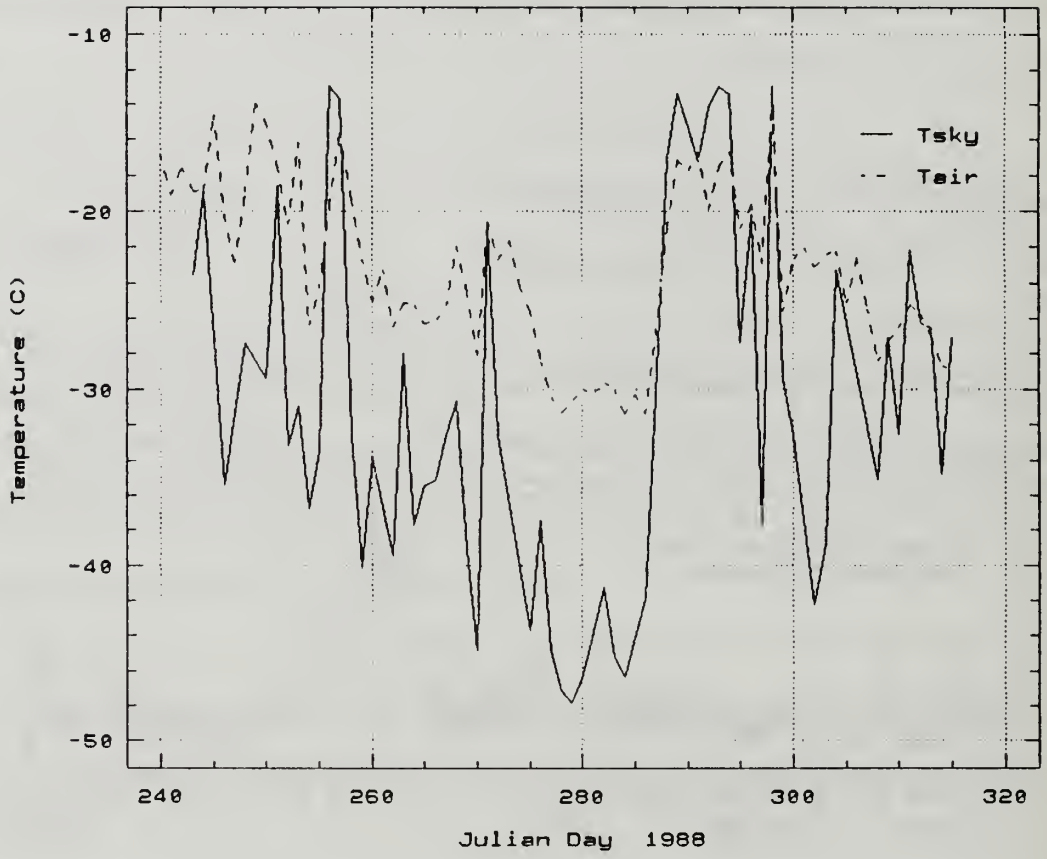

Figure 6 Time Series of 14 Meter Air Temperature (dashed line) and Sky Temperature (solid line) during the CEAREX Drift.

where σ = 5.67 x $10^{-8}Wm^{-2}K^{4}$ is the Stefan-Boltzmann constant. The air temperature, T_{air}, in Figure 6, is usually very close to the sky temperature, except for a few periods of colder sky temperatures.

The periods when T_{air} was close to T_{sky} were cloudy periods, while the periods when T_{sky} was colder occurred during clear periods. This is illustrated by scatterplots of T_{air} vs. T_{sky} for overcast and clear sky conditions (Figures 7 and 8). A link between T_{air} and T_{sky} exists for all sky conditions. This is because the dry snow surface has a low heat capacity and low thermal conductivity and therefore the snow surface temperature quickly responds to changes in surface energy balance caused by changes in downward radiation. The snow surface is then closely linked to the ABL air temperature by turbulent heat flux as discussed above.

During low level overcast periods, a better correlation between air temperature and surface temperature exists (Figure 8). T_{air} and T_{sky} are never more than a few degrees different from each other. During these overcast periods, the surface is not only linked by radiation with the surface, it is also turbulently linked if the cloud bottom is within the ABL. ABL turbulence effectively transfers heat between the surface and the top of the ABL during overcast conditions.

A conclusion of OG was that longwave radiational cooling of the snow surface causes the lower atmosphere to cool during the dark seasons. The temperature of the air near the surface is determined by a balance between upward radiation at the snow surface and downward radiation from the isothermal layer (with a small effect due to heating from the ocean through leads and ice). This study proposes that these conclusions be modified for situations when the ABL is cloud-capped. During these periods, important radiational exchanges are occurring at the cloud top rather than at the surface.

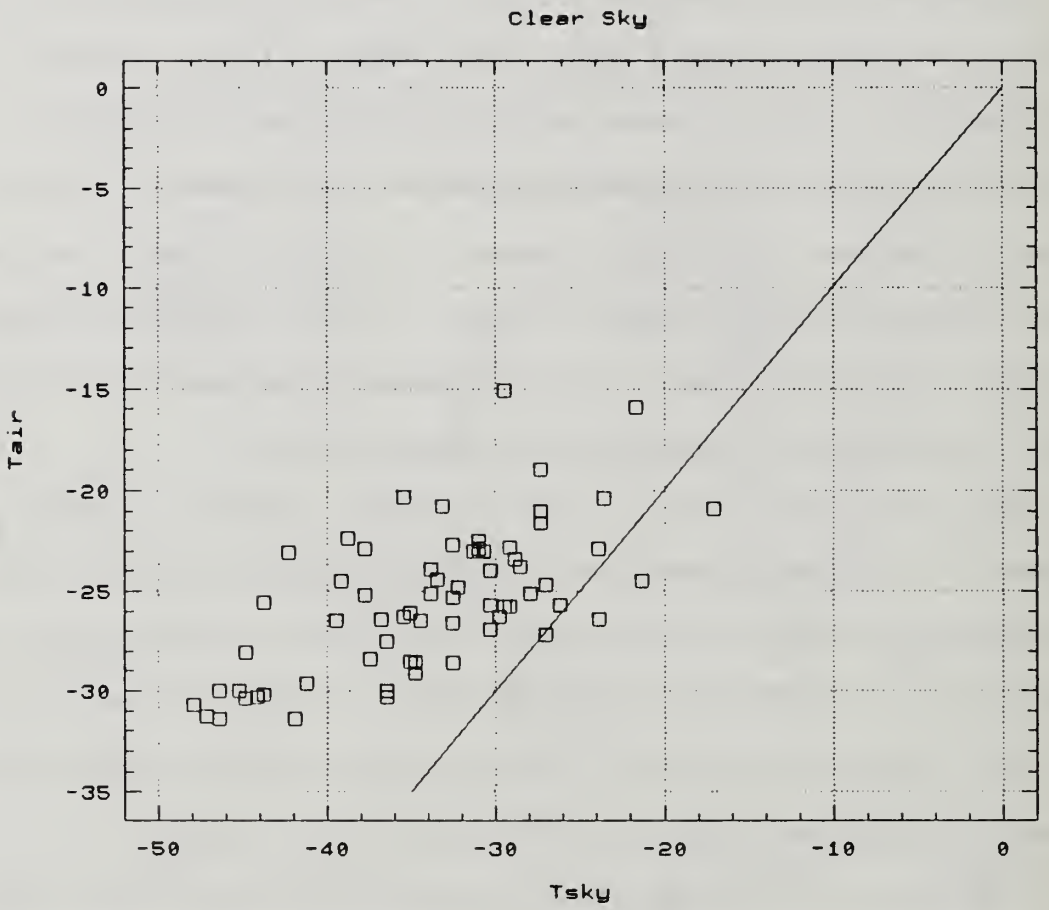

Figure 7 Scatterplot of Sky Temperature vs. 14 Meter Air Temperature for Clear Sky Conditions during the CEAREX Drift. The line represents surface temperature equal to sky temperature.

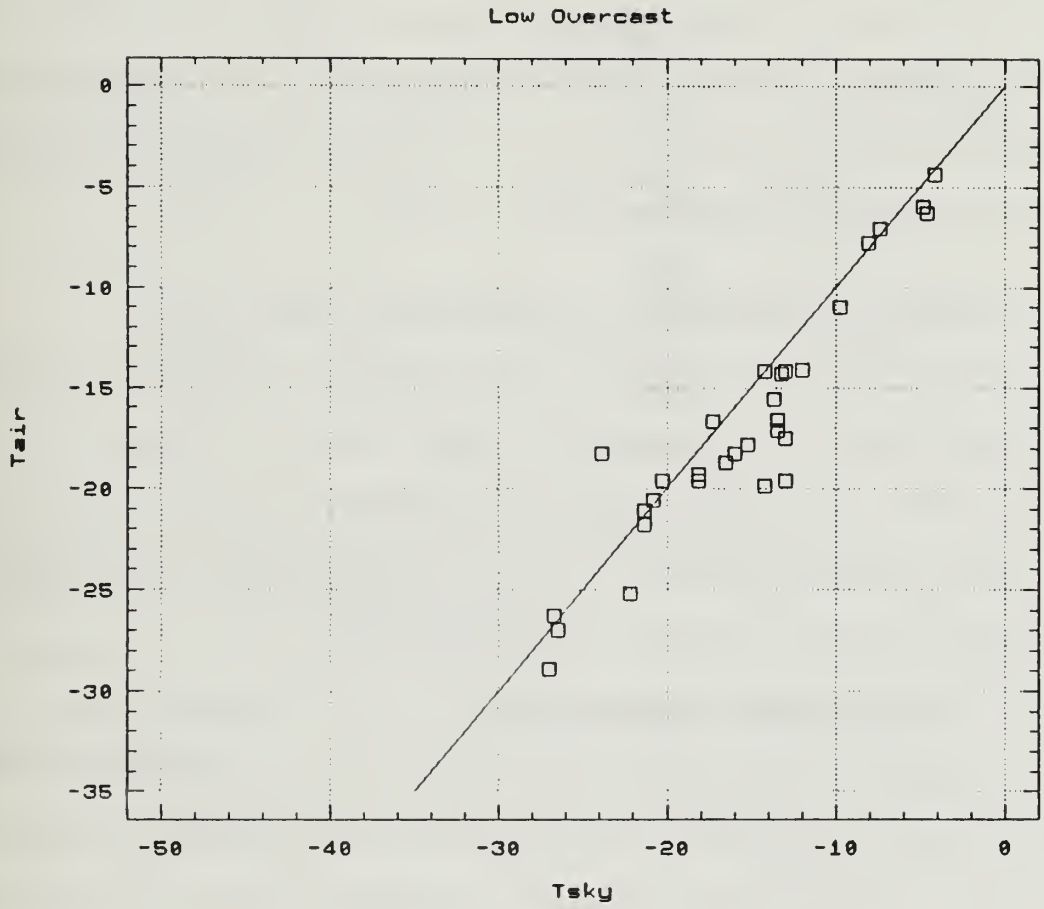

Figure 8 Same as Figure 7 but for Low Overcast Conditions.

Overland and Davidson (1992), hereafter referred to as OD, found that wind stress was affected by a measure of the external or background atmospheric stratification based on the difference in temperature between the surface and an upper level (900 or 850 mb), assumed to be in the isothermal layer. When ABL clouds exist, the surface is no longer directly connected by radiation to the upper level. In this case, an external stability parameter defined by the difference in temperature between the cloud top (instead of the surface) and an upper level may be appropriate, since it is at the cloud top that the direct radiational linking between the surface and the upper levels is actually occurring.

C. CLOUDS AND BOUNDARY LAYER THERMAL STRUCTURE

To determine the effect of clouds on wind stress, it is important to understand how clouds affect or are associated with ABL structure. Two parameters for describing ABL structure were derived from hundreds of different MIZEX and CEAREX rawinsonde soundings. These were (1) height of the lowest inversion base, Z_i, and (2) "type" of boundary layer, described below.

1. Inversion Height - Average Values

Low cloud cases have a higher average Z_i than clear sky cases. This is shown in Table 3 for locations within the pack ice, in the MIZ and in the adjacent open ocean. Average inversion heights are considerably higher for cloudy skies compared to clear skies. This is true for the various locations shown in Table 3 and also is true for any data set grouped by season, platform, wind direction regime (off-ice, on-ice) or wind speed regime (not shown).

TABLE 3
MEAN AND MEDIAN Z_i FOR DIFFERENT LOW CLOUD CONDITIONS AND LOCATIONS

Cloud Condition		Location: Pack ice[1]	MIZ[2]	Open Ocean[3]
Overcast	median	220	400	610
	mean	270	480	730
	sd[4]	210	390	470
Clear	median	100	60	420
	mean	160	220	450
	sd[4]	240	370	340

[1]50 km or more from ice edge (primarily CEAREX drift data)

[2]<50 km from ice edge but still over sea ice

[3]over open ocean but within 200 km of ice edge

[4]sd = standard deviation These values represent natural variations, not experimental errors.

The large standard deviations of the Z_i values show that other factors besides clouds affect ABL structure. An analysis of variance shows that 22% of the variation in Z_i values not associated with distance from the ice edge can be attributed to cloud conditions. The higher average Z_i values associated with low clouds are not due entirely to the direct effect of clouds on the ABL. Cloud occurrence is associated with warm advection, low pressure systems, high wind speeds and moist marine air masses. All of these would be associated with higher Z_i values even without cloud effects.

In this section, Z_i vs cloud relationships were examined, and in the previous section, the coupling between longwave radiation and ABL air temperature for different cloud conditions was discussed. Results from both topics can be combined by plotting the difference between T_{sky} and T_{air} vs. Z_i for clear and low overcast conditions (Figure 9). Several differences between overcast and clear conditions are apparent. Overcast conditions are characterized by T_{sky} being nearly equal or slightly greater than T_{air}, and by having higher average inversion bases when compared with clear cases. Surface-based inversions ($Z_i = 0$) are extremely rare during cloudy skies, but clear skies do not guarantee that a surface inversion will be present.

2. Inversion Height and u. Scaling

It has been observed since early explorations (Sverdrup, 1933) that the value of Z_i is related to surface wind speed. Increasing wind speed generates more turbulent kinetic energy, TKE, due to turbulent shear production, which is able to extend mixing to higher levels. Attempts to scale or predict Z_i or the ABL depth, h, for stable or neutral ABLs invariably use parameters related to the mechanical production of turbulence: the friction velocity, u_*, an eddy viscosity coefficient, K,

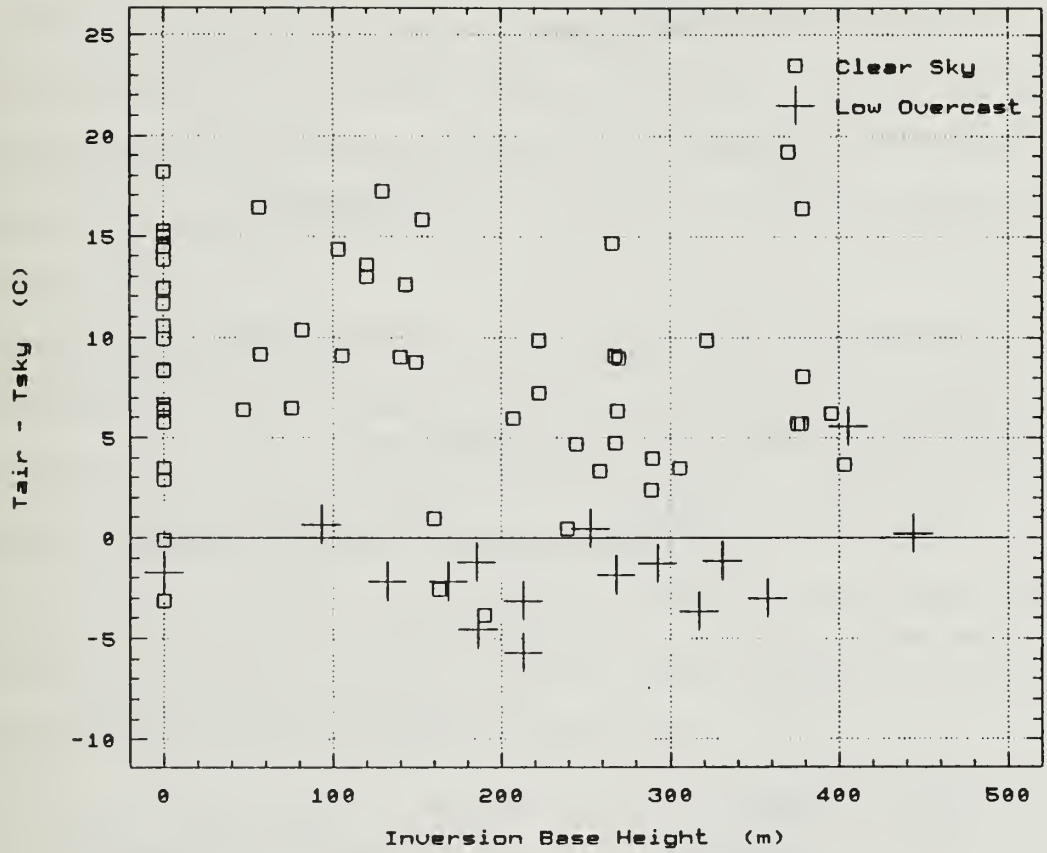

Figure 9 Scatterplot of the Difference Between the 14 Meter Air Temperature and the Sky Temperature vs. Inversion Base Height for Clear (squares) and Low Overcast (plusses) Sky Conditions.

the bulk Richardson number, Ri_B, or a wind speed or wind shear parameter. The following scales for equilibrium ABL height, h_e, have been proposed for stable and neutral ABLs.

Neutral ABL and Free Atmosphere:

$$h_e = \pi\left(\frac{2K}{f}\right)^{\frac{1}{2}} \qquad \text{Ekman depth}$$

$$h_e = 0.2\left(\frac{u_*}{f}\right) \qquad \text{e.g. Panofsky and Dutton (1984)}$$

Stable Surface Layer, Neutral Free Atmosphere:

$$h_e = L = -\frac{\theta_v u_*^3}{kg\,\overline{w'\theta_v'}} \qquad \text{Obukhov length scale}$$

$$h_e \propto \left(\frac{u_* L}{f}\right)^{\frac{1}{2}} \qquad \text{Zilitinkevich (1972, 1974)}$$

$$h_e \propto \frac{Ri_B U_h^2\,\theta}{g(\theta_h - \theta_o)} \qquad \text{Hanna (1969), Wetzel (1982)}$$

Neutral Surface Layer, Stable Free Atmosphere:

$$h_e \propto \frac{u_*}{N};\ N^2 = \frac{g}{\theta_v}\frac{\partial \theta_v}{\partial z} \qquad \text{OG , Kitaigorodskii (1988), Kitaigorodskii and Joffre (1988)}$$

The parameter $\frac{u_*}{N}$ was shown by OD to be relevant for scaling the Arctic winter boundary layer, when surface fluxes are usually small and an external or background stability limits the height of the ABL. OD used data from the

CEAREX drift to verify this relationship. A re-analysis of these data confirms that Z_i was correlated (R^2 = 0.34) with u_* or wind speed during the CEAREX drift data (Figure 10). A similar correlation (R^2 = 0.21) occurs for the data set containing all MIZEX and CEAREX soundings made by our group in the Arctic (Figure 11) when all sky condition cases are included. However, when either data set is divided into categories depending on cloud conditions, it is found that the wind speed (or u_*) dependence completely disappears ($R^2 < 0.05$) for the low overcast cases (Figures 12 and 13).

The wind dependence noted by OD and others apparently occurs only during clear sky periods. This lack of wind speed dependence for Z_i during overcast conditions was observed in the MIZ during the summer in MIZEX-84 (Guest and Davidson, 1987b) and in the spring during MIZEX-87 (Guest *et al.*, 1988) as well as over pack ice during the fall/winter CEAREX drift (Guest and Davidson, 1991a). Therefore, low clouds appear to reduce the relative influences of surface layer mechanical production of turbulence on the Z_i values.

The latter conclusion seems to contradict some basic assumptions about the factors that control ABL depth in a stable atmosphere. The lack of a wind speed vs. Z_i correlation could have several explanations. (1) Z_i, as defined here, is not always a good measure of ABL height, h. For the modeling studies, the ABL height, h, is arbitrarily defined as the height at which TKE becomes 10% of the surface value. Clouds may create a sharp inversion which defines the Z_i value when mixing is actually limited to a lower level which cannot be identified from the rawinsonde data. (2) The boundary layer under clouds in the Arctic is usually unstable and therefore buoyant production of TKE may dominate over mechanical production at times. (3) Cloud top cooling and wind shear, both of which often

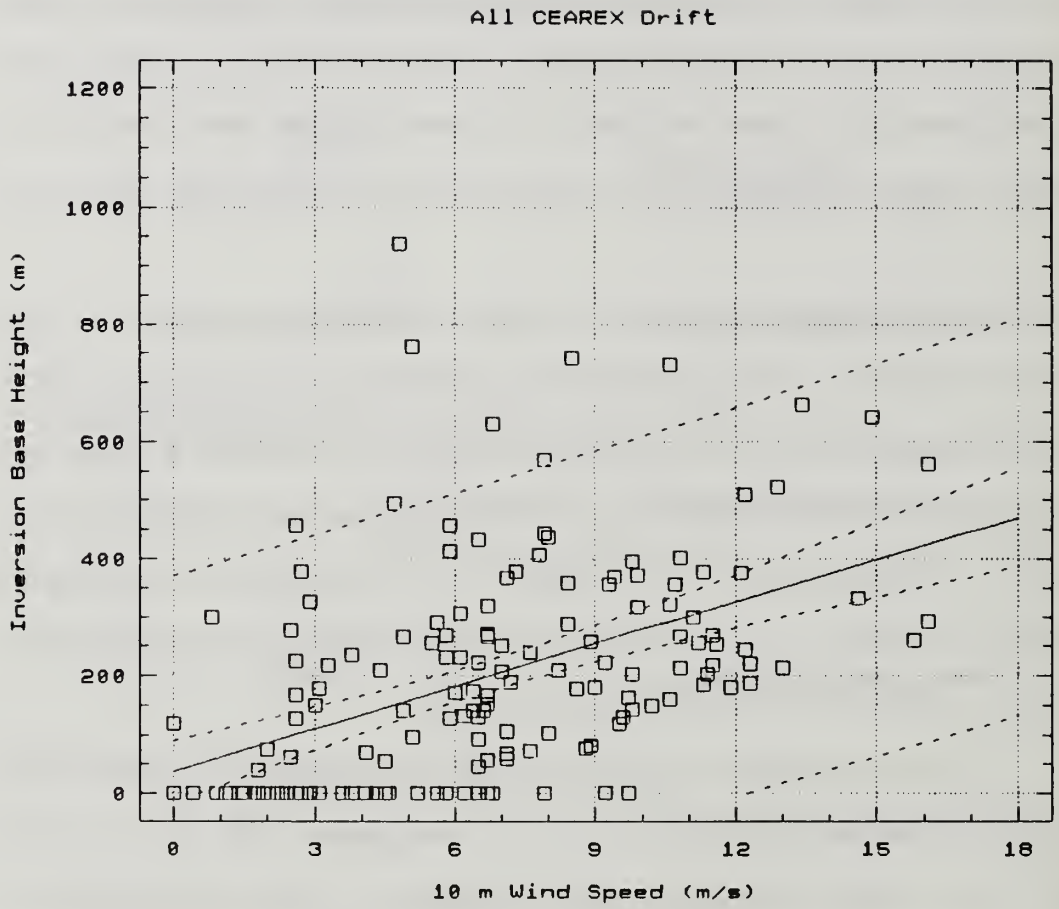

Figure 10 A plot of Inversion Height vs. Wind Speed during the CEAREX Drift. The solid line is the linear regression fit, the inner dashed lines are the 95% confidence intervals of the regression and the outer dashed lines are the 95% data range limits.

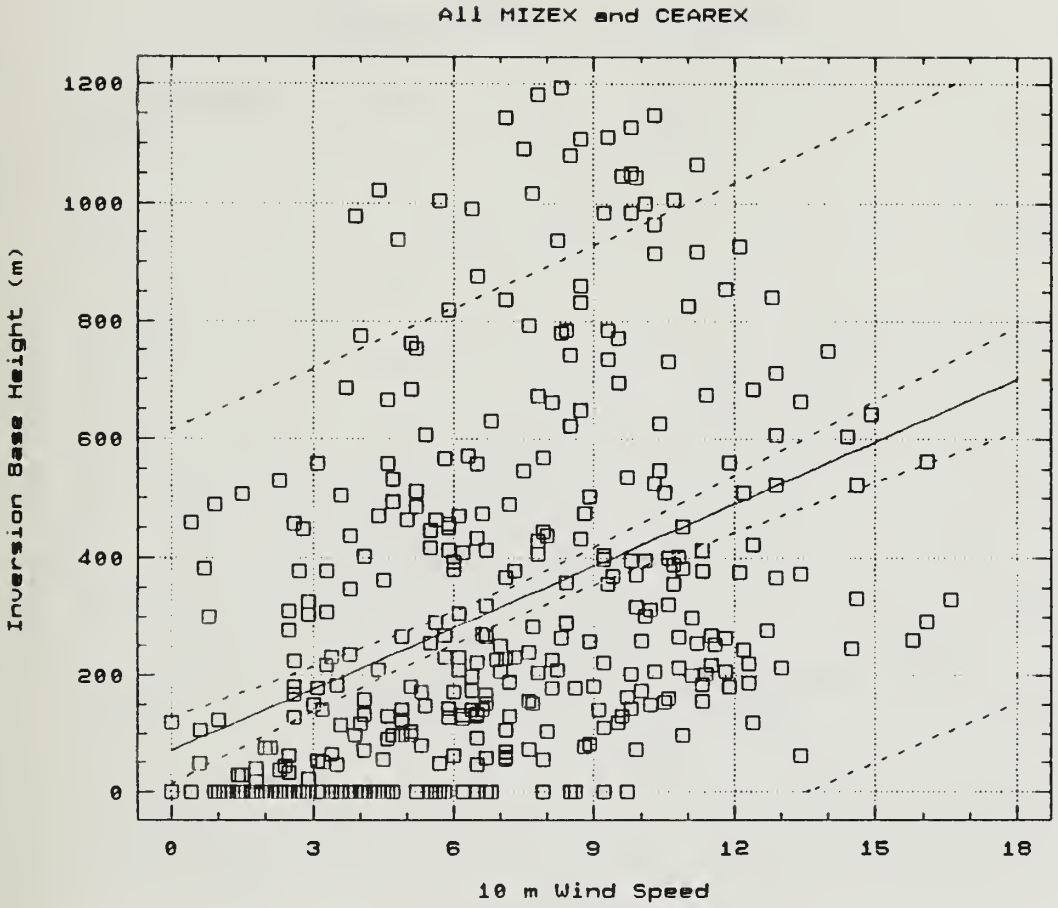

Figure 11 Same as Figure 10 but using All Data from MIZEX-84, MIZEX-87 and CEAREX.

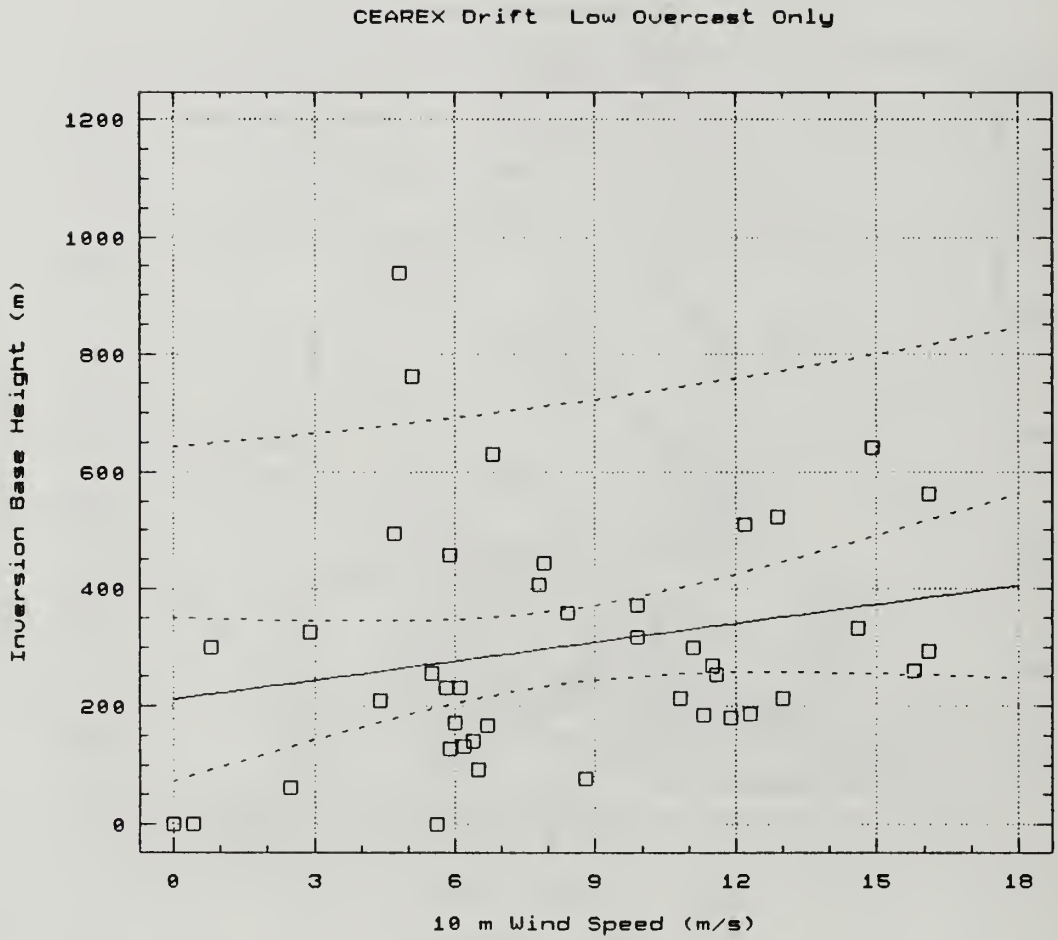

Figure 12 Same as Figure 10 but for Low Overcast Cases Only.

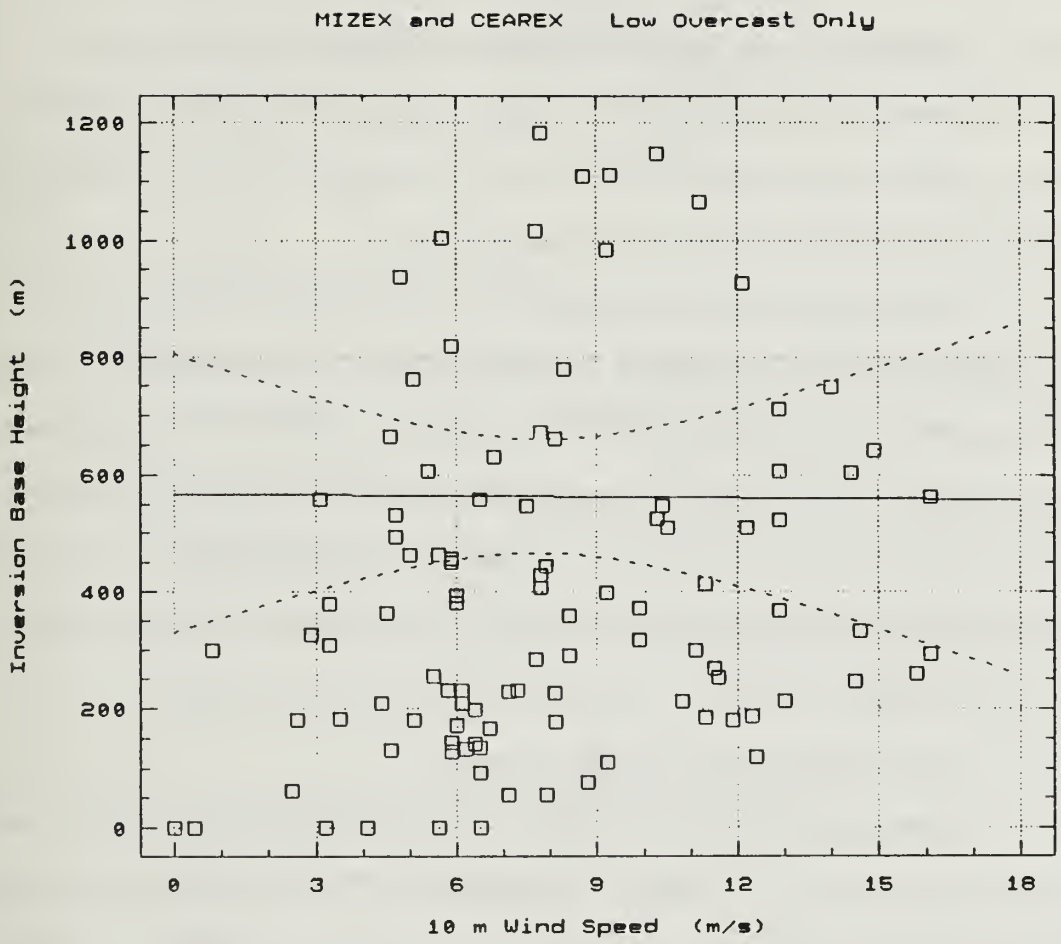

Figure 13 Same as Figure 11 but for Low Overcast Cases Only.

occur at the top of the ABL, may be more important than surface processes in controlling Z_i during overcast conditions. (4) Advection of moisture at certain levels may fix Z_i at that level regardless of surface conditions. (5) Cloud top entrainment instability, CTEI, (Lilly, 1968) is another process not directly related to surface wind stress. A necessary condition for CTEI is that the equivalent potential temperature of the air in ABL must be greater than the air just above ABL. This condition is rare in the Arctic; therefore CTEI cannot be common.

Although this sub-section concerned the effect of wind stress on an ABL structure parameter, Z_i, the focus of this study remains the more subtle reverse process: the effect of cloud-influenced ABL structure on wind stress. These results have illustrated how the surface wind stress influence on boundary layer structure is strongly dependent on cloud conditions. Scaling inversion height with u_* is not valid during low overcast conditions, which provides further evidence that clouds have a strong effect on ABL structure.

3. Types of Atmospheric Boundary Layers

Another way to describe ABL thermal structure is to classify each measured ABL according to a scheme summarized in Table 4, where the number assigned each type is arbitrary. For types 0, 3, and 5, the specification of Z_i is straightforward since these represent "classic" ABLs where a clearly defined inversion exists at the surface or above a surface-based well-mixed layer. For the other types the Z_i specification is more ambiguous because either no inversion exists or weakly stable layers exist below a more obvious inversion. In these cases, Z_i is still defined as the lowest inversion base, but probably is not a good measure of ABL depth, h.

TABLE 4
TYPES OF ATMOSPHERIC BOUNDARY LAYERS

Type	
-1	No inversion in lower 2500 m
0	Strong surface-based inversion (height of top of inversion ,Z_{top} > 200 m or potential temperature increase within the inversion, θ_{jump} > 3 C)
1	Weak sfc-based inversion below mixed layer (Z_{top} < 200 m and Z_{top} > 100 m and θ_{jump} < 3 C)
2	Elevated inversion above stable layer; stable layer not inverted.
3	Elevated inversion above mixed layer
4	Miscellaneous category (complicated structure)
5	Two inversions with mixed layer between
0.5	Combination of 0 and 5; A strong surface-based inversion below a well-mixed layer capped by an upper level inversion.

All rawinsonde profiles we have collected in the Arctic during MIZEX and CEAREX (over 1300) have been classified according to ABL type and amount of low clouds. The percentage of total of profiles for each type is listed in Table 5.

As indicated previously (Figure 9), surface-based inversions are rare during low overcast conditions and common during clear skies. All the low level inversions occurred over ice and during clear skies, with the exception of four cloudy cases when strong warm advection over cold ice in the MIZ caused a surface-based inversion to form. During the CEAREX drift, there were no surface-based inversions, Type 0, with overcast skies. This is a significant observation with respect to the wind stress because during these very stable, low inversion periods atmospheric stability determines how wind stress is related to geostrophic forcing (Overland, 1985; and later in this dissertation). During less stable, higher inversion periods, changes in surface roughness are more important than atmospheric stability in affecting wind stress. Clouds play an important role in destroying or preventing the formation of strong surface-based inversions.

Multiple upper-level inversions (Type 5) were twice as common for overcast vs. clear skies. Most of the Type 5 clear cases had high relative humidities at the bottom of the upper inversions, which may indicate evidence of previous clouds. Arctic clouds can form mixed layers capped by inversions which are de-coupled from the ABL.

When surface-based inversions existed below an upper-level inversion (Type 0.5, 12 cases), only one case had clouds associated with the upper inversion. Clouds prevent surface inversions from forming even if they are de-coupled from the surface.

TABLE 5

A CROSS TABULATION OF BOUNDARY LAYER TYPE BY LOW-LEVEL CLOUD CONDITIONS EXPRESSED AS PERCENTAGE OF ALL CEAREX DRIFT SOUNDINGS[1]

/

ABL Type[2]	Low Cloud Amount		
	Clear	Partial	Overcast
Surfaced-based inversion Type 0 or 0.5	13.3	4.4	0.7
Inversion above mixed layer Type 3 or Type 5	34.8	11.1	26.7
Two inversions Type 5 or 0.5	23.7	12.6	17.0
Unclear inversion location Type 1, 2 or 4	4.4	2.2	2.3

[1]Based on 135 rawinsonde profiles. Total of all categories is 153%. This is because 14% of the soundings were Type 0.5, which are both surface-based and two inversions and 39% of the soundings were Type 5 which is both mixed surface layer and two inversions.

[2]Type numbers are defined in Table 4.

D. CLOUDS AND SURFACE FLUXES

One way clouds can affect surface wind stress is by their influence on the surface layer stratification. This section is an examination of how observed sky conditions and sky condition changes are related to measured surface sensible heat fluxes. Turbulent heat flux at the surface determines surface layer stability which affects the value of the surface drag coefficient by the well-verified Monin-Obhukov similarity theory (Dyer, 1974). Also, surface heat fluxes can affect wind stress by influencing entrainment into the ABL. Entrainment brings momentum characteristic of upper-level air into the ABL, causing a short term effect on surface wind stress. Entrainment also changes the ABL depth, h, which can have a long term effect on wind stress. Results from numerical models of these processes are presented in Chapter V.

Thirty-one periods from the CEAREX drift were identified when the wind direction was favorable for surface heat flux measurements, meteorological conditions remained constant and several consecutive ten minute heat flux values were similar. Low cloud cover was correlated with surface sensible heat flux (Figure 14). The average heat flux was -5 Wm^{-2} and 1 Wm^{-2} during clear skies and low overcast skies respectively. A better correlation occurred between measured sensible heat flux and downward longwave radiation at the surface (Figure 15) or net surface radiation (Figure 16), although scatter remains. The zero-flux calm wind cases are not shown. All the measured heat fluxes from the CEAREX drift were small compared to typical radiative terms and MIZ or lead turbulent heat fluxes. However, the largest changes in the effect of stability on wind stress occurred in the

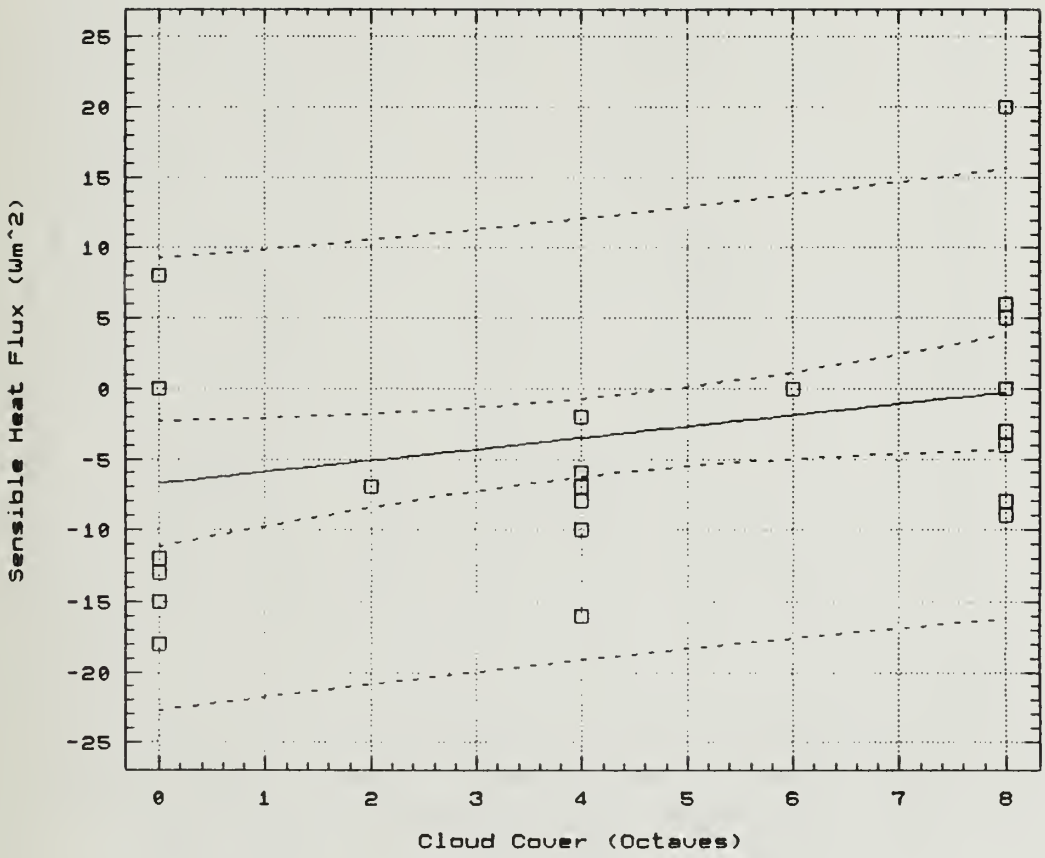

Figure 14 Surface Sensible Heat Flux (positive upward) as a Function of Cloud Cover Octaves from Selected CEAREX Drift Periods. Lines represents statistics described in Figure 9 caption.

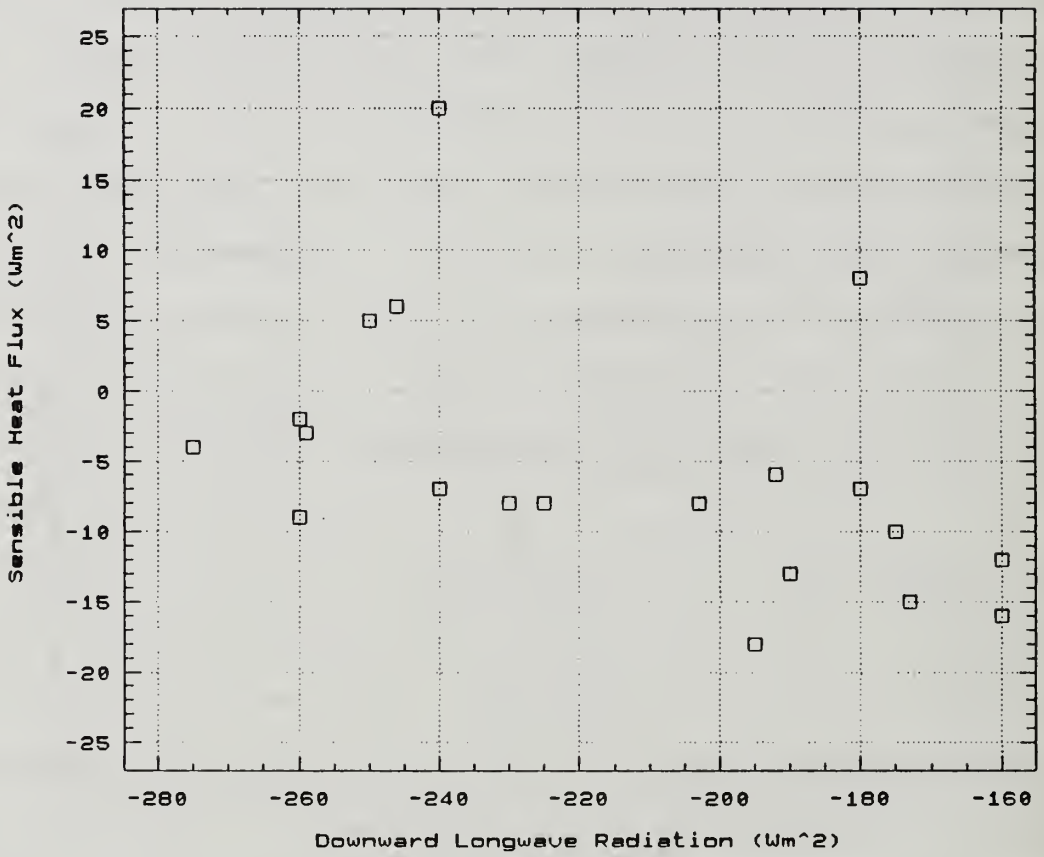

Figure 15 Surface Sensible Heat Flux as a Function of Downward Longwave Radiation (Wm^{-2}). Very low winds cases are not shown.

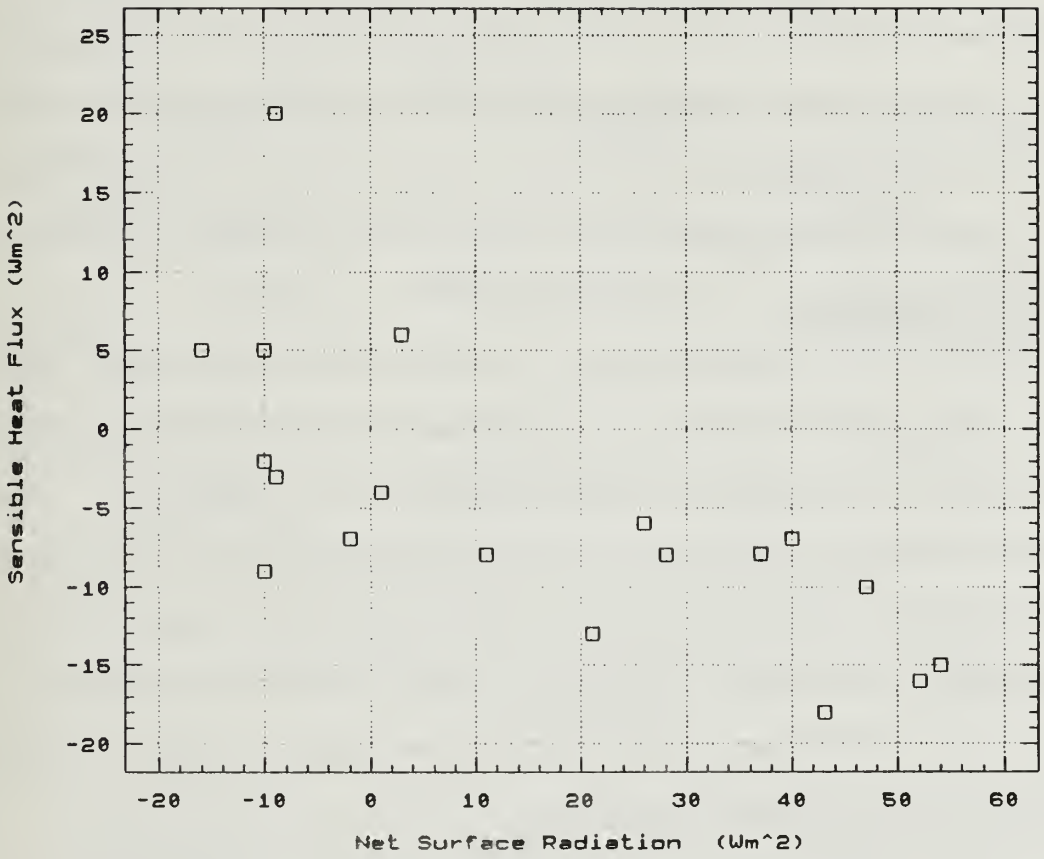

Figure 16 Surface Sensible Heat Flux as a Function of Net Longwave Radiation (Wm^{-2}).

near-neutral regime (e.g. Brown and Liu, 1982), so even small differences in heat flux and surface stability may significantly affect wind stress.

Most periods represented by these data had quite constant meteorological conditions, including cloud cover. Larger sensible heat fluxes were measured immediately after changes in cloud conditions. This is best illustrated in a case study (Figure 17) of a period from the CEAREX drift. Note the close correlation between cloud conditions and surface sensible heat flux for this case. Cloud clearing is closely linked to a change from unstable to stable surface conditions while the reverse occurs for cloud forming. Several other similar examples exist from the CEAREX drift period.

Sixteen sharp cloud change events (eight totally clear to low overcast changes within an hour, eight low overcast to clear changes) were identified during periods when surface flux measurements were available. The surface layer of the atmosphere changed from unstable to stable in all the clearing cases. The surface layer changed from stable to unstable in five of the "clouding" cases. The other three clouding cases showed no significant change in heat fluxes or stability. It is obvious that surface fluxes are closely related to changes in cloud conditions, particularly immediately after clearing events.

E. FACTORS INFLUENCING SURFACE HEAT FLUX

Instantaneous and integrated turbulent surface heat fluxes affect the ABL structure and, therefore, the ability of the atmosphere to transfer momentum to the surface. It has been shown that changes in cloud conditions are often associated with changes in the surface turbulent heat flux. But other factors can also induce heat flux changes. In order to evaluate the significance of the effect of clouds on

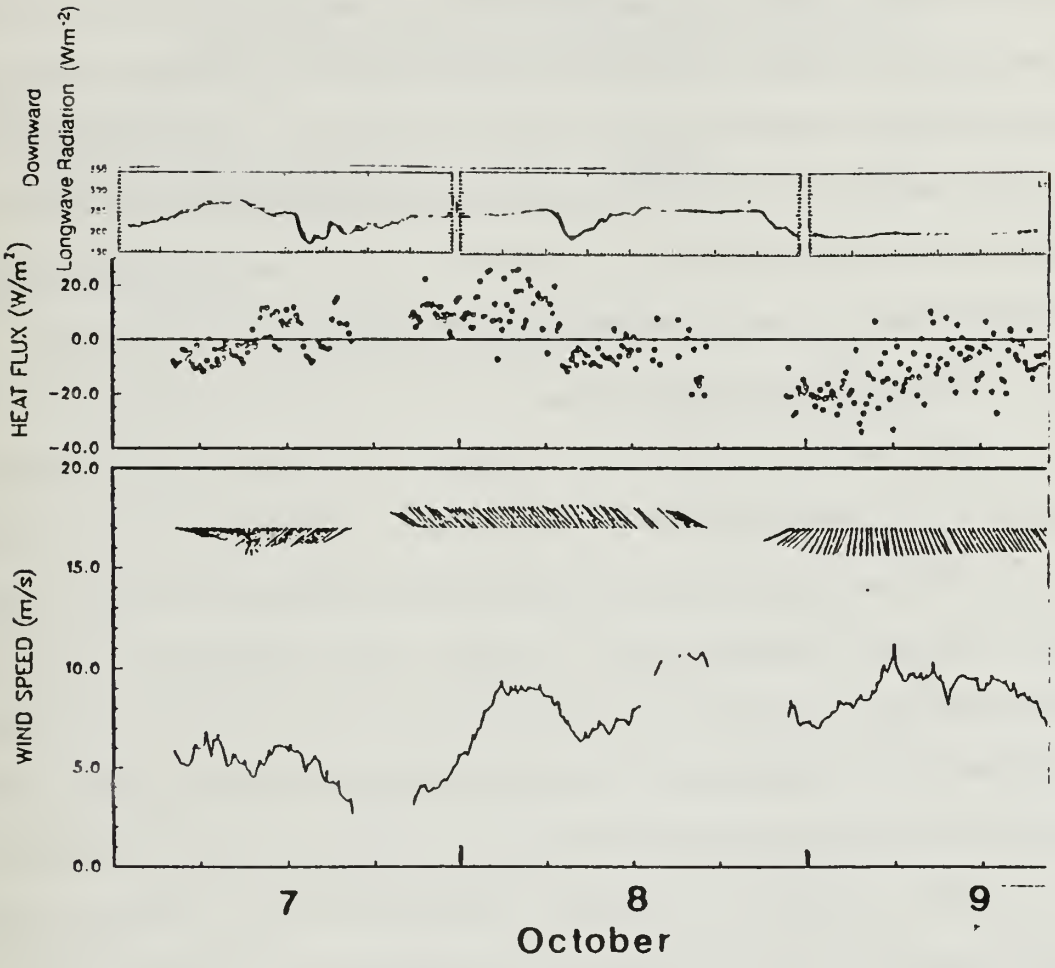

Figure 17 Time Series of Downward Longwave Radiation, Surface Sensible Heat Flux, Wind Direction (barbs) and Wind Speed from 7 October through 9 October during the CEAREX drift. Gaps represent missing data.

wind stress in the central Arctic winter, the effect of downward longwave radiation, i.e. cloud conditions, on surface heat fluxes must be compared with other processes that can generate a surface heat flux. This section describes a method for classifying a non-neutral ABL according to the mechanism driving the surface turbulent heat flux. The classification scheme will then be applied to the CEAREX drift data to evaluate the relative importance of changes in surface radiation conditions in generating surface heat fluxes relative to other mechanisms.

1. General Classification Scheme

With no outside forcing or advection, the turbulent surface heat flux drives the T_{air} - T_{sfc} difference toward zero over time. As shown in section A, these two parameters are closely linked unless no turbulence exists in the surface layer. Surface heat flux counteracts some "outside" forcing mechanism creating a difference between T_{air} and T_{sfc}. There are two types of outside forcing mechanisms: Type R (radiational) ones that act directly to change T_{sfc} and Type A (advective) ones that act directly to change T_{air}. In Type R ABLs, the surface is controlling the temperature in the ABL through surface fluxes; changes in T_{sfc} precede changes in T_{air}. In Type A ABLs, the temperature in the ABL is controlling T_{sfc} through surface fluxes; changes in T_{air} precede changes in T_{sfc}. These two mechanisms can be distinguished by comparing the signs of the surface heat flux and $\frac{\partial T_{air}}{\partial t}$. For Type R they are the same sign while for Type A they are opposite signs. This concept is summarized in Table 6.

TABLE 6
TYPES OF TURBULENT HEAT FLUX EVENTS

Type R - Radiational

Downward (upward) turbulent surface heat flux
Cooling (warming) ABL and surface

Type A - Advective

Downward (upward) turbulent surface heat flux
Warming (cooling) ABL and surface

Type R is identified as "radiational" because changes in T_{sfc} not caused by sensible heat fluxes are closely linked to changes in radiation conditions. The only other factor affecting T_{sfc} is conductive heat flux through the snow/ice. This can be considered a passive process because snow and ice conditions do not change much on the time scales of a few hours being considered here. Type R ABLs are common over land where diurnal variations in temperature are large, particularly in the summer when solar radiation is intense and the soil is dry. Because advection of soil or snow is insignificant, pure Type R ABLs are by definition caused by a one-dimensional process.

Changes in radiation conditions in the Arctic winter are strongly related to cloud conditions. These radiational changes are an order of magnitude less than diurnal solar radiation changes at lower latitudes, where Type R ABLs are common. However, it will be shown that the winter Arctic ABL often has Type R characteristics. This is because the temperatures of the dry snow surface and shallow ABL quickly adjust to radiation changes.

Type A ABLs are caused by any process, other than turbulent surface heat flux, that changes the temperature within the ABL. Note that this is termed "advective" in Table 6. This is because advection is assumed to be the dominant non-radiative process controlling the structure of the ABL. Type A ABLs occur over open water regions with SST gradients and anywhere following an atmospheric frontal passage.

2. Scale Analysis

To evaluate the factors which change ABL temperature, consider the following equation for the time rate of change of the vertically-integrated potential temperature of the ABL.

$$\boxed{1} \qquad \boxed{2}$$

$$\frac{\partial \overline{\theta}}{\partial t} \; - \; \overline{\mathbf{u} \cdot \nabla \theta} \; =$$

$$\boxed{3} \qquad \boxed{4}$$

$$\langle w'\theta' \rangle_{sfc} \; - \; \langle w'\theta' \rangle_{h}$$

$$\boxed{5} \qquad \boxed{6} \qquad \boxed{7} \qquad \boxed{8}$$

$$+ \; \frac{R_{upsfc}}{\rho \, c_p} \; - \; \frac{R_{downsfc}}{\rho \, c_p} \; + \; \frac{R_{uph}}{\rho \, c_p} \; - \; \frac{R_{downh}}{\rho \, c_p}$$

$$\boxed{9} \qquad \boxed{10}$$

$$+ \; \frac{\partial \overline{Q_L}}{\partial t} \frac{L_{evap}}{c_p} \; + \; \frac{\partial \overline{Q_I}}{\partial t} \frac{L_{sublim}}{c_p} \qquad (5)$$

The overbar represents a vertical integral through the ABL:

$$\overline{x} \; = \; \int_0^h x \, dz$$

$\boxed{1}$ = time derivative

$\boxed{2}$ = advection ($\mathbf{u}$ = vector wind in ABL)

$\boxed{3}$ = surface flux (< > represents time average)

$\boxed{4}$ = entrainment flux

$\boxed{5}$ = radiation up from surface

$\boxed{6}$ = radiation into surface

$\boxed{7}$ = radiation up from ABL

$\boxed{8}$ = radiation down into ABL

$\boxed{9}$ = latent heat of evaporation

$\boxed{10}$ = latent heat of sublimation

Measurements or estimates from the CEAREX drift, during periods when reliable data were available, were used to derive ranges of the values for each of the terms in Equation (5) and are given in Table 7. The time derivative (Term 1), advection (Term 2) and cloud top cooling (Terms 7 and 8) dominate the mean temperature equation. Surface fluxes (Term 3) and entrainment (Term 4) are an order of magnitude smaller and clear air radiation divergence (Terms 5, 6, 7 and 8) and latent heat (Terms 9 and 10) are almost another two orders of magnitude smaller. The smallness of the latent heat term justifies ignoring latent heat when considering the effect of clouds on ABL temperature. This is based on periods when ABL temperatures are below -20 C. As shown by Curry (1986), the latent heat term can be important in the summer when ABL temperatures are near 0 C.

3. Graphical Representation of ABL Temperature and Surface Heat Flux Events.

Only terms 1 and 3 in Equation (5) were directly measured; the others were estimated for typical Arctic conditions. A plot of the measured terms, Term 1 vs. Term 3, provides a visualization of factors affecting ABL temperature (diagrammed in Figure 18). The vertical axis represents surface turbulent heat flux while the horizontal axis represents time change in ABL temperature. This represents a heat flux-temperature change or F-C diagram. A steady-state equilibrium (no turbulent surface heat flux) situation is represented by the origin in Figure 18. The dashed lines in Figure 18 represent lines of constant Term 2 + Term 4 through 9. These lines will be termed "isoadvects" because advection is usually the dominant term, although factors other than advection may be important for individual cases.

TABLE 7
SCALE ANALYSIS OF ABL TEMPERATURE EQUATION
(units are Wm^{-2})

Term	Percentile 5	95	Median Magnitude
1.	-121	86	34
2.	-110	100	35
3.	-12	11	4
4.	0	10	3
5.+6.+7.+8. (Clear)	-1	1	<1
5.+6.+7.+8. (ABL Cloud)	-90	0	35
9.+10.	-3	3	1

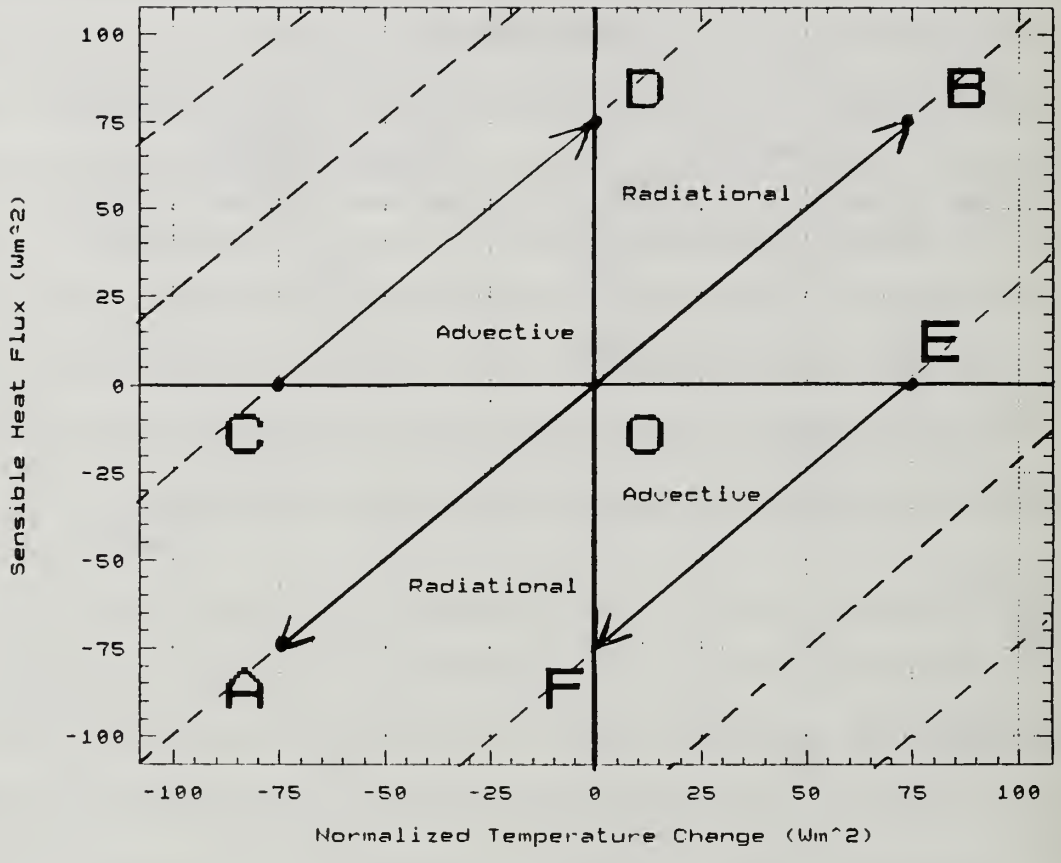

$$\frac{\partial \overline{\theta}}{\partial t} \rho C_p$$

Figure 18 F-C Diagram Showing Characteristics of Different Types of Sensible Heat Flux Events. The X-Axis represents the local time derivative of temperature times ABL depth and volumetric heat capacity (Wm^{-2}) and the Y-axis represents sensible heat flux (Wm^{-2}). Pure Type R events fall along line AB while pure Type A events fall along line segments CD or EF.

Pure Type R situations (i.e. Terms 1 = Term 3) would have points only along the zero isoadvect, which is represented by line AB in Figure 18. A cloud-clearing event occurring in a situation which was previously in equilibrium would cause the representative location in Figure 18 to move from the origin to Point A as the negative surface fluxes respond to the radiation change. Eventually, the cooling of the ABL will counteract the fluxes caused by the new radiation conditions and the representative location will move back to the origin. Similarly, a cloud-forming event will move the representative location toward Point B and then back to the origin. Note that for pure Type R situations, the cloud-clearing or cloud forming must occur above the ABL; clouds within the ABL can affect ABL temperature directly, a Type A process.

A pure Type A situation (surface temperature driven entirely by the turbulent heat flux) would begin at a point on the X-axis because at first the ABL temperature will not have changed and the fluxes will be zero. For example, at the onset of steady cold advection, the representative location would be on the X-axis at the value of the advection, such as Point C. Eventually the cooling ABL will generate positive fluxes and the isoadvect will be followed until Point D is reached. At this time, the ABL has cooled enough so that the positive heat flux is balanced by the advection and a steady-state is reached. Alternatively, a warm advection event would cause the representative location to move from Point E to Point F. Note that line AB is entirely within the upper right or lower left quadrants, where the signs of Term 1 and Term 3 are the same. Lines CD and EF are in the upper left and lower right quadrants where the signs of Term 1 and Term 3 are opposite. This is consistent with the earlier, more general definitions of Type R and Type A situations which were defined in Table 6. "Pure" Type R and "pure" Type A events

were shown in Figure 18. In nature, completely "pure" situations almost never occur and advection is not constant. The more general definitions for Type A or Type R categories will be used for this study. Therefore any situation with changing temperatures and surface heat fluxes must be either Type A or Type R.

F. EXAMPLES FROM CEAREX DRIFT

Term 1 vs. Term 3 from Equation (5) for the entire CEAREX drift period when surface flux measurements were available is plotted in Figure 19. The data are averaged over one hour intervals. The vertical scale in Figure 19 is exaggerated compared to Figure 18 so that the isoadvects are almost vertical. The majority of the points are clustered toward the center where fluxes and temperature changes are small. There is too much noise (randomness) in the data to detect any discernable patterns in the central data cluster.

The large heat flux events (high y-axis magnitude points in Figure 19) are examined more closely because these have the potential to strongly influence the effect of atmospheric stability on wind stress. Unlike the center of the scatterplot, the outer points in Figure 19 show some definite trends. The largest negative heat fluxes (below -15 Wm^{-2}) usually occur during periods of dropping temperatures. This is consistent with a cloud clearing event which cools the ABL by first cooling the surface. Type R events are more common than Type A events for explaining large negative heat fluxes. This study will concentrate on Type R events, since these are the situations when clouds have the strongest effects on wind stress.

A good example of a Type R event occurred from 1800 8 October to 1200 9 October (Figure 20). At the beginning of this period, the representative locations on the F-C diagram were near the origin, but then they moved down and to the left.

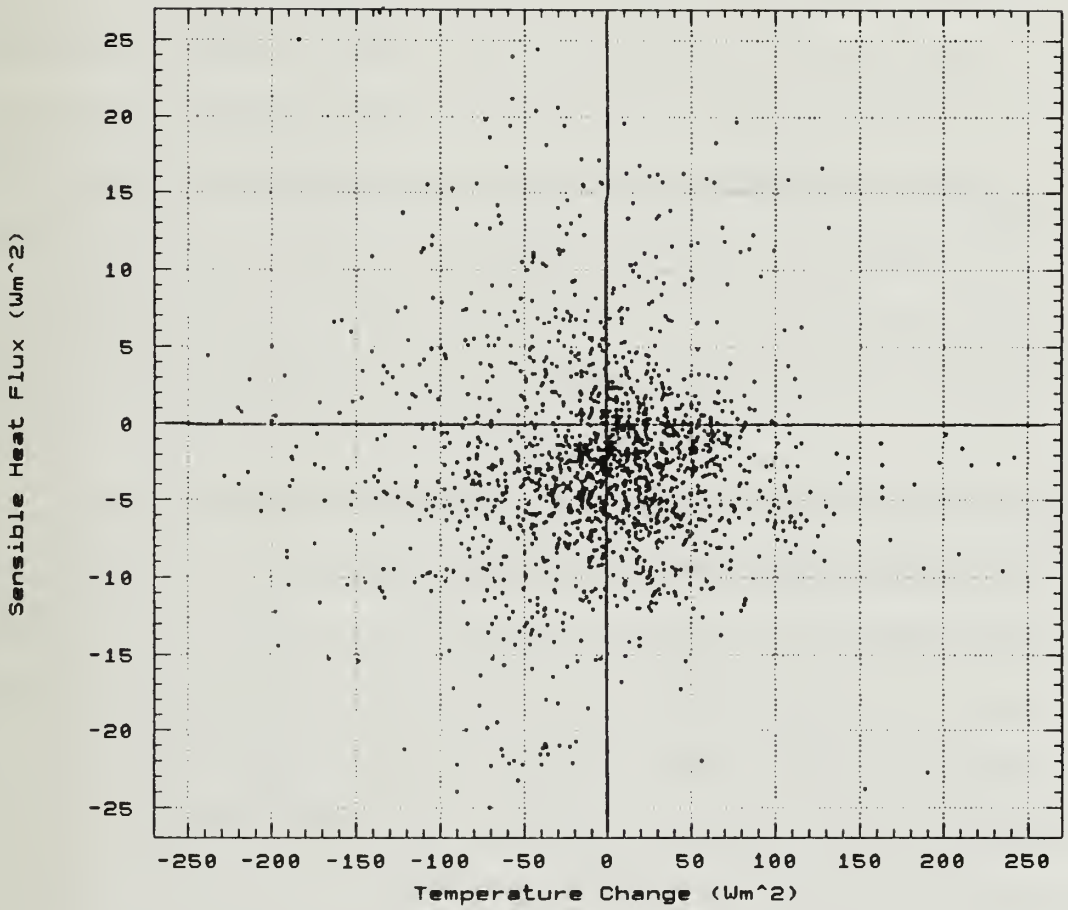

Figure 19 F-C Diagram of Entire CEAREX Drift. Heat flux scale exaggerated compared to Figure 16.

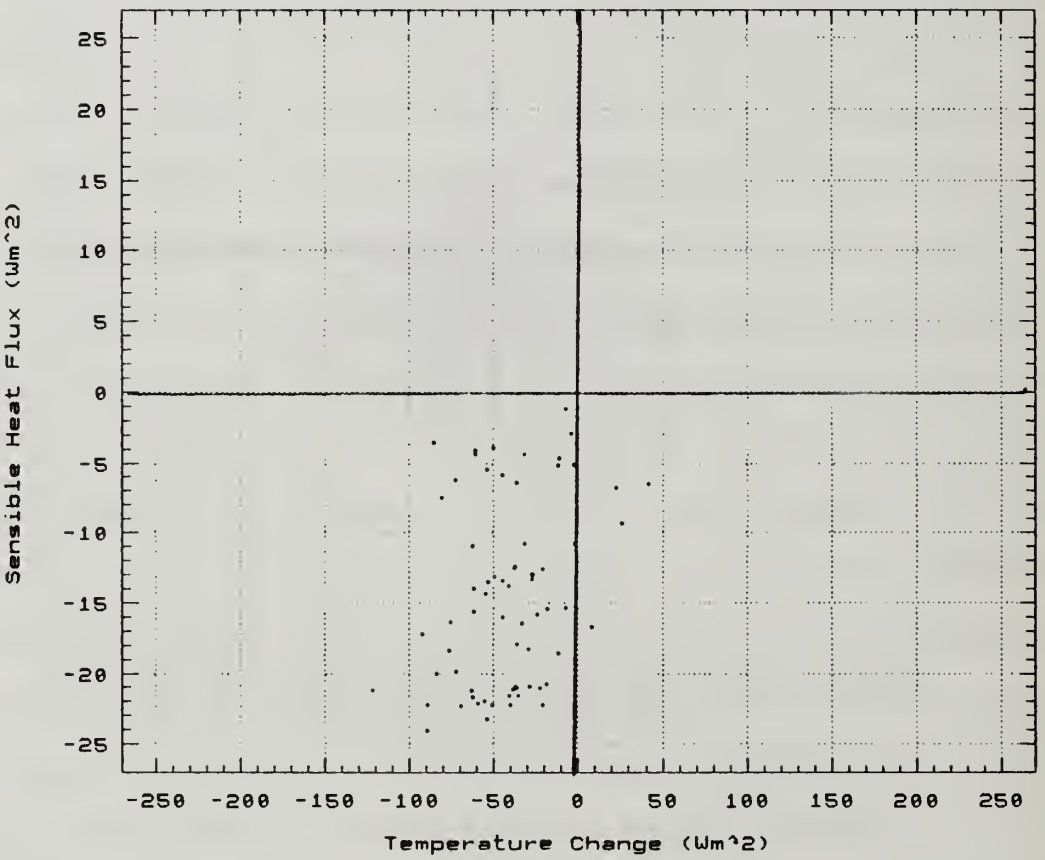

Figure 20 F-C Diagram of Clearing Event From CEAREX Drift 1800 8 Oct to 1200 9 October. The axes scaling is different compared to Figure 18.

Longwave radiation and sky observations (not shown) clearly indicate that the observed decrease in temperature and in negative sensible heat flux was associated with a change in cloud conditions. This is a Type R case since the points are near the zero isoadvect.

Most points in the lower left quadrant of Figure 19 are to the left of the zero advect. This means that the ABL cooling cannot be entirely explained by a one-dimensional, Type R, surface heat flux argument for most cases. The one-dimensional reasoning would require that cloud clearing occur everywhere at once. This does not happen; the cloud edge moves horizontally, usually in the same direction as the air parcels in the ABL. Therefore, the cooling that occurs after cloud clearing is more intense because the air parcels have been exposed to the clear conditions and cold surface for a longer period than the time after the cloud clearing event at any particular location on the surface.

Large upward (positive) sensible heat fluxes are equally divided between Type A and Type R events (top of Figure 19 to the left and right respectively). Cloud-forming events do not seem to dominate the positive upward heat flux cases to the extent that cloud clearing dominates negative heat flux events.

The largest temperature increases (to the right of 150 Wm^{-2} in Figure 19) are all associated with negative fluxes, a Type A situation. But large temperature increases (to the left of -150 Wm^{-2}) can occur with both upward and downward heat fluxes. Again, this indicates that cloud-clearing events are a relatively more important cause for surface heat fluxes than cloud-forming events. This means that the magnitude of the ABL warming associated with cloud formation is less than the magnitude of the ABL cooling associated with cloud clearing.

Two reasons explain the difference in surface heat flux response between cloud-forming and cloud-clearing situations. The first reason is that cloud-forming events often involve ABL clouds. The radiational warming is counteracted by cloud top cooling so that there are large positive fluxes at the surface but the ABL temperature does not warm. Cloud-clearing has no counteracting radiational warming in the ABL. The second reason is that the depth of the ABL is usually lower for cloud-clearing than cloud-forming events. Shallow ABLs respond more quickly to surface heat fluxes than do deep ABLs.

Several conclusions concerning the effect of clouds on ABL processes can be derived from the CEAREX drift data discussed in this sub-section. Type R ABL events occurred at about the same rate as type A events when all data are considered. Therefore, cloud condition changes appear to be as important as other factors in affecting surface heat fluxes when all cases are considered. Large negative heat fluxes are particularly well-correlated with cloud condition changes.

This section demonstrates that clouds are often important to surface heat fluxes. Therefore, much of the wind stress variation caused by surface heat fluxes over sea ice or ABL stability effects can be attributed to cloud condition changes.

G. CONCLUSIONS ON CLOUD EFFECTS ON ATMOSPHERIC THERMODYNAMIC STRUCTURE

This examination shows the strong association between cloud conditions and the thermodynamic structure of the lower atmosphere over sea ice in winter. Observed data show that clouds have a large effect on surface temperature which in turn is closely linked to the ABL properties by turbulent fluxes. Clouds prevent the formation of surface-based inversions and are associated with higher inversion bases and multiple-level inversions. The presence of low clouds leads to no correlation

between the inversion height and wind speed. During the CEAREX drift, clouds had as great an effect on surface layer stability as all other factors combined. Cloud clearing events were especially effective at generating relatively large negative surface heat fluxes and cooling the ABL.

IV. THE EFFECT OF CLOUDS ON SURFACE LAYER STABILITY, THE SNOW/ICE LAYER AND WIND STRESS

A. DEFINING SURFACE LAYER STABILITY EFFECTS

The quadratic geostrophic drag coefficient, C_G^2, parameterizes the effect of surface and ABL physics on wind stress. The physical processes which affect C_G^2 can be divided into two categories (1) surface layer effects and (2) outer ABL layer effects. The quadratic geostrophic drag coefficient can be expressed as

$$\begin{aligned} C_G^2 &= \left(\frac{u_*}{U_G}\right)^2 \\ &= \left(\frac{u_*}{U_{10}}\right)^2 \left(\frac{U_{10}}{U_G}\right)^2 \\ &= C_d \; C_{UG} \; . \end{aligned} \tag{6}$$

where U_{10} is the wind speed 10 meters above the surface, which is near the top of the surface layer. Surface layer effects on wind stress are parameterized by the surface drag coefficient, C_d, while outer ABL processes are parameterized by the quadratic reduction factor, C_{UG}.

Surface heat fluxes cause surface layer stability effects which change the value of C_d. The changes in C_d caused by clouds will be analyzed in this chapter. The next chapter will include the effects of clouds on the reduction factor.

B. PURPOSE OF SURFACE LAYER STABILITY STUDIES

Discussion in Chapter III addressed how changes in cloud conditions caused heat fluxes and stratification at the surface. Here, these heat fluxes will be

analytically and numerically modeled assuming pure Type R events, i.e. no advection, entrainment or diabatic ABL cooling other than surface fluxes. One purpose of this section is to determine analytical expressions for important time scales related to Type R heat flux events. Another purpose is to determine the most important parameters for predicting heat flux and wind stress on various time scales over sea ice.

OG modeled the effect of an instantaneous change in downward radiation on T_{air} and surface heat flux (Figure 21) to describe changes in conditions above the ABL from cloudy to clear and back to cloudy. They did not consider the wind stress implications of the radiational changes. Heat flux values from Figure 21 indicated that there were periods (the first two hours of day 2) when turbulence and wind stress would be almost completely suppressed and other periods (first hour of day 6) when it would be enhanced by 30%. These conclusions were based on surface layer Monin-Obukhov similarity theory (MO). Inclusion of ABL changes would magnify the surface layer stability effects. Although the OG case (Figure 21) had low wind speeds and therefore may not be significant to wind stress variations, it shows that for certain conditions, changes in cloud cover can have large relative effects on wind stress for short time periods.

C. CONDUCTION OF HEAT THROUGH SNOW/ICE (ANALYTICAL MODEL)

A skin depth, d_{skin}, is defined as the effective or e-folding distance that longwave radiation penetrates the snow/ice surface. If there is an instantaneous change in downward surface radiation, F_{rad}, from a previously equilibrium (no net

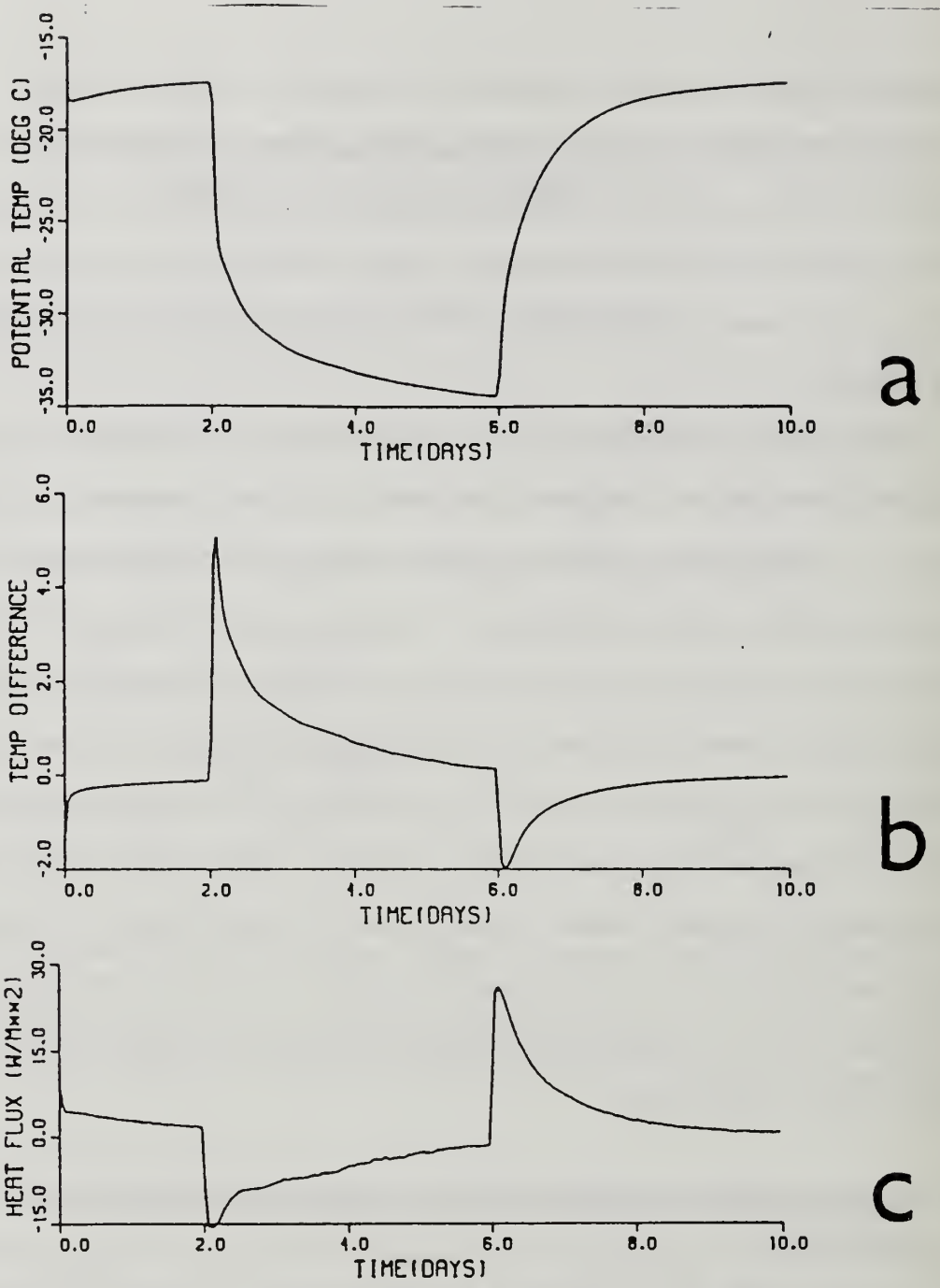

Figure 21 Model Simulation Time Series of (a) Surface Temperature, (b) Difference between Surface and 10 meter Air Temperature, (c) Surface Sensible Heat Flux. A change from cloudy to clear occurs at 2 days and becomes overcast again after 6 days. From Overland and Guest (1991).

flux) situation, then the surface temperature, T_{sfc}, cannot change temperature any faster than

$$\frac{\partial T_{sfc}}{\partial t} = \frac{F_{rad}}{d_{skin} C_{skin}}, \qquad (7)$$

where C_{skin} is the volumetric heat capacity of the snow or ice at the surface.

The heat conduction within the snow or ice cover is governed by the one-dimensional heat flux equation (Semtner, 1976)

$$C\frac{\partial T}{\partial t} = k\frac{\partial^2 T}{\partial z^2}, \qquad (8)$$

where k is the thermal conductivity of the snow or ice and C is the volumetric heat capacity. In the first few seconds following a change in radiation conditions, the surface temperature has not changed enough to generate sensible turbulent fluxes. Therefore, all the radiational imbalance not stored in the skin layer must be counteracted by a conductive flux, F_C, from the skin layer to the snow just below.

$$F_{rad} = F_C = k_{sfc}\left(\frac{\partial T}{\partial z}\right)_{sfc} \qquad (9)$$

If it is assumed that C and k are constant to infinite depth and d_{skin} is infinitesimal, the only parameters governing the value of T_{sfc} are F_{rad} ($Js^{-1}m^{-2}$), C ($Jm^{-3}K^{-1}$), k ($Jm^{-1}s^{-1}K^{-1}$) and the time since the change in radiation conditions, t (s). From dimensional analysis

$$T_{sfc}(t) = T_{sfc}(0) - \Pi F_{rad}\left(\frac{t}{Ck}\right)^{\frac{1}{2}} . \qquad (10)$$

The dimensionless constant (Π) was determined to be equal to 1.13 based on results from a numerical model similar to Semtner (1976), with 1000 computational levels in the snow layer and a time step of 0.01 seconds.

A time scale, t_{skin}, can be derived from Equations (7) and (10) which represents the time required to heat the skin layer enough so that all the radiational heat imbalance is conducted to the lower layers and $\frac{\partial T_{sfc}}{\partial t}$ no longer depends on storage of heat in the skin layer:

$$t_{skin} = \frac{(\Pi d_{skin})^2}{\nu_{skin}} , \qquad (11)$$

where $\nu_{snow} = \frac{k_s}{C}$ is the thermal diffusivity. At approximately $t < t_{skin}$ Equation (7) is applicable while at $t > t_{skin}$ Equation (10) applies. Note that t_{skin} is independent of F_{rad}. Using a value of 1 mm for d_{skin} and $\nu = 1.0 \times 10^{-7}$ which are characteristic values for feathery new snow (Stull, 1988), t_{skin} has the value of 12.8 seconds. For an ice surface, t_{skin} equals 1.4 seconds. Old snow has intermediate values. In nature, downward longwave radiation changes usually takes a few minutes; therefore the heat storage represented by Equation (7) is not significant for downward radiation. Equation (7) would be more applicable to downward solar shortwave radiation, which is not present in the winter. Shortwave radiation can change within a few seconds as the sun goes behind a cloud and penetrates several centimeters into the snow/ice.

Equation (10) is not valid after the time, t_{turb}, when T_{sfc} has changed enough so that the surface turbulent heat flux, F_{sens}, is significant, assumed to be when the sensible heat flux is 10% of the initial radiational imbalance

$$F_{sens} \geq \frac{F_{rad}}{10} \quad . \tag{12}$$

The turbulent heat flux can be approximated by

$$F_{sens} = \Delta T \, \rho \, c_p \, U_{10} \, C_H \quad , \tag{13}$$

where ρ is the density of air, c_p is the specific heat of air at constant pressure, ΔT is the difference in potential temperature between the surface, T_{sfc}, and a reference height near the top of the surface layer, T_{10}. U_{10} is the wind speed at the reference height, and C_H is the heat transfer coefficient. Assuming that Equation (10) is valid and T_{10} remains equal to T_{sfc} $(t = 0)$ when $t <= t_{turb}$, an approximate expression for t_{turb} can be derived using Equations (10), (12) and (13):

$$t_{turb} = \frac{Ck}{(10 \, \rho \, c_p \, U_{10} \, C_H \, \Pi)^2} \quad . \tag{14}$$

This time scale represents the time required for the turbulent heat fluxes to become significant after a change in radiation conditions. Some values for various snow/ice types are listed in Table 8. The low values of t_{turb} explain the previously described measurements of the close coupling between the turbulent heat fluxes and radiation.

TABLE 8

VALUES OF T_{turb} (seconds) FOR $U_{10} = 5\ ms^{-1}$, $C_H = 1.0 \times 10^{-3}$

New feathery snow (Stull, 1988)	0.7
Old packed snow (Stull, 1988)	44.8
Ice (Stull, 1988)	614.0
Snow (Semtner, 1976)	33.9
Ice (Semtner, 1976)	604.0
CEAREX drift top 3 cm (estimated)	20.0

E. CONDUCTION OF HEAT THROUGH SNOW/ICE (NUMERICAL MODEL)

1. Model Description

The analytical models described above are useful for determining simple formulae for time scales associated with radiation changes and surface temperature and can be accurate for predicting T_{sfc} for the first few seconds or minutes. However, a numerical multi-level model is better suited for predicting T_{sfc} when the radiational change is "felt" at lower levels in the ice/snow, where k and C may not be constant.

The numerical snow/ice thermodynamic model used was based on Semtner (1976). This model numerically solves Equation (8) for each level. The surface temperature, T_{sfc}, is determined by assuming a balance of net radiation, turbulent sensible and latent heat fluxes, and heat conduction through the ice at the surface. The value of T_{sfc} for the next time step is based on analytical expressions for the partial derivatives of each of the fluxes with respect to a change in T_{sfc}. Semtner (1976) prescribed the turbulent fluxes since he was studying long term processes associated with ice growth and climate. For this study, time dependent expressions for the effect of turbulent fluxes on T_{sfc} have been added.

2. Model Time Scales

The purpose of this sub-section is to provide a guide for choosing enough vertical layers so that turbulent fluxes can be accurately modeled. Appropriate time scales associated with various snow/ice model parameters are described. These time scales can be used to determine how many layers are needed in the snow/ice

model to accurately predict turbulent surface fluxes. A forward differencing scheme with time step Δt, and model layer depth d, should be numerically stable if

$$\Delta t < \frac{d^2}{\nu} . \qquad (15)$$

Model predicted T_{sfc} changes instantly in response to changes in surface heat balance. The analytical formulae for ΔT_{sfc} (Equations (7) and (10)) show that actual changes in $T`_{sfc}$ cannot be instantaneous. This is because the top of the snow conducts and stores some heat. This change is not resolved by the numerical model. Therefore, the T_{sfc} change after a radiation change requires an amount of time, t_{start}, which may be different than the model time step, Δt. For Semtner's (1976) model with prescribed turbulent fluxes, this time scale can be approximated by

$$t_{start10} = \frac{d^2}{\Pi^2 4\,\nu} \qquad (16)$$

if $t_{start10} < t_{turb}$.

The time scale, $t_{start11}$, would represent the time required for the snow/ice to absorb the amount of heat which the model artificially created in one time step.

$$t_{start11} = \frac{d^2}{8\,\nu} \qquad (17)$$

The version of the snow/ice model used for this study included the effects of atmospheric sensible and latent heat fluxes in the prediction of T_{sfc}. In this case

$$t_{start12} = \frac{\left(\frac{k}{\Pi \frac{dF_a}{dT_{sfc}} + \frac{2k}{d}} \right)^2}{\nu}, \qquad (18)$$

where $\frac{dF_a}{dT_{sfc}}$ is the predicted change in total atmospheric heat flux due to a change in surface temperature. This equation reverts to Equation (16) when $\frac{dF_a}{dT_{sfc}}$ is set to zero. Equation (18) is only valid when $t_{start} < t_{turb}$.

A more accurate estimate of t_{start}, which can be applied to cases when $t_{start} > t_{turb}$, is

$$t_{start13} = t_{start12} \left(\frac{F_{rad}}{\overline{F_A}} \right)^2, \qquad (19)$$

where $\overline{F_A}$ is a weighted average total atmospheric heat flux (radiation and turbulence terms), which was determined based on the best fit to the "true" t_{start} defined below. $t_{start13}$ is always greater than $t_{start12}$ because turbulent fluxes into the atmosphere buffer the change in surface temperature.

A summary of the values of the surface temperature jump in the initial time step, $\Delta T_{sfcinit}$, $t_{start12}$, $t_{start13}$ and a "true" t_{start} for various snow/ice conditions is presented in Table 9. The value of the "true" t_{start} is derived from the amount of time required to have T_{sfc} change by $\Delta T_{sfcinit}$ based on a 1000 snow layer model with a slab atmosphere. The snow, ice and ABL parameters used for the "standard case"

TABLE 9

TEMPERATURE JUMP, $\Delta T_{sfcinit}$, AND VARIOUS PREDICTIONS OF THE TIME ELAPSED IN THE FIRST STEP* OF A NUMERICAL SNOW/ICE MODEL

	Number of snow layers in model				
	1	2	10	30	1000
Standard Case (old snow) t_{turb} = 44.8 secs					
$\Delta T_{sfcinit}$ (C)	4.80	4.07	1.835	0.773	0.027
$t_{start12}$ (secs)	563	405	82.4	14.6	0.017
$t_{start13}$	5014	2133	148.7	18.4	0.017
t_{start}	3197	1838	148.0	18.3	0.017
New feathery snow t_{turb} = 0.7 secs					
$\Delta T_{sfcinit}$	5.76	5.68	5.09	4.05	0.37
$t_{start12}$	16.7	16.3	13.1	8.2	0.078
$t_{start13}$	407	354	151	43.0	0.078
t_{start}	861	643	280	55.0	0.070
Snow replaced by ice t_{turb} = 614 secs					
$\Delta T_{sfcinit}$	2.36	1.475	0.370	0.129	0.004
$t_{start12}$	2510	985	61.8	7.5	0.007
$t_{start13}$	5553	1559	68.7	8.1	0.007
t_{start}	4875	1491	68.5	7.6	0.007

*after an instantaneous change in radiation conditions

are described in the next subsection. The standard case represents typical central Arctic winter conditions with old packed snow. For comparison, a case with C_s and k_s characteristic of new feathery snow (Stull, 1988) and a case with C_s and k_s equal to ice values are also shown in Table 9. The snow is assumed to be 0.2 m deep; divide this into the number of snow layers in the model to get the model layer thickness, d.

This table shows that Equation (18) is accurate when $t_{start} < t_{turb}$ and Equation (19) is reasonably accurate for all cases except the one and two snow-layer models. The one snow-layer model shown in Table 9 has the same parameters as the OG case. Note that the temperature change predicted in the first time step takes 3197 seconds or 53 minutes, which is much larger than the numerical model time step. In order to fully resolve the period when surface turbulent fluxes are important, the normal model time step, Δt, should be smaller than t_{turb}. During these first 50 minutes the turbulent fluxes have already reached their maximum values.

The results of this sub-section showed that, for snow conditions typical of the CEAREX drift, the Semtner model with one snow layer, as in OG, did not have enough vertical resolution to predict accurately surface temperature and surface fluxes during the first few minutes after a change in radiation conditions. The first time step of the 30 layer model required only 18 seconds; this is small enough to provide accurate representation of turbulent fluxes and changes in C_d during the time period immediately after a radiation change. The 30 layer version with Equation (19) used to predict t_{start} was used to derive the results presented below.

3. Snow/Ice Model Predictions of Surface Layer Stability Effects on Wind Stress

An analysis is performed in this subsection on how surface layer stability affects wind stress. The snow/ice model simulates the time variation and magnitude of wind stress following a cloud condition change. The turbulent heat and momentum fluxes into the atmosphere are based on transfer coefficients which have been corrected for stability using MO scaling. The expressions for the fluxes are implicit so that an iterative numerical procedure is required. The ABL above 10 meters is assumed to mix heat instantly to a prescribed ABL depth, h. The wind speed at 10 meters is fixed. These last two assumptions are unrealistic but the purpose is to analyze only surface layer effects; later an ABL model will be used to examine how the outer layer (the ABL above the surface layer) affects h, U_{10} and wind stress.

a. Standard (Reference) Case

A standard case is defined based on conditions which are typical of the CEAREX drift period. The values of various parameters which were used for the standard case are shown in Table 10. The initial snow and ice temperatures were determined by running the snow/ice model for 60 days from an initial profile of 0 C. This simulates the change from summer to early winter conditions.

For the initialization run, the turbulent fluxes were zero. The downward longwave radiation was prescribed to be -221.3 Wm^{-2}, corresponding to the "previous sky temperature" value of -23.19 C given in Table 10. This value was chosen because the surface temperature becomes exactly -20.0 C after 60 days. At this surface temperature, the upward radiation is 232.9 Wm^{-2}. The net radiation loss at the surface is counteracted by a conductive heat flux through the snow of 11.6 Wm^{-2}. This compares well with the value of 12.9 Wm^{-2} that was estimated by

TABLE 10
STANDARD CASE VALUES

Parameter	Symbol	Value	Units
		Constants (varied for non-standard cases)	
Wind speed	U_{10}	6	ms^{-1}
ABL depth	h	50	m
Initial net radiat.	F_{rad}	-80	Wm^{-2}
Snow depth	d_{snow}	0.2	m
Snow conductivity	k_s	0.310	$Jm^{-1}s^{-1}K^{-1}$
Snow heat capacity	C_s	6.9×10^5	$Jm^{-3}K^{-1}$
Ice depth	d_{ice}	2.0	m
Ice conductivity	k_i	2.03	$m^{-1}s^{-1}K^{-1}$
Ice heat capacity	C_i	1.88×10^6	$Jm^{-3}K^{-1}$
Snow density	ρ_{snow}	330	$Kg\ m^{-3}$
		Initial value of time-dependent parameters	
Snow surface temp.	T_{sfc}	-20	C
ABL and 10 m temp.	$\theta_{10}, \theta_{ABL}$	-20	C
Snow/ice temps	T(z)	(see text)	
Previous sky temp	T_{sky1}	-23.19	C
		Other constants	
Neutral drag coeff.	C_{dn10}	2.3×10^{-3}	dimensionless
Neutral heat coeff.	C_{hn10}	1.5×10^{-3}	dimensionless
Air density	ρ_{air}	1.4	$kg\ m^{-3}$
Air heat capacity	C_p	1005	$J\ kg^{-1}K^{-1}$
Ocean temp.	T_{sea}	-1.7	C
Surface emissivity	ϵ	1.00	
MO constants	(Guest and Davidson, 1987; Large and Pond, 1981, 1982)		

Maykut (1982) for Arctic pack ice greater than 0.8 thickness in October. After 60 days of constant conditions, the upper part of the ice floe is essentially in equilibrium so that the conductive fluxes are nearly constant with depth, z, and T_{sfc} is nearly constant with time.

After the initialization period, the downward radiation is instantly changed by an amount represented by F_{rad}, which is -80 Wm^{-2} for the standard case. The standard case represents an instant change from cloudy to clear conditions. The cloud layer is above the ABL so that it does not cool the ABL; the only cloud effect is on downward radiation reaching the surface. The change in radiation of -80 Wm^{-2} and the snow and ice parameters are the same as used by OG. The transfer coefficients represent values for central Arctic pack ice in undisturbed areas during early winter based on measurements (OG, Guest and Davidson, 1991a, and unpublished data).

The surface temperature, T_{sfc}, ABL temperature, θ_{ABL} and turbulent sensible heat flux, F_{sens}, for the 24-hour period following a change in downward radiation for the standard case is shown in Figures 22 and 23. Immediately following the radiation change, T_{sfc} decreases rapidly as the surface experiences a net radiation loss (Figure 23). After 48 seconds ($t = t_{turb}$) T_{sfc} has dropped enough so that the turbulent sensible heat flux is able to start decreasing the ABL temperature. After about 0.9 hours θ_{10} decreases at the same rate as T_{sfc} and the turbulent heat flux, F_{sens}, is at a minimum (maximum magnitude). This time will be represented as t_{max}. After t_{max}, T_{sfc} decreases slower than θ_{ABL} so that the difference between them becomes less and the magnitude of F_{sens} decreases, but remains above 10 Wm^{-2} for 10 hours.

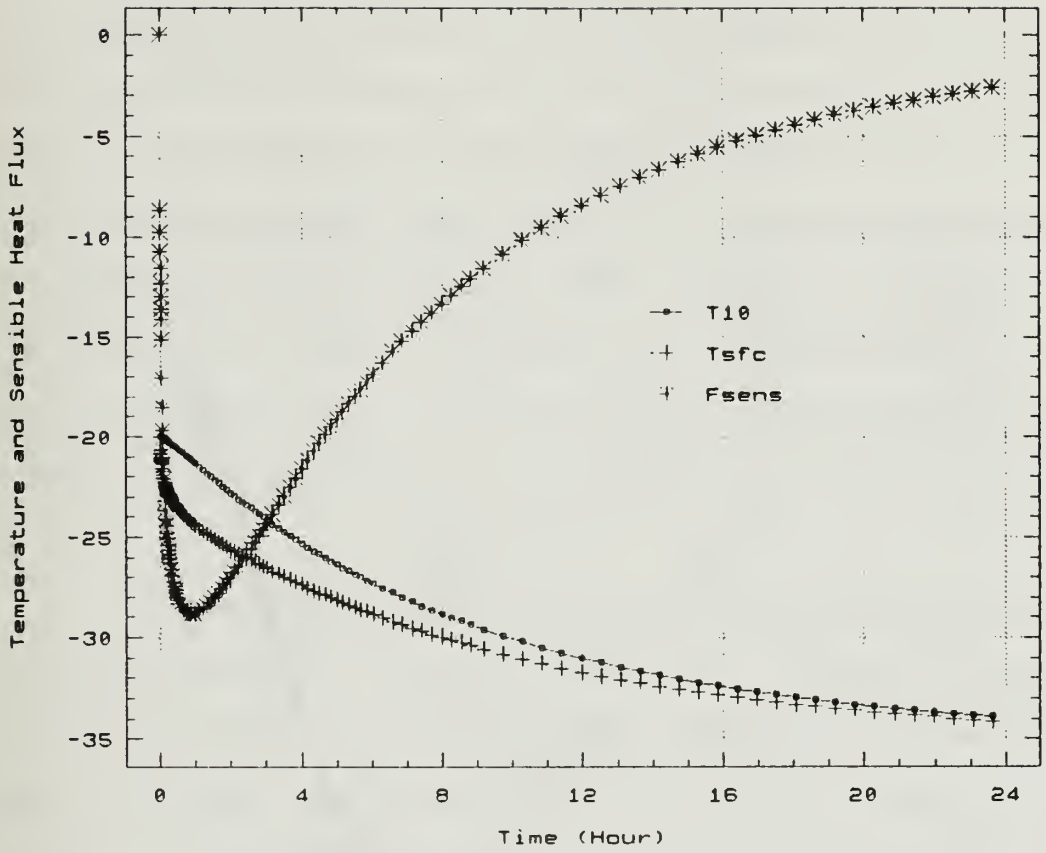

Figure 22 Slab Model Standard Case Simulation Time Series of 10 Meter Air Temperature C (small squares), Surface Temperature C (plusses) and Surface Sensible Heat Flux Wm^{-2} (asterisks). The time scale on this and the following figures in this chapter represents the time after an instantaneous change in downward radiation.

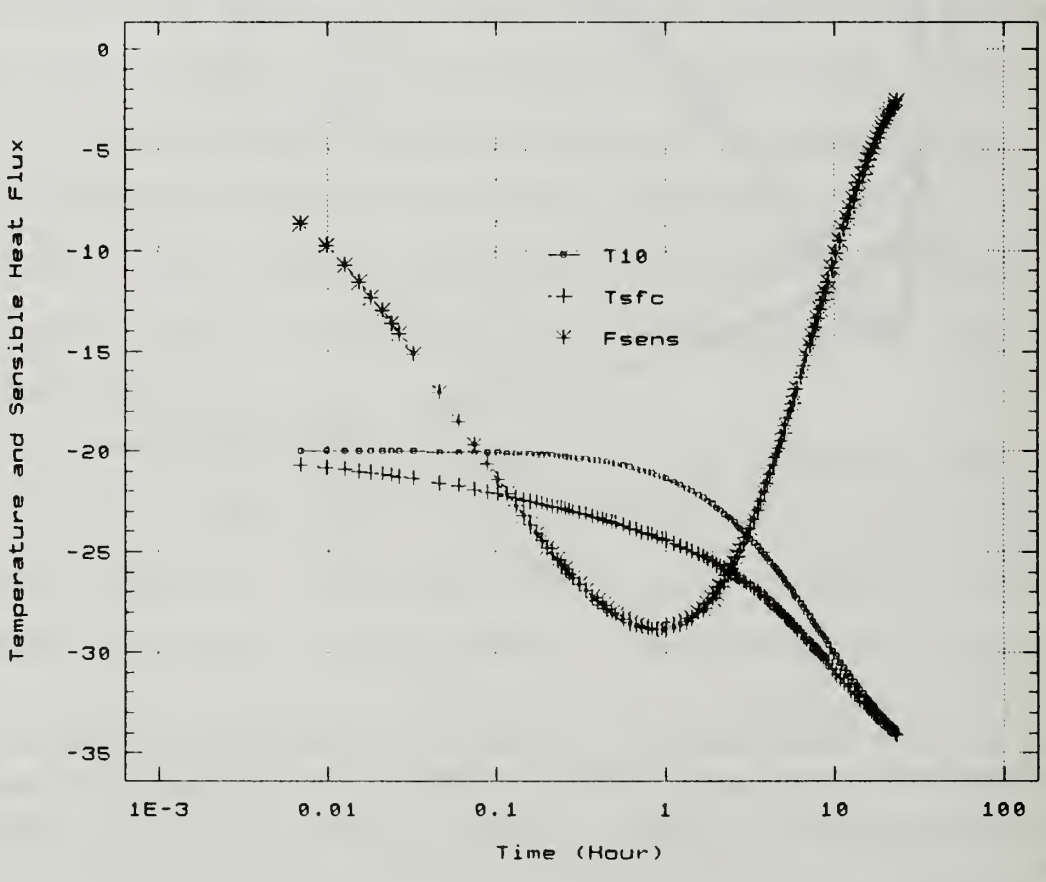

Figure 23 Same as Figure 21a but Logarithmic Time Scale.

At all times the radiation deficit at the surface, R_{netsfc}, must equal the conductive heat flux through the snow, F_{snow}, minus the air-snow turbulent flux, F_{sens}. During the first few seconds after the radiation change the radiation deficit is counteracted mostly by a conductive heat flux through the snow, F_{snow} (Figure 24). At time t_{max}, about 55% of the radiation deficit is counteracted by F_{snow} while the rest goes into the atmosphere (Figures 24 and 25). The sensible turbulent heat flux remains below -10 Wm^{-2} for ten hours. After a day, F_{sens} has become small and R_{netsfc} is again almost totally counteracted by F_{snow}. The magnitudes of both F_{sens} and R_{netsfc} will continue to decrease for several days as the surface cools off, but will eventually approach an equilibrium as T_{sfc} becomes just few degrees warmer than T_{sky}.

The results from the standard case, single-layer ABL, multi-layer snow/ice model show that surface layer fluxes cause a maximum 30% change in wind stress due to surface layer stability changes. Unlike what is implied by models without multiple snow layers such as used by OG, the effect on wind stress is not instantaneous; some time is required to change the surface temperature before stability is affected.

Because the atmospheric model is simplistic, the actual magnitude of the wind stress change in nature might be different. However, the purpose of this section is to examine the relative importance of various parameters in affecting surface layer stability. Inclusion of complicated ABL physics would mask the surface layer stability effects which are the focus of this chapter. The important results here are in the comparison of the effect of various parameters, not in the quantitative effects on wind stress during an actual radiation change event.

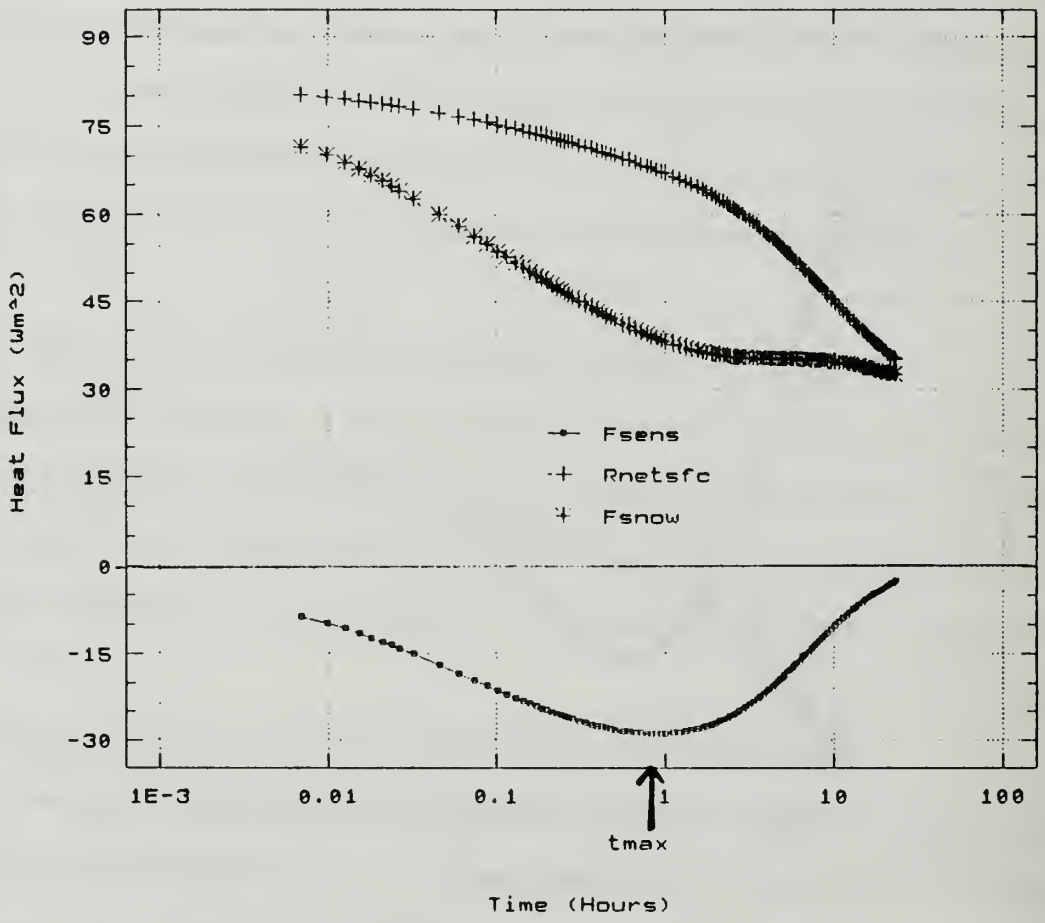

Figure 24 Slab Model Standard Case Simulation Time Series of Net Longwave Radiation (plusses), Conductive Heat Flux at top of Snow (asterisks) and Surface Sensible Heat Flux (small squares). The time scale is logarithmic.

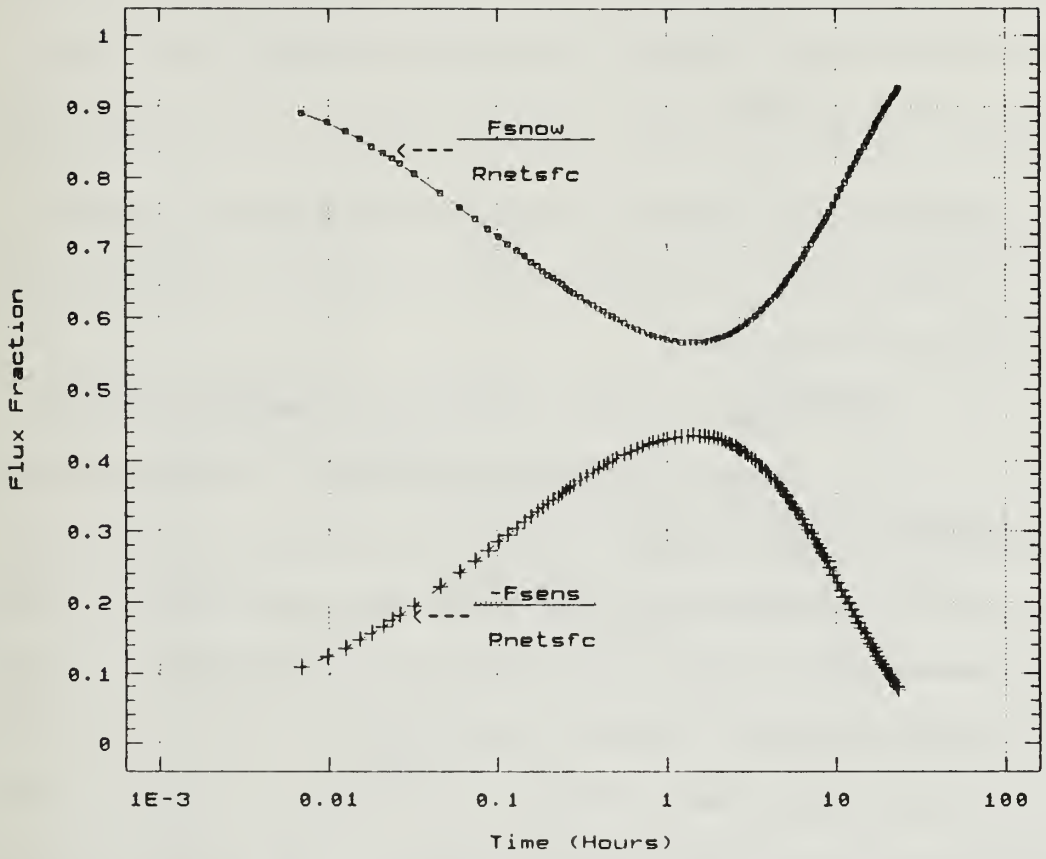

Figure 25 Slab Model Standard Case Simulation Time Series of Conductive Heat Flux at Top of Snow Divided by Net Longwave Radiation (small squares) and Negative Surface Sensible Heat Flux divided by Net Longwave Radiation (large squares). This figure shows how the energy deficit created by the longwave cooling at the surface is partitioned between turbulent fluxes with the atmosphere and conductive fluxes through the snow.

In the following subsections, the results from the standard case will be compared with cases with different initial radiation imbalances, wind speeds, ABL depths, snow type and snow depth. The following figures indicate the stability wind stress effect with the ratio of the 10-meter drag coefficient to the neutral 10-meter drag coefficient, $\frac{C_{d10}}{C_{dn10}}$ or C_{d10}^{*}. Because the ten meter wind speed is fixed, this ratio is equivalent to the change in wind stress from the initial neutral value. In each of the following cases one parameter is varied, while all the other parameters are set to the standard case values.

b. Initial Radiation Imbalance, Wind Speed and ABL Depth Effects

The standard case represented a change from totally clear to overcast conditions above the ABL. Changes in the reverse direction, clear to cloudy, are just as common as the standard case. Also, partial changes in cloud cover are often observed in the Arctic. These cases are modeled by setting the value of the initial radiation imbalance, F_{rad}, to 80 Wm^{-1} (clouding), 40 Wm^{-1} (partial clouding), -40 Wm^{-1} (partial clearing) or -80 Wm^{-1} (clearing, standard case). The surface layer effects of these radiation changes on wind stress are shown in Figures 26 and 27. Note that for the same magnitude F_{rad}, clearing produces a greater effect than clouding. This is because MO theory predicts that the heat flux into the ABL will be suppressed by the stable conditions following clearing and enhanced by the unstable conditions following clouding. Therefore, θ_{10} is slower to follow T_{sfc} and the time of maximum stability effect, t_{max}, is greater for clearing cases compared to clouding cases. The slower response of θ_{10} during clearing causes larger surface layer temperature gradients and greater stability effects.

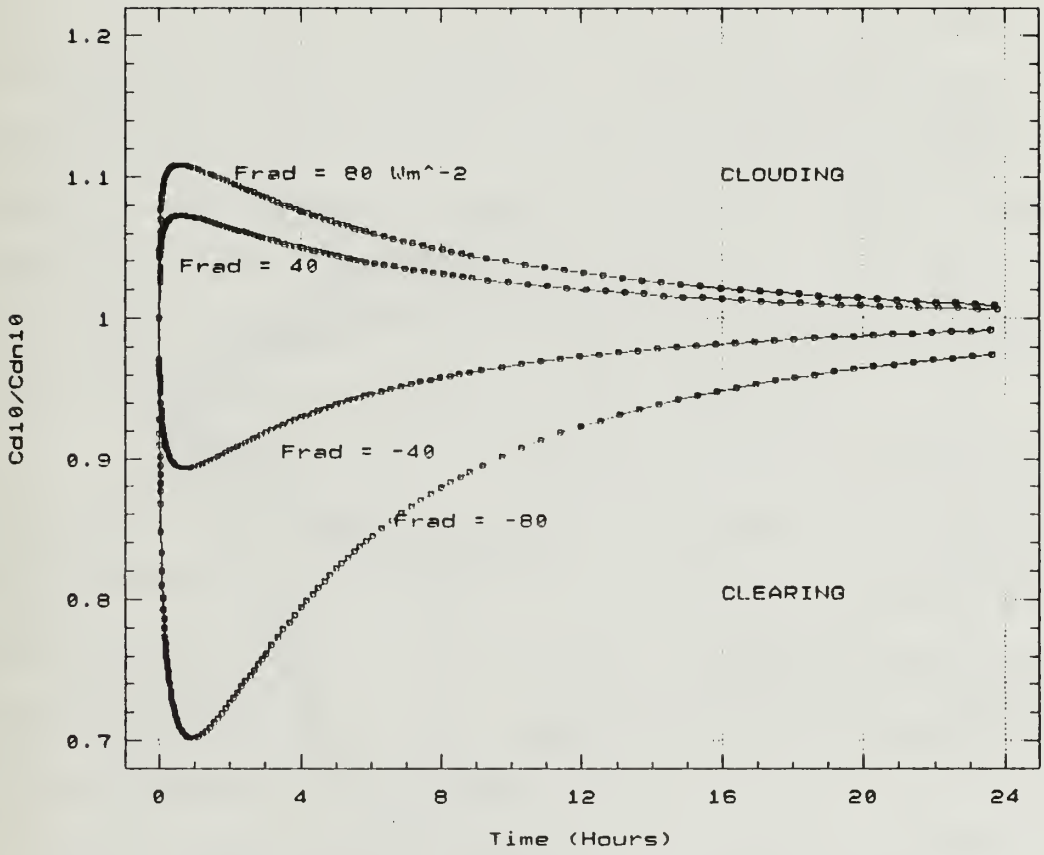

Figure 26 Slab Model Simulation Time Series of Drag Coefficient Ratio after Different Cloud Change Events.

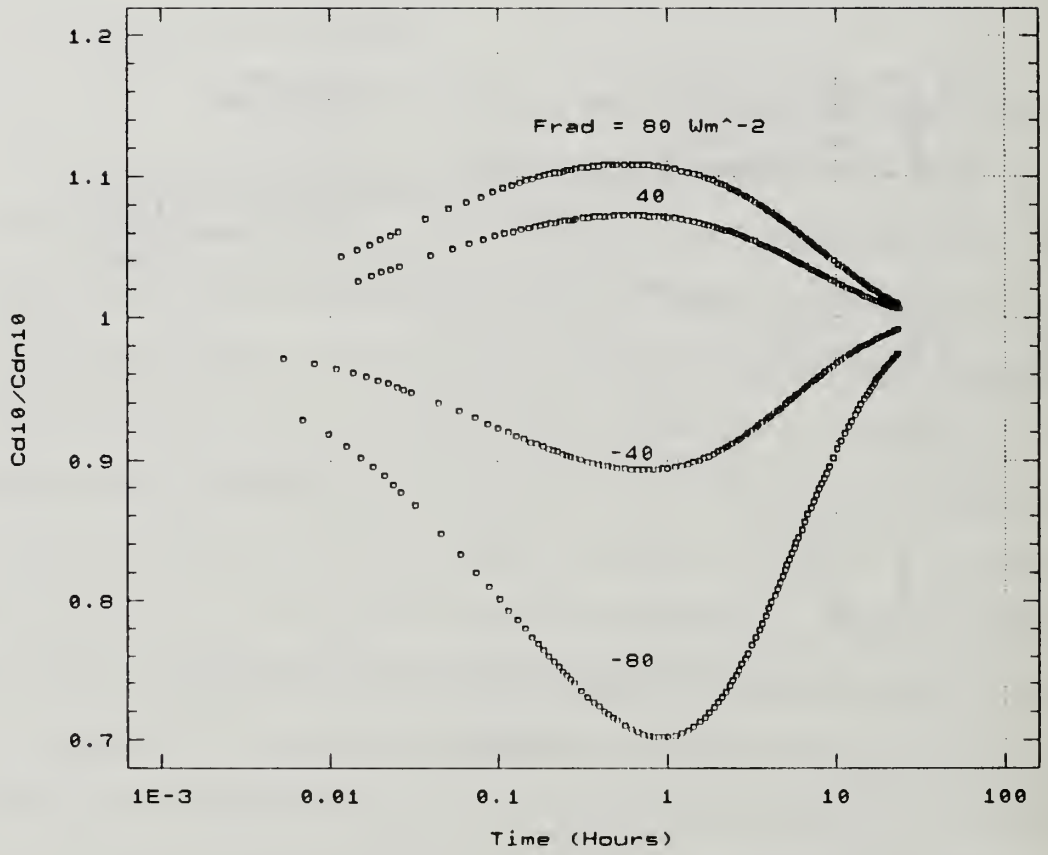

Figure 27 Same as Figure 24 but Logarithmic Time Scale.

Different wind speeds were tested in another experiment (Figures 28 and 29). The largest relative (Figures 28 and 29) and absolute (Figure 30) changes in wind stress after a radiation change event occur during the lightest winds. The maximum wind stress reduction was only 9% for the 9 ms^{-1} wind case, compared to a 30% reduction for the standard 6 ms^{-1} case and a 58% reduction for the 5 ms^{-1} case. At wind speeds below 4.5 ms^{-1}, the wind stress becomes zero after about an hour (not shown) because MO theory predicts complete suppression of turbulence and heat and momentum fluxes. The CEAREX drift period from 2 November 1988 to 5 November 1988 (Figure 5) is an example of a situation when fluxes have been completely suppressed during light winds. The results show that surface layer stability effects on wind stress are important in the central Arctic during average wind conditions, i.e. $U_{10} = 5\ ms^{-1}$. During high wind periods, $U_{10} > 10\ ms^{-1}$, the surface layer stability effect is almost negligible.

The ABL depth, h, is important to surface layer stability changes after a radiation change (Figures 31 and 32). The temperature of the ABL, θ_{10}, responds slower to changes in the surface temperature, T_{sfc}, when h is large. In nature, wind stress effects for an initial large h are less than what is shown in Figures 31 and 32 because during these stable periods a new low-level inversion would form and h would become much less after a few minutes.

c. Snow Characteristics Effects

Snow characteristics effects must also be considered. For such examinations, different standard case initializations were necessary because different snow/ice depths or conductivities result in different equilibrium temperature profiles. New 60 day initializations were based on the same downward

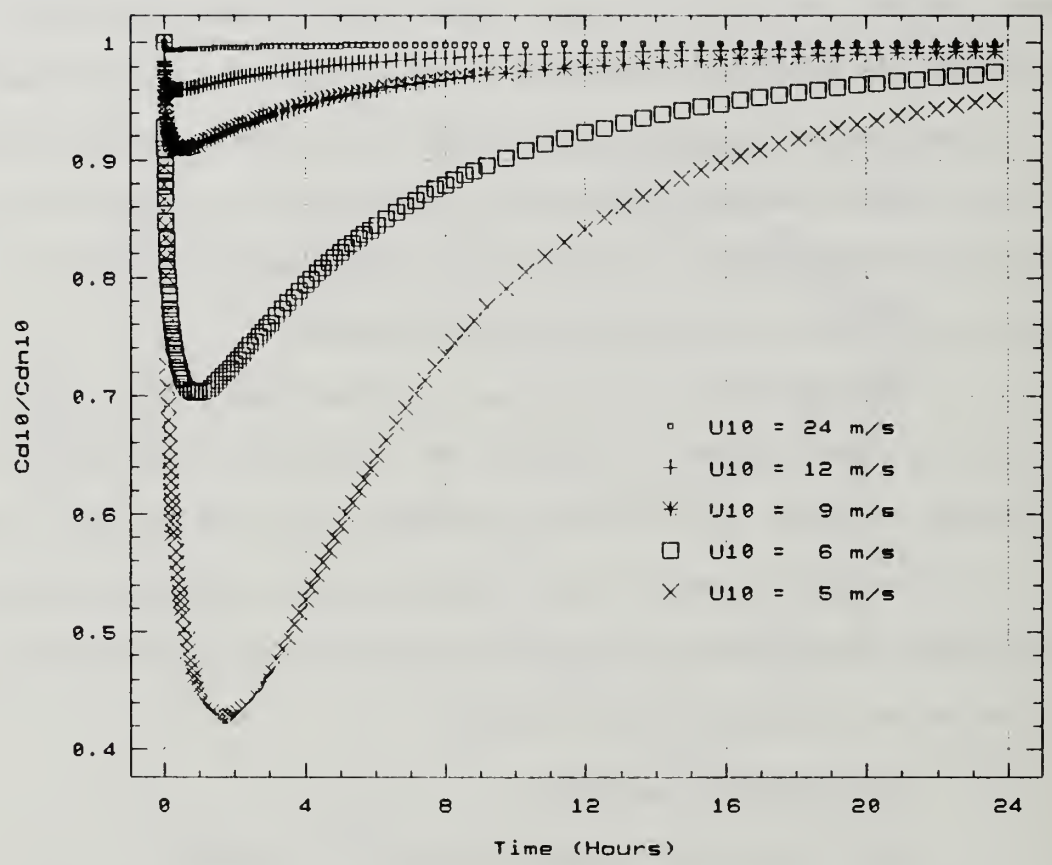

Figure 28 Slab Model Simulation Time Series of Drag Coefficient Ratio For Different Wind Speeds.

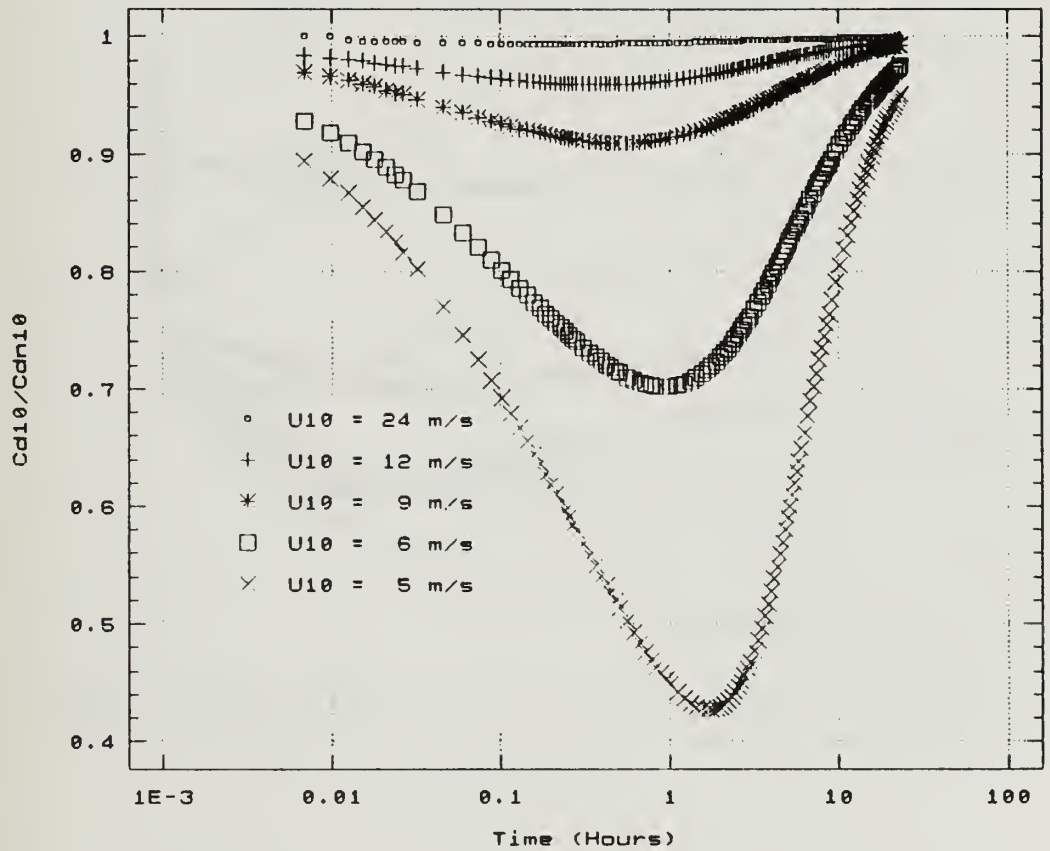

Figure 29 Same as Figure 28 but Logarithmic Time Scale.

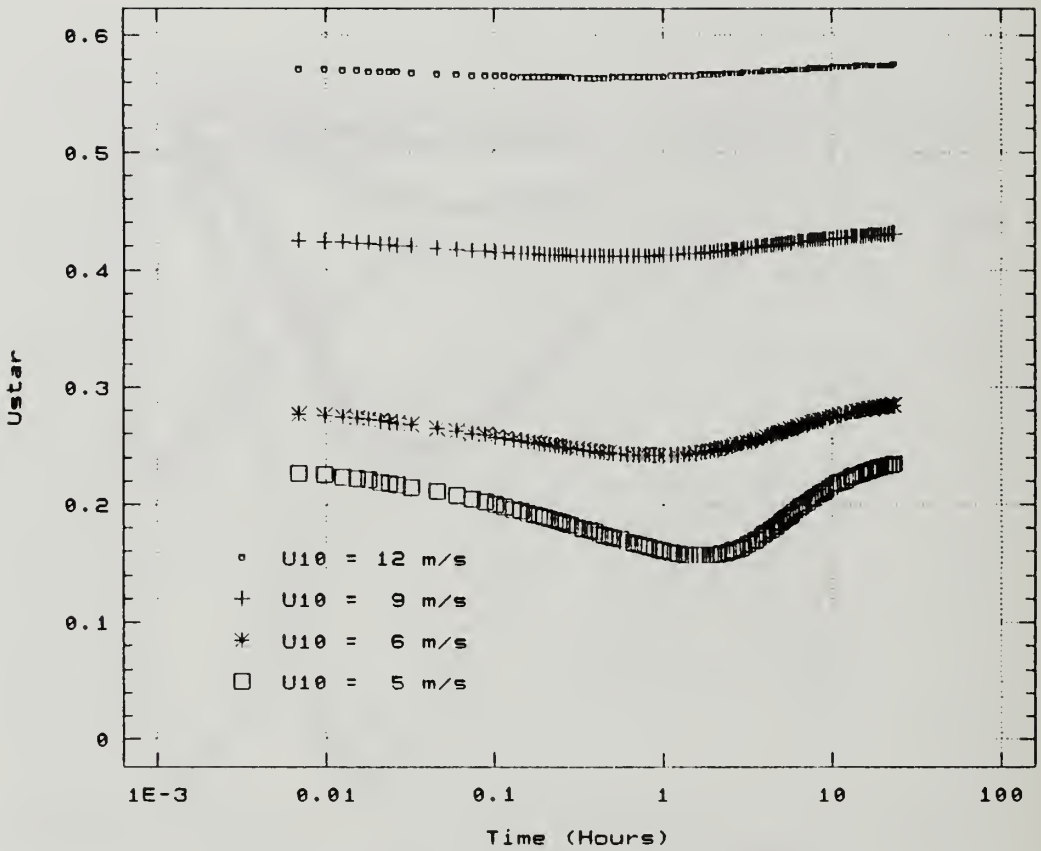

Figure 30 Slab Model Simulation Time Series of u_* for Different Wind Speeds.

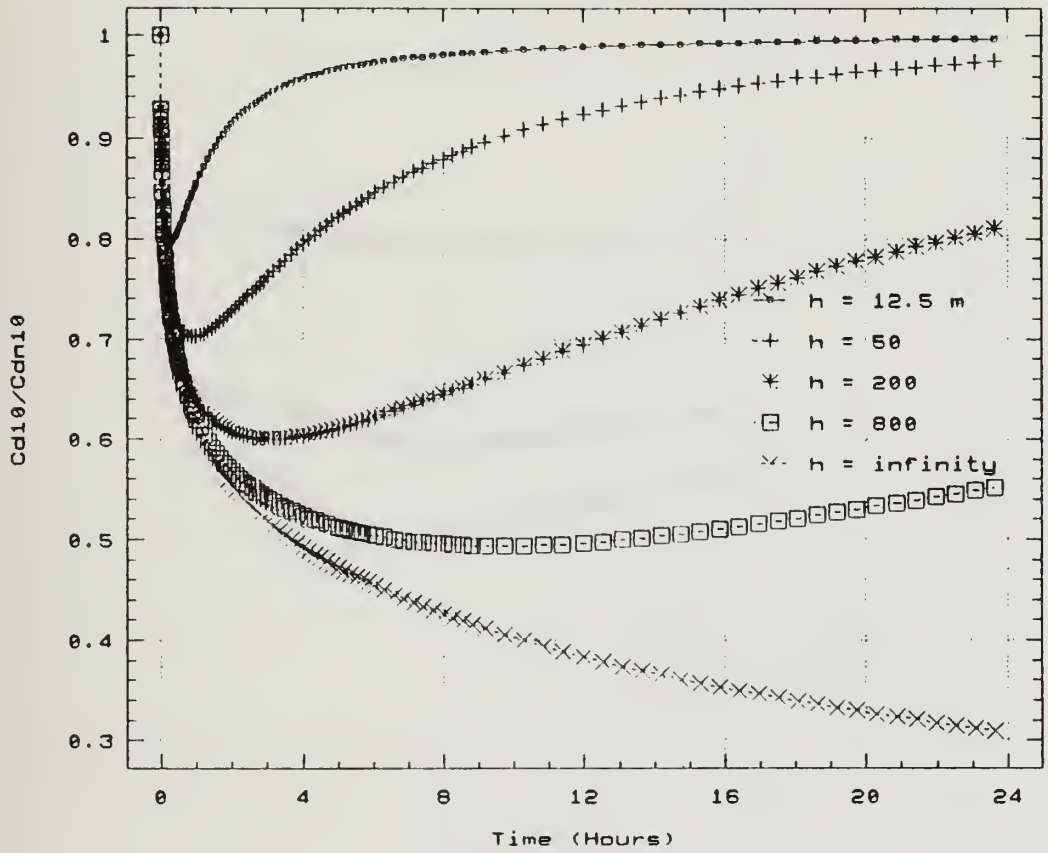

Figure 31 Slab Model Simulation Time Series of Drag Coefficient Ratio for Different ABL Depths.

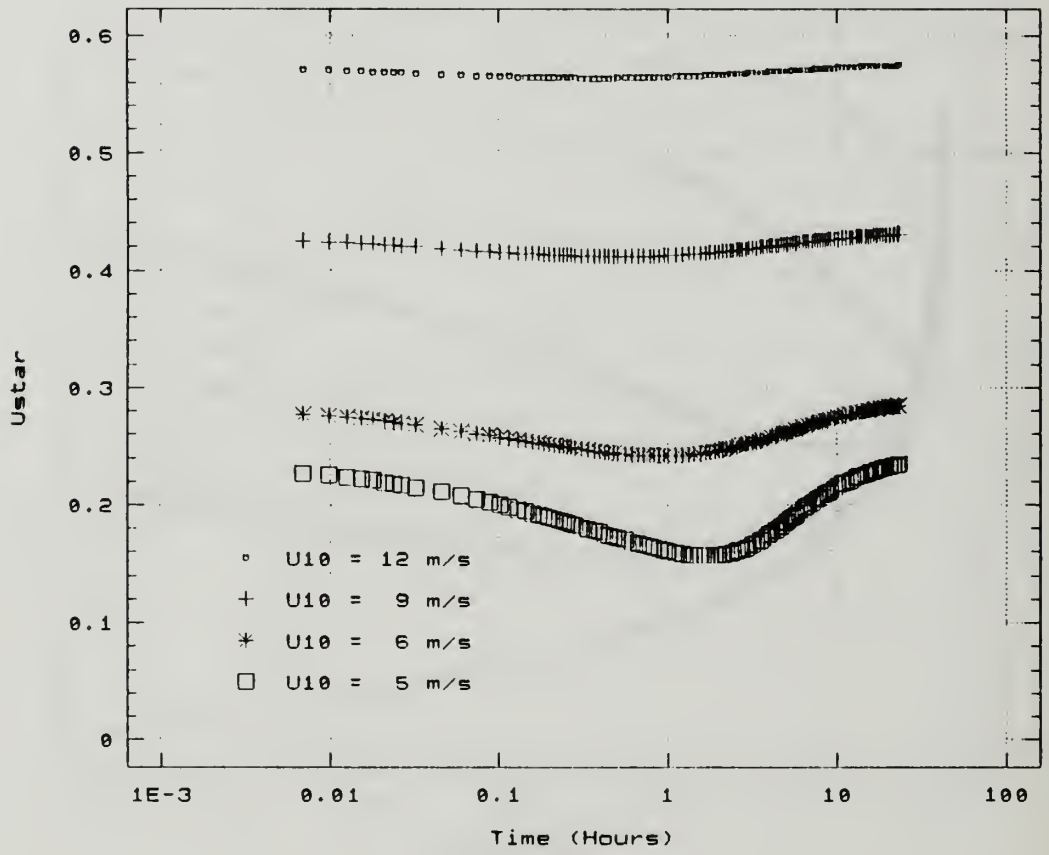

Figure 30 Slab Model Simulation Time Series of u_* for Different Wind Speeds.

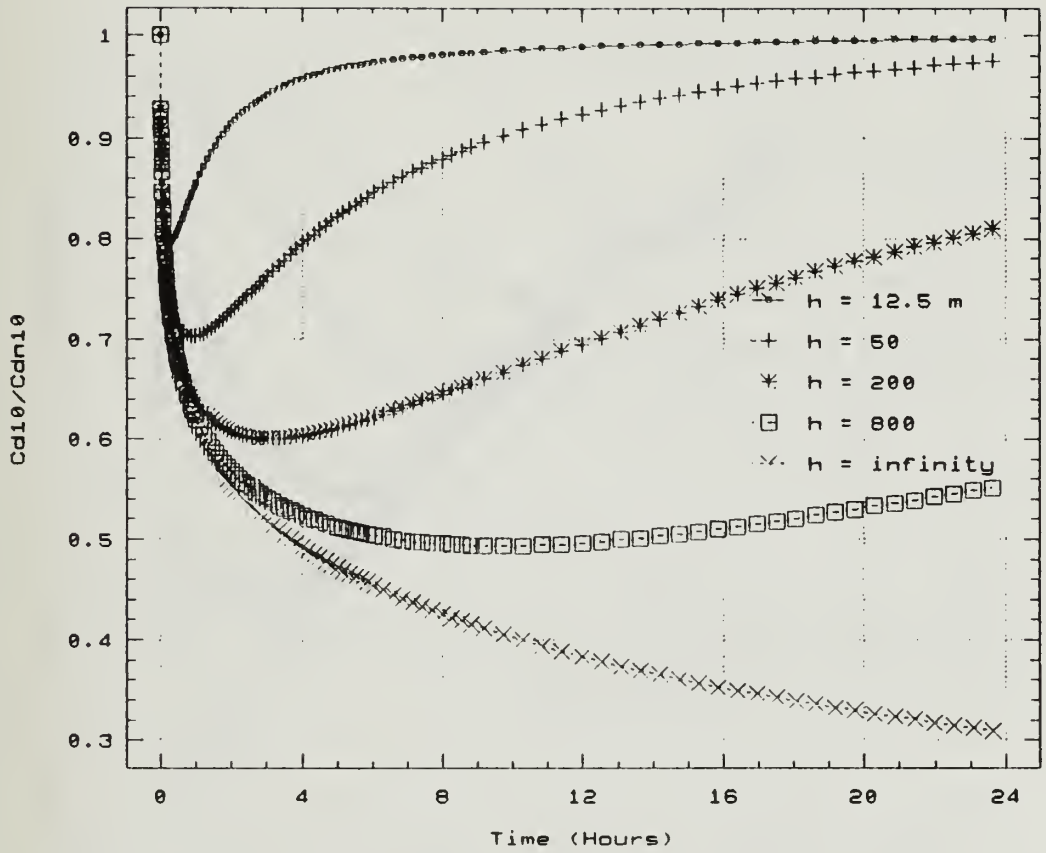

Figure 31 Slab Model Simulation Time Series of Drag Coefficient Ratio for Different ABL Depths.

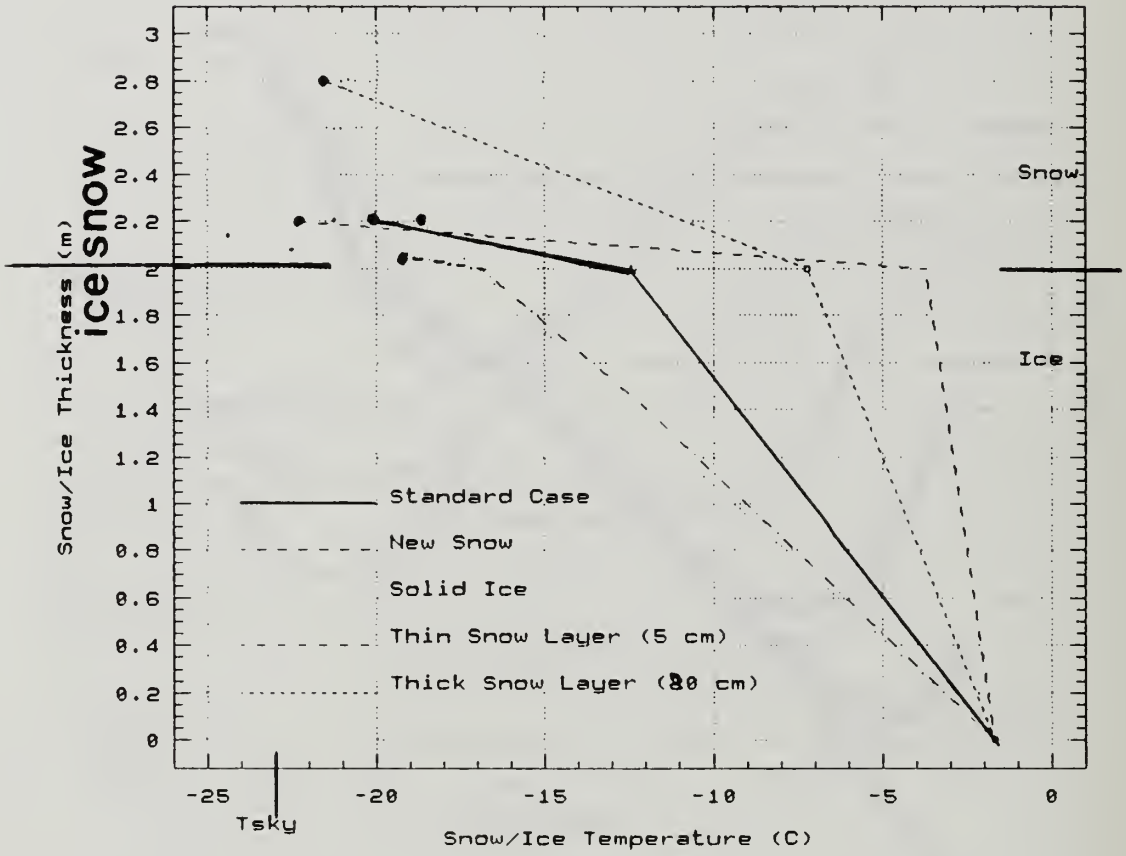

Figure 33 Temperature (X-Axis) as a Function of Snow and Ice Depths (Y-Axis) after 60-day Slab Model Simulation. Different simulations for various snow types and thicknesses are shown.

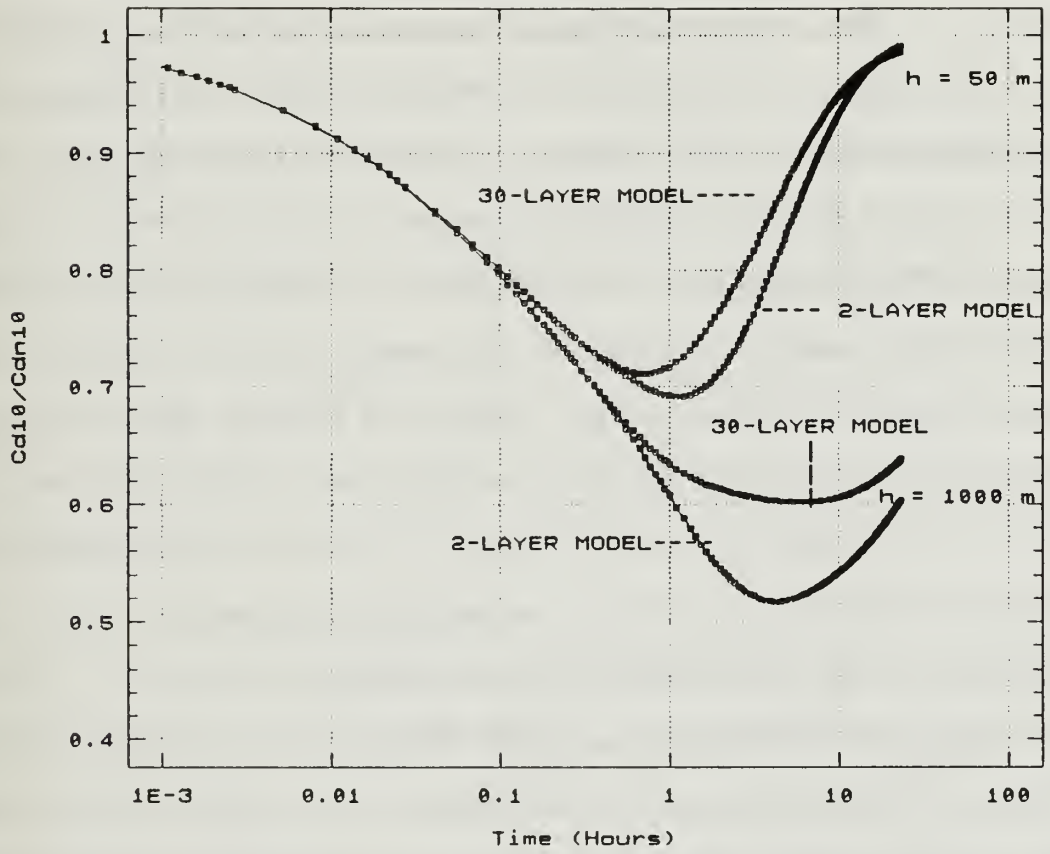

Figure 34 Errors Resulting from Using Too Few Ice Levels in the Numerical Snow/ice Model. Slab model drag coefficient ratio time series results using snow depth of 5 cm or 1/4 or the standard case values. Two different ABL depths, h, and two different numbers of ice layers are shown.

layers. Using more than 30 ice layers results in virtually identical results as the 30 ice layer version shown in Figure 34; 30 ice layers is enough resolution for accurate modeling of all cases. The error was much less for snow depths of 0.2 m or more. When this error was significant, the number of ice layers was increased from 2 to 30.

The surface of the pack ice can consist of ice or various types of snow. Different surfaces are modeled by changing the volumetric heat capacity, C_s, and thermal conductivity, k_s, of the upper 0.2 m of the floe (Figures 35 and 36). The values C_s and k_s used for the different surfaces are the same as used for Table 10 with an additional category represented by C_s and k_s values between the old packed and new feathery values, representing an intermediate snow type. The results in Figures 35 and 36 show that the wind stress after a radiation change is strongly dependent on snow type. Light new snow is a better insulator and has less volumetric heat capacity than denser old snow; both characteristics cause T_{sfc} to change more rapidly and generate larger surface layer stability effects for light snow vs. dense snow. Volumetric heat capacity, C_s, is proportional to density, ρ_s. Thermal conductivity, k_s, is proportional to ρ_{snow}^{2} (Stull, 1988). Initially, the change in T_{sfc} is therefore proportional to $\rho_{snow}^{-3/2}$, using Equation (10). After time t_{turb}, the difference in T_{sfc} changes between ice types is less than implied by Equation (10), but still significant enough to cause large differences in the maximum magnitudes of heat flux and wind stress reduction stability effect. For example, after one hour, which is approximately t_{max}, wind stress for ice, intermediate snow and old packed snow has been reduced by 12%, 44% and 63%, respectively, compared to 30% for the standard case.

The insulating characteristics of snow allow significant stability effects on wind stress to occur over the central Arctic. Liquid water has a greater

volumetric heat capacity than snow and a much greater thermal conductivity (due to turbulence); therefore the stability effects that have been discussed could not occur over open ocean regions.

The snow cover depth, d_s, of pack ice can vary from no snow to tens of centimeters. The surface layer stability effect on wind stress for three different snow depths and no snow is shown in Figures 37 and 38. For the standard case, with ABL depth equal to 50 meters, there is virtually no difference between the 0.2 m deep snow and the 0.8 m deep snow. The 0.05 m thick snow case shows small differences from the thicker cases after 0.5 hours. The t_{max} occurs 25% sooner and there is about a 20% less stability effect after one hour for the 0.05 m snow case compared to the standard 0.2 m case. These are minor relative differences compared to the solid ice case which had much less stability effect during the first 4 hours than all the snow cases.

d. Physical Time Scales

When the height of the ABL is increased to 1000 m, there is more difference in the results for the different snow depths (Figure 39) than the h = 50 case (Figure 36). Initially, the stability effects are identical as long as some snow is present. After 1.5 hours, the 0.05 snow thickness case has 10% less stability effect than the 0.2 m or 0.8 m snow thickness cases. Note that this time scale (1.5 hours) was identical for both h = 50 m and h = 1000 m cases. This is also the time after which the 2 ice layer model begins to show some error (Figure 34). This time represents the time elapsed, t_{deep}, before the ice layer below the snow can "feel" the different radiation conditions and begin to affect the temperature within and on top of the snow layer. The value of t_{deep} depends on the thermal diffusivity, ν_{snow}, and depth, d_{snow}, of the snow layer. From dimensional analysis

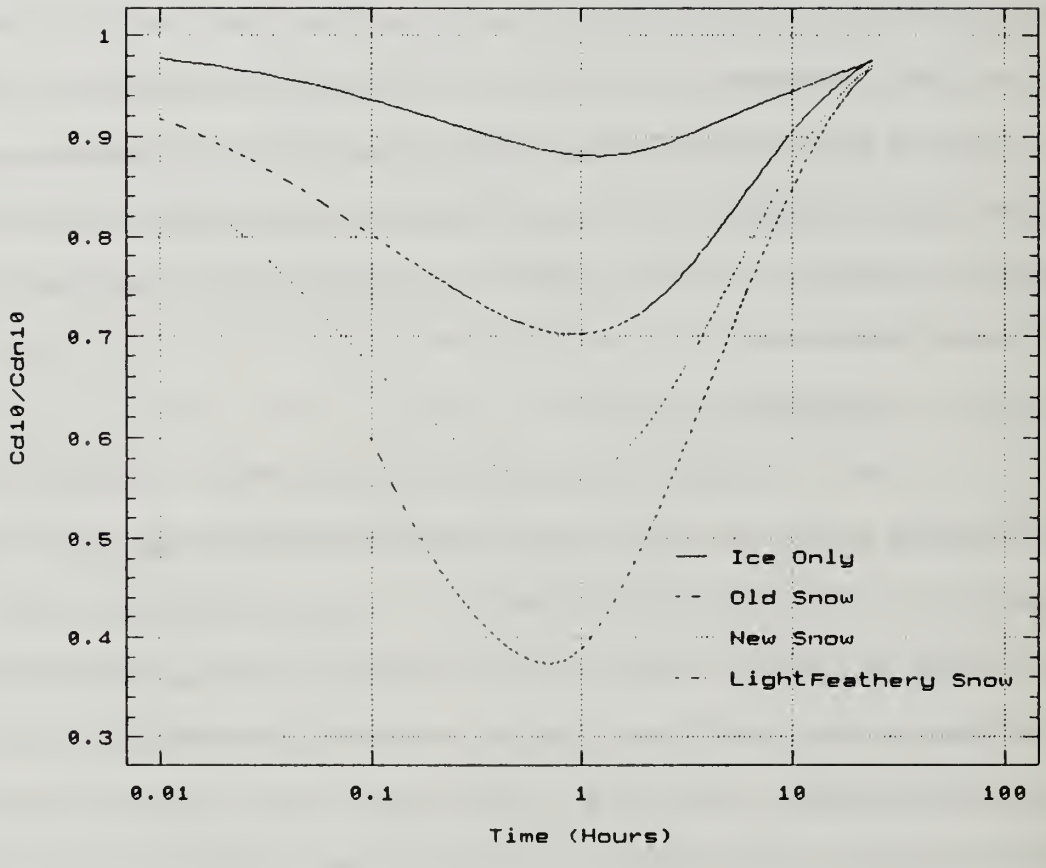

Figure 36 Same as Figure 35 but Logarithmic Time Scale.

volumetric heat capacity than snow and a much greater thermal conductivity (due to turbulence); therefore the stability effects that have been discussed could not occur over open ocean regions.

The snow cover depth, d_s, of pack ice can vary from no snow to tens of centimeters. The surface layer stability effect on wind stress for three different snow depths and no snow is shown in Figures 37 and 38. For the standard case, with ABL depth equal to 50 meters, there is virtually no difference between the 0.2 m deep snow and the 0.8 m deep snow. The 0.05 m thick snow case shows small differences from the thicker cases after 0.5 hours. The t_{max} occurs 25% sooner and there is about a 20% less stability effect after one hour for the 0.05 m snow case compared to the standard 0.2 m case. These are minor relative differences compared to the solid ice case which had much less stability effect during the first 4 hours than all the snow cases.

d. Physical Time Scales

When the height of the ABL is increased to 1000 m, there is more difference in the results for the different snow depths (Figure 39) than the h = 50 case (Figure 36). Initially, the stability effects are identical as long as some snow is present. After 1.5 hours, the 0.05 snow thickness case has 10% less stability effect than the 0.2 m or 0.8 m snow thickness cases. Note that this time scale (1.5 hours) was identical for both h = 50 m and h = 1000 m cases. This is also the time after which the 2 ice layer model begins to show some error (Figure 34). This time represents the time elapsed, t_{deep}, before the ice layer below the snow can "feel" the different radiation conditions and begin to affect the temperature within and on top of the snow layer. The value of t_{deep} depends on the thermal diffusivity, ν_{snow}, and depth, d_{snow}, of the snow layer. From dimensional analysis

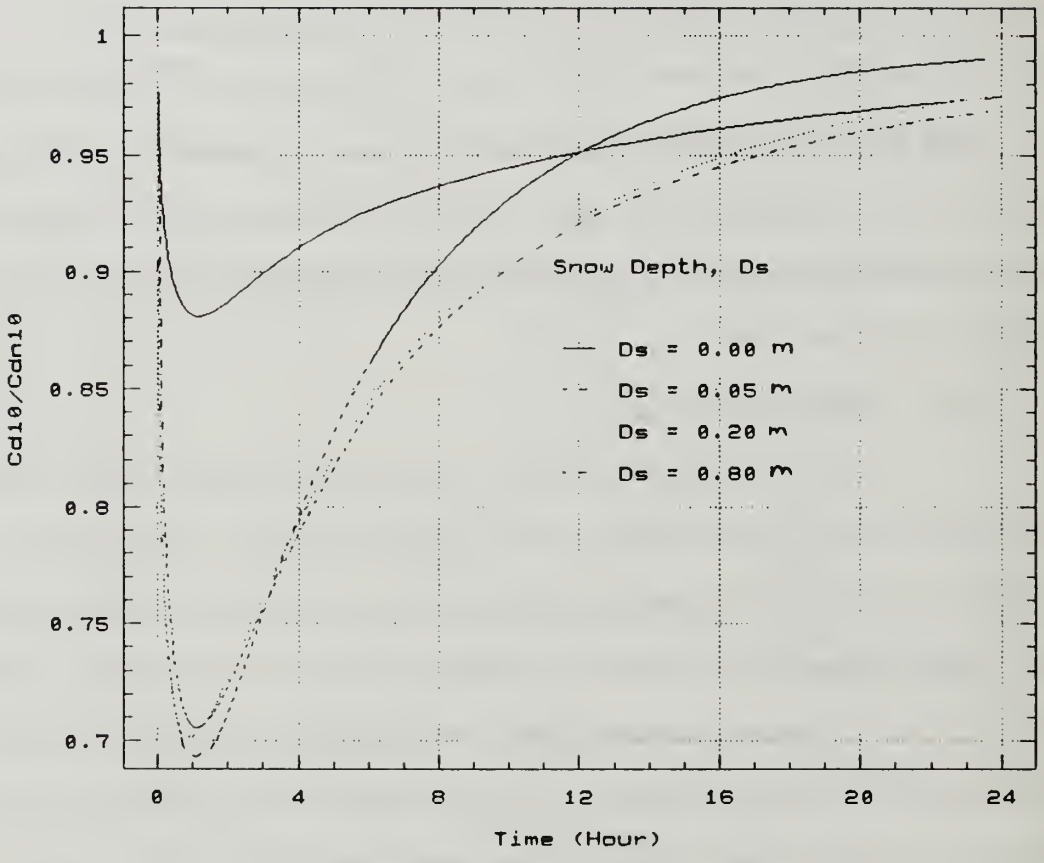

Figure 37 Slab Model Simulation Time Series of Drag Coefficient Ratio for Different Snow Depths.

$$t_{deep} = C_2 \frac{d_{snow}^2}{\nu_{snow}}, \qquad (20)$$

where C_2 is a dimensionless constant. The value of C_2 depends on what magnitude of ice layer effect is deemed significant. If significant is defined as a 1% effect on the wind stress, then the constant C_2 has a value of about 0.3. If significant is defined as a 10% effect on the wind stress, then the constant C_2 has a value of about one (see Figure 39). Analytical (Equation (20) with C_2 = 1.0) and numerical (Figure 39) results using both imply that t_{deep} is approximately equal to 1.5 and 24 hours for d_{snow} = 0.05 m and 0.2 m respectively.

Because t_{deep} equals 24 hours for 0.2 m thick snow and 384 hours for 0.8 m thick snow, a significant difference between the two cases should be noticeable after 24 hours. There is an obvious difference at 24 hours for the h = 1000 m case (Figure 39) but it is less obvious for the h = 50 m case (Figure 36). The reason that the effect of depth is not very noticeable for the h = 50 m case is because after 24 hours the ABL has already adjusted to the changes in surface temperature and heat fluxes are small, i.e. $t >> t_{max}$. The stability effect has become small, so relative differences of 10% correspond to a small absolute difference in stability effect. In order for the snow depth to have an effect on wind stress, t_{deep} must be less than an atmospheric time scale, t_{ABL}, which represents the amount of time required before the atmosphere has adjusted to the change in surface temperature. According to the simple ABL slab model, at any time, t, after a surface radiation change, the following equality will exist

$$t = \frac{\rho_{air} c_p \Delta T_{ABL} h}{F_{sens}}, \qquad (21)$$

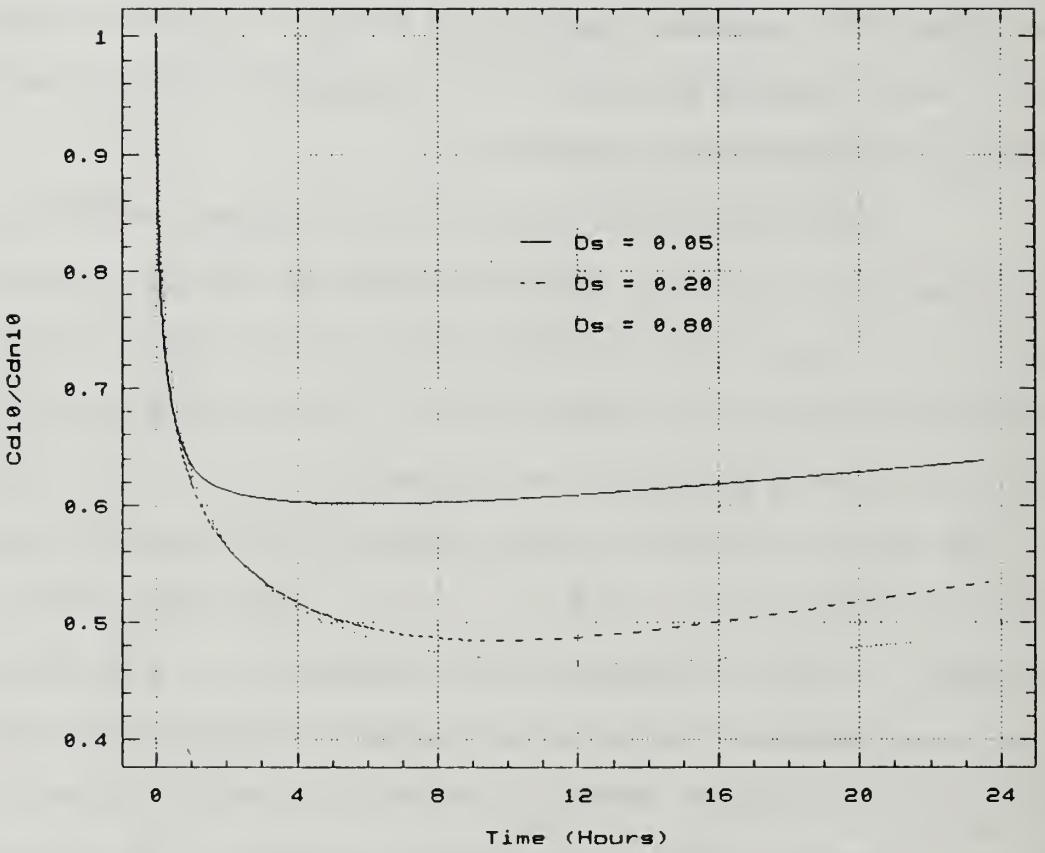

Figure 39 Slab Model Simulation Time Series of Drag Coefficient Ratio for Different Snow Depths Using an ABL Depth of 1000 m or 20 Times The Standard Case Value.

$$t_{deep} = C_2 \frac{d_{snow}^2}{\nu_{snow}}, \qquad (20)$$

where C_2 is a dimensionless constant. The value of C_2 depends on what magnitude of ice layer effect is deemed significant. If significant is defined as a 1% effect on the wind stress, then the constant C_2 has a value of about 0.3. If significant is defined as a 10% effect on the wind stress, then the constant C_2 has a value of about one (see Figure 39). Analytical (Equation (20) with C_2 = 1.0) and numerical (Figure 39) results using both imply that t_{deep} is approximately equal to 1.5 and 24 hours for d_{snow} = 0.05 m and 0.2 m respectively.

Because t_{deep} equals 24 hours for 0.2 m thick snow and 384 hours for 0.8 m thick snow, a significant difference between the two cases should be noticeable after 24 hours. There is an obvious difference at 24 hours for the h = 1000 m case (Figure 39) but it is less obvious for the h = 50 m case (Figure 36). The reason that the effect of depth is not very noticeable for the h = 50 m case is because after 24 hours the ABL has already adjusted to the changes in surface temperature and heat fluxes are small, i.e. $t >> t_{max}$. The stability effect has become small, so relative differences of 10% correspond to a small absolute difference in stability effect. In order for the snow depth to have an effect on wind stress, t_{deep} must be less than an atmospheric time scale, t_{ABL}, which represents the amount of time required before the atmosphere has adjusted to the change in surface temperature. According to the simple ABL slab model, at any time, t, after a surface radiation change, the following equality will exist

$$t = \frac{\rho_{air} c_p \Delta T_{ABL} h}{F_{sens}}, \qquad (21)$$

where ΔT_{ABL} is the change in ABL potential temperature, and F_{sens} is the average sensible heat flux. By picking appropriate scales for ΔT_{ABL} and F_{sens} a non-dimensional time, t^*, can be derived. Since the ABL temperature change is dictated by the change in downward radiation, a reasonable scale for ΔT_{ABL} is ΔT_{sky} which expresses the radiation change in terms of change in sky temperature. A scale to use for F_{sens} is the maximum sensible heat flux, $F_{sensmax}$. Using these scales the nondimensional time can be defined as

$$t^* = \frac{t}{t_{ABL}} , \qquad (22)$$

where

$$t_{ABL} = \frac{\rho_{air}\, c_p\, \Delta T_{sky}\, h}{F_{sensmax}} . \qquad (23)$$

At $t^* = 1$ the ABL has adjusted to the change in surface conditions. This occurs at $t = t_{ABL}$. For the standard case, t_{ABL} equals 15 hours, which corresponds well with the time period over which wind stress is affected by surface stability after a change in radiation conditions.

The model results show that the maximum sensible heat fluxes occur at approximately

$$t^* = \frac{1}{15} . \qquad (24)$$

The dimensional time of the maximum sensible fluxes, t_{max}, therefore occurs at

$$t_{max} = \frac{t_{ABL}}{15} . \qquad (25)$$

change represents a time change different from the model time step. An expression for this time period was derived.

Model simulations show that, unlike results from single snow layer surface models such as that used by OG, the surface fluxes require some time to "kick in" after a cloud cover change. Analytical expressions for this time period, as well as expressions for the time of maximum surface layer stability effect and the entire time period over which surface layer stability effects are important were derived. Assuming constant ABL depth, the surface layer stability change is inversely related to wind speed, as expected. At wind speeds greater that 9 ms^{-1} the surface layer stability effect is negligible. The specified value of ABL depth can strongly affect the surface flux changes. The temperature of a deep ABL cannot respond quickly to changes in surface temperature and therefore flux magnitudes and stability effects are larger and stay large for longer periods than for shallow ABLs.

The thermodynamic characteristics of an ice floe surface can vary from mostly solid ice to light feathery snow. The type of surface strongly affects surface fluxes following a cloud cover change. However, the depth of the snow layer on top of the pack ice may or may not affect surface fluxes. Analytical expressions based on snow and ABL characteristics can be used to determine when snow depth is an important parameter.

TABLE 11.
SUMMARY OF TIME SCALES RELATED TO EFFECTS OF h AND d_{snow} ON SURFACE LAYER STABILITY

Condition	Influence on wind stress[1]
$t < t_{turb}$	small stability effects
$t < t_{deep}$	d_{snow} has no effect
$t < t_h$	h has no effect
$t = t_{max}$	time of maximum effect
$t > t_{ABL}$	again small stability effects
$t_{deep} > t_{ABL}$	d_{snow} never has an effect
$t_{ABL} > t_{deep} > t_{max}$	d_{snow} has small effect on stability*
$t_{deep} < t_{max}$	d_{snow} has large effect on stability*

[1]"no" means < 1% effect
"small" means > 1% and < 10% effect
"large" means > 10% effect

*Assuming $t_{deep} < t < t_{ABL}$

change represents a time change different from the model time step. An expression for this time period was derived.

Model simulations show that, unlike results from single snow layer surface models such as that used by OG, the surface fluxes require some time to "kick in" after a cloud cover change. Analytical expressions for this time period, as well as expressions for the time of maximum surface layer stability effect and the entire time period over which surface layer stability effects are important were derived. Assuming constant ABL depth, the surface layer stability change is inversely related to wind speed, as expected. At wind speeds greater that 9 ms^{-1} the surface layer stability effect is negligible. The specified value of ABL depth can strongly affect the surface flux changes. The temperature of a deep ABL cannot respond quickly to changes in surface temperature and therefore flux magnitudes and stability effects are larger and stay large for longer periods than for shallow ABLs.

The thermodynamic characteristics of an ice floe surface can vary from mostly solid ice to light feathery snow. The type of surface strongly affects surface fluxes following a cloud cover change. However, the depth of the snow layer on top of the pack ice may or may not affect surface fluxes. Analytical expressions based on snow and ABL characteristics can be used to determine when snow depth is an important parameter.

V. CASE STUDIES OF THE EFFECT OF CLOUDS ON WIND STRESS

The influence of clouds on the wind stress resulting from their effect on stability dependent surface layer drag coefficient was examined in the previous chapter. In that examination, the relationship between downward radiation changes due to cloud cover changes and the surface stability changes was considered for Type R situations. Because the wind speed is the primary factor in the wind stress, the effect of clouds on surface wind speeds as well as stability requires examination, based on Arctic boundary layer characteristics. Clouds can affect the surface wind vector by being radiatively cooled at the top and by influencing the entrainment of air into the ABL. Entrainment and cloud top cooling within the ABL are non-Type R phenomena.

Unlike the simple Monin-Obukhov surface layer theory used to determine radiation effects on surface layer stability in Chapter IV, the combined effect of these processes is too complicated to describe with analytical equations or simple numerical models. Therefore, this chapter will examine the combined effect of all physical processes which may link wind stress to cloud conditions by examining the results of numerical ABL simulations, with cloud and radiation physics included, and *in situ* observations from the CEAREX drift.

Three case studies are presented which use numerical model results, initialized and verified using CEAREX observations, to quantify the various cloud effects on wind stress. The case studies will be used to show realistic examples of how various cloud conditions and changes in cloud conditions can influence wind stress in the Arctic. The purpose of the case studies presented here is to use the

longwave radiation with model predictions based on a concurrent rawinsonde sounding.

In this study, the original model was found to significantly underpredict the downward longwave radiation at the surface during clear winter Arctic conditions. When Thompson and Burk (1990) used this radiation code to model an Arctic front, they were forced to set the surface temperature to a constant value since the incorrect radiation was causing a snow/ice relaxation scheme to predict surface temperature values that were too low. The problem only occurred at temperatures below 0 C and only became obvious when the model was compared to the CEAREX drift measurements. For this study, the radiation code was modified (Burk, personal communication) and the model radiation values compared well with the clear sky measurements during cold clear weather on the average. There was considerable scatter remaining.

The radiation model also underpredicted the absorption/emission of longwave radiation in Arctic winter clouds. Arctic clouds contain a relatively small amount of particulate water but are observed to be quite black. The model is based on lower latitude measurements, as are all radiation schemes, and does not account for ice particles and variations in particle size spectra which may occur in the Arctic. Information on the characteristics of cloud particulates was not available concurrently with the data used for this dissertation; therefore a detailed study of the radiation characteristics of Arctic clouds was not attempted. By increasing the absorptivity of particulate water in the clouds by a factor of 30, a good match (average difference 3.5 Wm^{-2}) between measurements of downward longwave radiation and model predictions during cloudy conditions was achieved. The match

potential temperature, θ_l (2) total water content, q_t (3) turbulent kinetic energy, TKE (4) the variance of θ_l (5) the variance of q_t (6) the cross correlation of θ_l and q_t (7) the east component of mean momentum, u, and (8) the north component of mean momentum, v. Other second-moment equations are solved with diagnostic equations. The turbulence closure occurs at level 2.5 and level 3 using Mellor and Yamada (1974) terminology. The second-order closure physics allows vertical virtual temperature fluxes to occur even when the gradient is zero (i.e. a mixed layer) as long as turbulence is present.

2. Cloud Model

By using thermodynamic turbulence statistics generated by the model, the method of Sommeria and Deardorff (1977) is used to predict the cloud cover at each level. With no turbulence, the cloud cover instantly changes from zero to total when the mean humidity reaches saturation. But with increasing turbulence, there is an expanding mean humidity range around 100% relative humidity where partial cloudiness is predicted.

When partial cloudiness exists at several levels, random overlapping is assumed (Harshvardhan *et al.*, 1987; Burk and Thompson, 1989). The radiation at each level is partitioned into the clear and cloudy air components.

3. Radiation Model

Radiative cooling/heating is based on a broadband radiative scheme with transmission functions at each level determined from the amount of water vapor, liquid water, carbon dioxide and aerosol (Oliver *et al.*, 1978; Lewellen *et al.*, 1976). The same radiation scheme has been tested for a variety of conditions, although not under Arctic conditions to my knowledge. The CEAREX measurements provided a good opportunity to compare measurements of downward

longwave radiation with model predictions based on a concurrent rawinsonde sounding.

In this study, the original model was found to significantly underpredict the downward longwave radiation at the surface during clear winter Arctic conditions. When Thompson and Burk (1990) used this radiation code to model an Arctic front, they were forced to set the surface temperature to a constant value since the incorrect radiation was causing a snow/ice relaxation scheme to predict surface temperature values that were too low. The problem only occurred at temperatures below 0 C and only became obvious when the model was compared to the CEAREX drift measurements. For this study, the radiation code was modified (Burk, personal communication) and the model radiation values compared well with the clear sky measurements during cold clear weather on the average. There was considerable scatter remaining.

The radiation model also underpredicted the absorption/emission of longwave radiation in Arctic winter clouds. Arctic clouds contain a relatively small amount of particulate water but are observed to be quite black. The model is based on lower latitude measurements, as are all radiation schemes, and does not account for ice particles and variations in particle size spectra which may occur in the Arctic. Information on the characteristics of cloud particulates was not available concurrently with the data used for this dissertation; therefore a detailed study of the radiation characteristics of Arctic clouds was not attempted. By increasing the absorptivity of particulate water in the clouds by a factor of 30, a good match (average difference 3.5 Wm^{-2}) between measurements of downward longwave radiation and model predictions during cloudy conditions was achieved. The match

is good because both adjusted model and observations have virtually black cloud bases if the cloud is thicker than 100 m.

During clear sky conditions, the model predictions of downward longwave radiation were less accurate, with an average difference of 22 Wm^{-2}, even after the modifications. It is doubtful that other radiation schemes could be significantly more accurate during clear skies. This is because large (> 30 Wm^{-2}) differences in measured downward radiation occurred between soundings which had very similar humidity and temperature profiles. No radiation model could predict these differences based on the rawinsonde profile alone.

Two explanations for the large variations in measured downward longwave radiation for similar rawinsonde profiles are (1) Varying amounts of small ice crystal concentrations and (2) Different temperature/humidity characteristics above the highest rawinsonde point. OG and Curry (1983) show how ice crystals or "diamond dust" are important to radiative transfer in the Arctic. Variable concentrations of diamond dust were personally observed during the CEAREX drift period. Assuming ice crystal concentrations are also variable throughout the entire atmosphere, it is reasonable to expect that the longwave radiation fluctuates due to the ice crystals. The additional downward longwave radiation at the surface due to ice crystals throughout the troposphere can vary from 15 to 80 Wm^{-2} (Curry *et al.*, 1989).

The model radiation predictions at the surface during clear weather were quite sensitive to the specification of temperature and humidity in the stratosphere, above the top level of most of the rawinsonde profiles. The temperature at the 100 mb level was adjusted so that the snow/ice model produced the measured clear sky surface temperature. The adjustment accounts for the unknown amounts of ice

longwave radiation over pack ice in winter (Chapter IV). Three choices for initial surface temperature are

(T1) the value produced by the snow/ice model using the measured radiation,

(T2) the value produced by the snow/ice model using the radiation value produced by the model radiation code and the measured temperature and humidity profiles or

(T3) the measured value.

These correspond to the following values of downward radiation:

(R1) the measured value,

(R2) the value given by the radiation code

(R3) the value required by the snow/ice model to produce the measured surface temperature.

Because the measured, radiation code and ice/snow model values differ, the longwave radiation and surface temperature values must be paired, i.e. R1 must be paired with T1, R2 with T2 etc., for the initialization to have an energy balance at the surface. Once the model run begins, the surface temperature is determined by the same method that was used to determine T2 during the initialization procedure. If either T1 or T3 is used at the start of the model, the model surface temperature will quickly jump toward T2, again because of an energy imbalance at the surface. Therefore the only pair which will not create a rapid change in surface temperature due to a surface energy imbalance at the start of the model run is R2 and T2. This is unsatisfactory because the (model-generated) surface temperature is determined

half of the surface geostrophic value. For this case, a low-level thermal wind was assumed, and the geostrophic winds above h were set to the true winds measured with a rawinsonde.

Advection could be simulated by having tendency terms for the prognostic variables. All tendencies were set to zero in the case studies shown here. An exception was that sometimes a sudden moisture tendency was imposed to force clouds to form or dissipate. Any moisture tendencies used will be discussed in the individual case study discussions.

5. Model Initialization

The 1-D ABL model is initialized from a rawinsonde or model profile of temperature, humidity and geostrophic wind vector and a modeled or specified surface temperature. But a classic problem arises: the values of different measured parameters are not in equilibrium with the model physics. Usually this problem is approached by having an adjustment or spin-up period before the actual model run; this method was used for several parameters. But for comparison between the modeled effect of clouds on wind stress and measurements, the spin-up should not substantially change the specification of clouds, the initial surface temperature and the low level temperature profile. The CEAREX drift measurements provided further information, such as measurements of longwave radiation, wind stress and heat flux, which should allow the initializations to match reality to a greater extent. However, the detailed CEAREX data provides the dilemma of having too much initialization information.

To illustrate this problem, consider the initialization of surface temperature. The surface temperature is strongly related to the downward

longwave radiation over pack ice in winter (Chapter IV). Three choices for initial surface temperature are

(T1) the value produced by the snow/ice model using the measured radiation,

(T2) the value produced by the snow/ice model using the radiation value produced by the model radiation code and the measured temperature and humidity profiles or

(T3) the measured value.

These correspond to the following values of downward radiation:

(R1) the measured value,

(R2) the value given by the radiation code

(R3) the value required by the snow/ice model to produce the measured surface temperature.

Because the measured, radiation code and ice/snow model values differ, the longwave radiation and surface temperature values must be paired, i.e. R1 must be paired with T1, R2 with T2 etc., for the initialization to have an energy balance at the surface. Once the model run begins, the surface temperature is determined by the same method that was used to determine T2 during the initialization procedure. If either T1 or T3 is used at the start of the model, the model surface temperature will quickly jump toward T2, again because of an energy imbalance at the surface. Therefore the only pair which will not create a rapid change in surface temperature due to a surface energy imbalance at the start of the model run is R2 and T2. This is unsatisfactory because the (model-generated) surface temperature is determined

with a different method from the rawinsonde air temperature. This will usually generate artificial turbulent surface heat fluxes, again resulting in a rapid jump in the surface temperature, this time toward the ABL temperature.

The only way to prevent an unwanted jump in surface temperature at the start of the model run is to specify radiation and snow, surface and ABL temperatures that are in equilibrium. Three methods to accomplish this are:

(1) alter the snow/ice model,

(2) alter the radiation model or

(3) alter the low-level measured temperature profile used for the initialization

The equilibrium surface temperature is not greatly sensitive to changes in snow depth or characteristics, as shown in Chapter IV. Large, unrealistic alterations to the snow characteristics would be required to make the snow/ice model produce the measured surface temperature, eliminating choice (1).

Further, it is desirable to preserve the measured thermal structure of the lower atmosphere as much as possible since this is expected to be an important link between clouds and wind stress. Therefore (3) is eliminated to have the thermal structure altered by modeled cloud and ABL physics, not artificially.

This leaves (2) altering the radiation model, as the best choice. It is realistic because the snow/ice model is quite sensitive to changes in longwave radiation, so that drastic changes are not required to produce the measured surface temperature. Also it was shown earlier how the radiation model has considerable

B. OCT 22 CASE STUDY - CLEARING EVENT

Three case studies were chosen to illustrate cloud effects on wind stress. The first two cases represent cloud forming and cloud clearing, respectively, above the ABL. The third case study involves cloud formation and dissipation within the ABL.

The first case study at the CEAREX drift location used a rawinsonde profile at 2300 October 21 to initialize the model at t = 0 hours (Figure 40). The case study ends at 1500 October 22, model t = 16 hours. All the case studies presented here are based on 16 hour model runs. Some moisture at cloud level was artificially removed from the model at t = 2 hours in order to simulate the observed cloud dissipation which occurred during the first three hours of this case study period.

During this period, overcast conditions changed to clear and the surface temperature underwent a sharp decrease (Figure 41b). The measured radiation value of almost 270 Wm^{-2} at t = 0 dropped to about 160 Wm^{-2} by t = 4 hours as the clouds dissipated (Figure 41a). Profile measurements of surface heat flux (not shown) averaged -20 Wm^{-2}, indicating a stable Type R event. This was one of the larger magnitude heat flux events measured with the profile tower during the CEAREX drift. This situation is similar to the standard case modeled in Chapter IV except that the surface wind speed was a little higher, about 6 ms^{-1} instead of 5 ms^{-1} and h adjusted to 124 m instead of the prescribed 50 m in the standard case.

The model surface heat fluxes were -30 Wm^{-2} to -50 Wm^{-2}. Despite the larger predicted heat loss compared to the measurements, the model air temperature decreased at only about one-half the rate of the measurements, although the shape of the temperature curves in Figure 41 are similar, resembling a negative exponential decrease with time (e^{-t}). The measurements indicated cold advection which magnified the temperature decrease and somewhat negated the large heat

In the final hours of the snow/ice model initialization, the value of the atmosphere-snow total heat flux (net radiation and turbulent fluxes) was chosen by trial and error which would result in the exact surface temperature which was measured at the start of the case study period. This prevents the type of energy imbalance at the start of the model run described above.

The ABL model performs a half-hour turbulence spin-up by keeping the mean prognostic variables fixed while allowing the second order variables and the TKE to adjust from an initial value of zero, except the TKE, which starts at a neutral atmosphere value (Burk and Thompson, 1989). Time equals zero after this spin-up.

The recommended method for initializing the mean wind velocity components is to set the true u and v wind components to the geostrophic value at all levels and let the model spin-down the winds after the start of the model run (Burk, personal communication). This prevents inertial oscillations and the adjustment usually requires only two or three hours. The problem with this method is that at the start of the model run, the surface wind speed is too high and may alter the structure of the ABL before adjustment occurs. This problem is more pronounced during common low Arctic inversion situations.

For the case studies, a preliminary run was used to provide the wind profiles for the start of the actual case study run and adjusted by trial and error to prevent inertial oscillations. These were compared with spin-down versions of the same cases. Generally, the cloud effects were similar using either method so this was not a crucial issue for studying the effect of clouds on wind stress.

B. OCT 22 CASE STUDY - CLEARING EVENT

Three case studies were chosen to illustrate cloud effects on wind stress. The first two cases represent cloud forming and cloud clearing, respectively, above the ABL. The third case study involves cloud formation and dissipation within the ABL.

The first case study at the CEAREX drift location used a rawinsonde profile at 2300 October 21 to initialize the model at t = 0 hours (Figure 40). The case study ends at 1500 October 22, model t = 16 hours. All the case studies presented here are based on 16 hour model runs. Some moisture at cloud level was artificially removed from the model at t = 2 hours in order to simulate the observed cloud dissipation which occurred during the first three hours of this case study period.

During this period, overcast conditions changed to clear and the surface temperature underwent a sharp decrease (Figure 41b). The measured radiation value of almost 270 Wm^{-2} at t = 0 dropped to about 160 Wm^{-2} by t = 4 hours as the clouds dissipated (Figure 41a). Profile measurements of surface heat flux (not shown) averaged -20 Wm^{-2}, indicating a stable Type R event. This was one of the larger magnitude heat flux events measured with the profile tower during the CEAREX drift. This situation is similar to the standard case modeled in Chapter IV except that the surface wind speed was a little higher, about 6 ms^{-1} instead of 5 ms^{-1} and h adjusted to 124 m instead of the prescribed 50 m in the standard case.

The model surface heat fluxes were -30 Wm^{-2} to -50 Wm^{-2}. Despite the larger predicted heat loss compared to the measurements, the model air temperature decreased at only about one-half the rate of the measurements, although the shape of the temperature curves in Figure 41 are similar, resembling a negative exponential decrease with time (e^{-t}). The measurements indicated cold advection which magnified the temperature decrease and somewhat negated the large heat

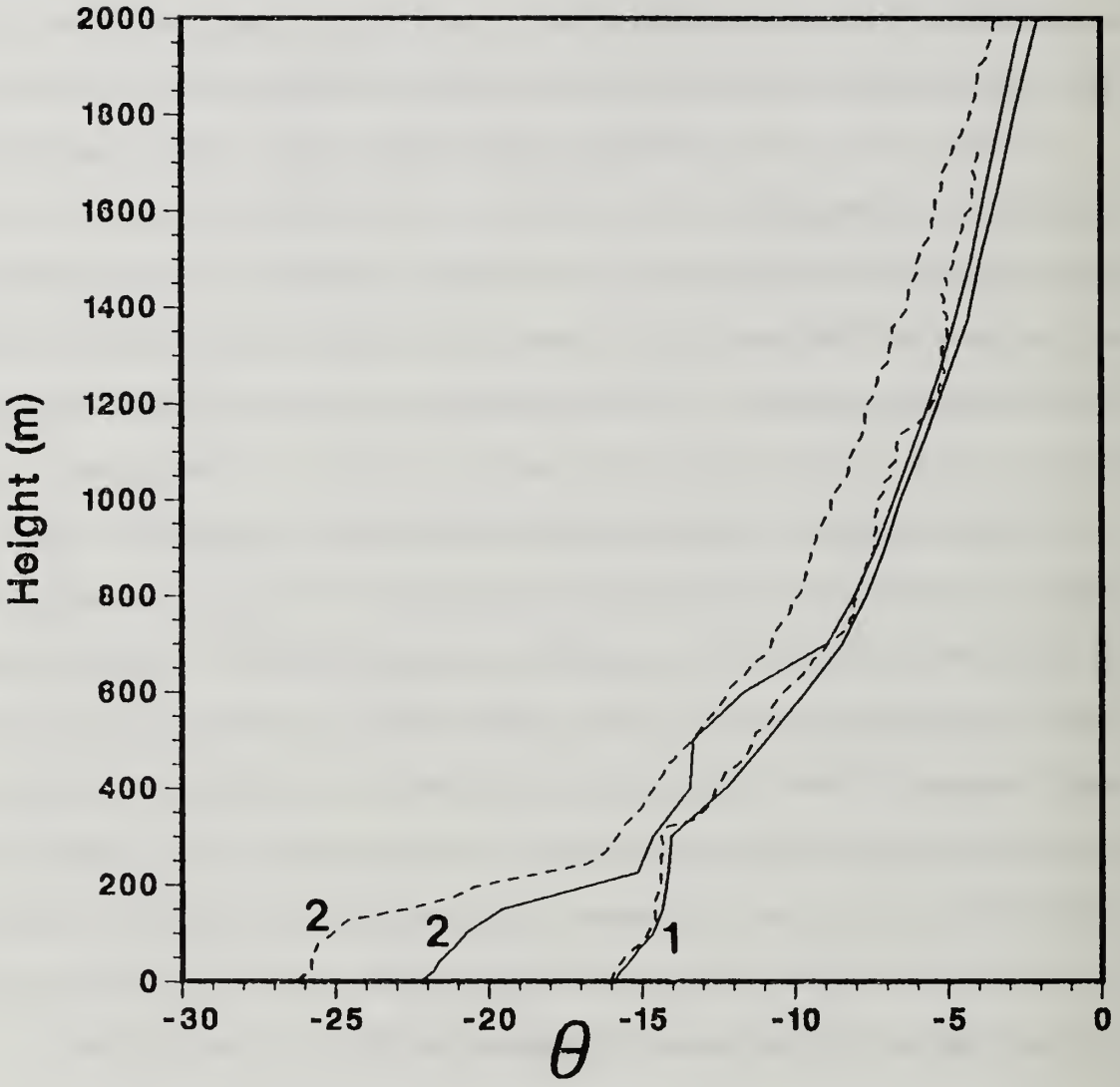

Figure 40 Model (solid line) and Measured (dashed line) Profiles of Potential Temperature for the October 21-22 Case Study. The lines labelled "1" are at model t = 0 hours and the lines labeled "2" are at t = 12 hours.

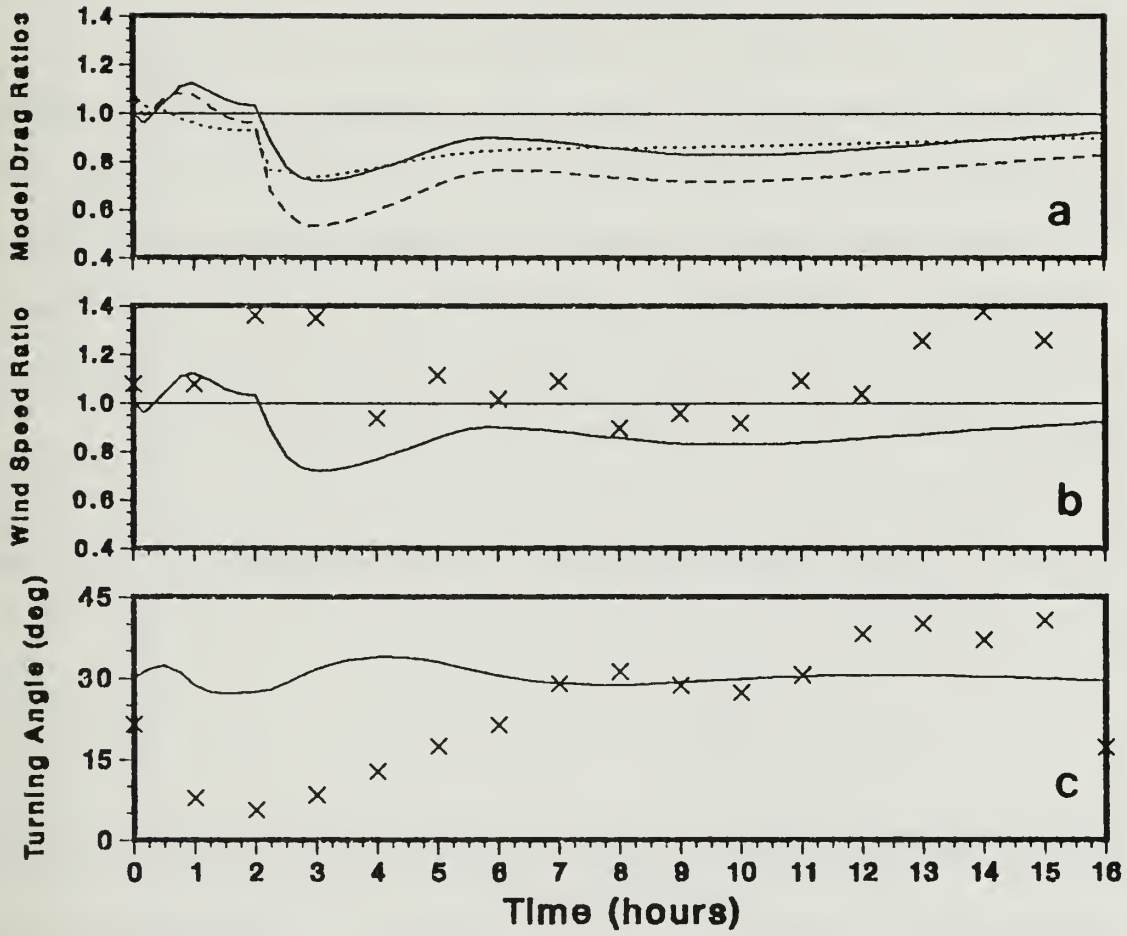

Figure 42 Model Output and Measured Values of Various Parameters Related to Wind Stress for the October 22 Case Study. The top panel (a) shows the model output for the normalized quadratic reduction factor (solid line), the normalized drag coefficient (dotted line) and the normalized quadratic geostrophic drag coefficient (dashed line). The middle panel (b) also shows the model output normalized quadratic reduction factor (solid line) and the measured values (x's). Both panels have a straight solid line to use as a reference for the average value of 1.0. The bottom panel (c) shows model output (solid line) and measured (x's) turning angle. See text for definitions of these parameters.

flux into the surface. The cold advection extended to at least 2000 m, as indicated by the measured line 2 in Figure 40, which has clearly shifted to the left of line 1 at all levels. The presence of cold advection can be explained by the air within the ABL, after the clearing event, being exposed to clear skies and cooling surface conditions for a much longer time than suggested by the local conditions.

Despite not accounting for cold advection, the model does a fairly good job of reproducing the internal boundary layer which forms after the clearing event. After twelve hours, both the model and measured ABL heights were about 100 m (Figures 40 and 41). The measured ABL height shown in Figure 40 was based on the height of the lowest temperature inversion. The model ABL height shown in Figure 41 was based on the level where the TKE reaches 10% of its near-surface value.

Measured and modeled parameters relating to wind stress are shown in Figure 42. One parameter plotted in Figure 42a is the normalized quadratic wind speed ratio, C_{UG}^{*} (solid line). This is defined as

$$C_{UG}^{*} = \frac{\left(\frac{U_{10}}{U_G}\right)^2}{0.347} \quad . \tag{28}$$

The 0.347 normalization factor is the average value of $\left(\frac{U_{10}}{U_G}\right)^2$ measured during the CEAREX drift. The value of the geostrophic wind speed, U_G, was determined from an array of pressure buoys which surrounded the *Polarbjoern* during the drift phase. The geostrophic wind was estimated to be accurate to within 1.5 ms^{-1}. This parameter represents a non-dimensional outer layer effect or wind speed effect.

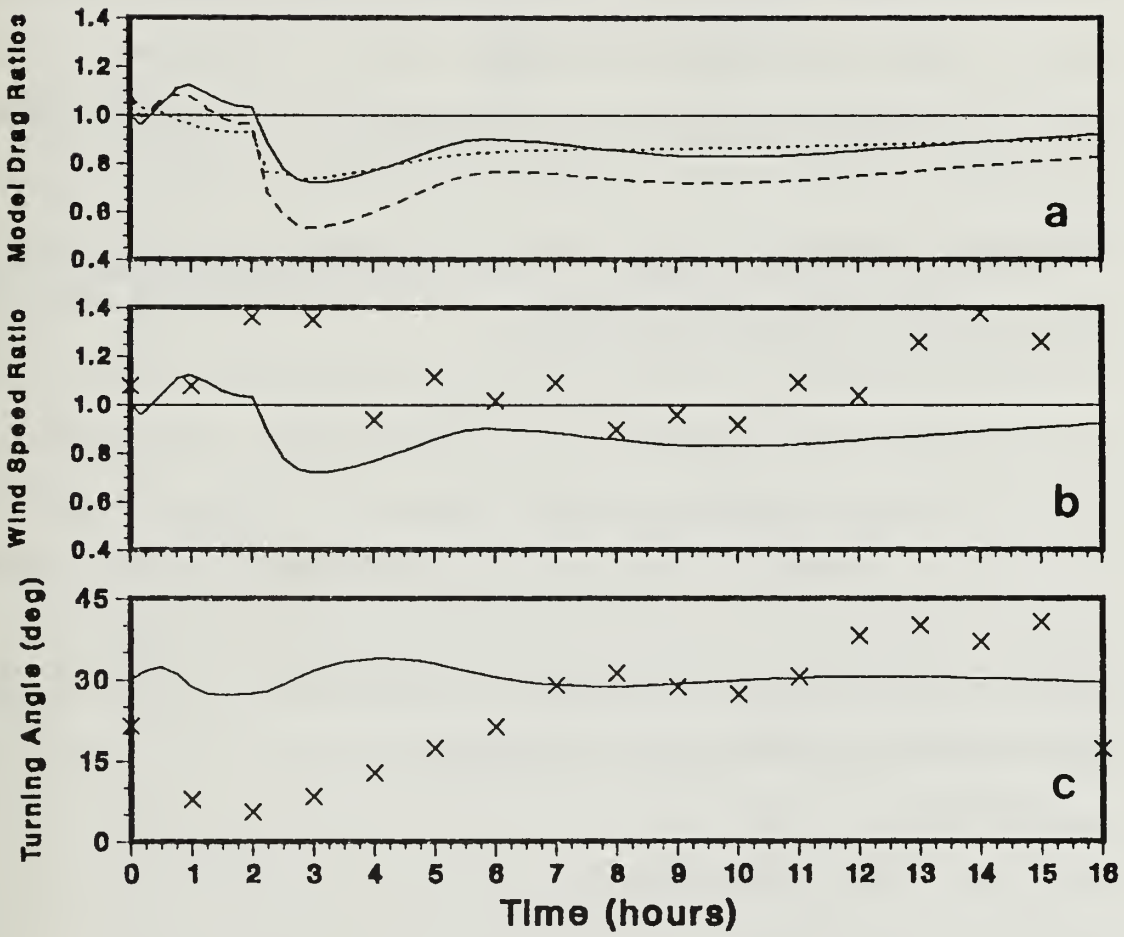

Figure 42 Model Output and Measured Values of Various Parameters Related to Wind Stress for the October 22 Case Study. The top panel (a) shows the model output for the normalized quadratic reduction factor (solid line), the normalized drag coefficient (dotted line) and the normalized quadratic geostrophic drag coefficient (dashed line). The middle panel (b) also shows the model output normalized quadratic reduction factor (solid line) and the measured values (x's). Both panels have a straight solid line to use as a reference for the average value of 1.0. The bottom panel (c) shows model output (solid line) and measured (x's) turning angle. See text for definitions of these parameters.

Another value in Figure 42a is the drag coefficient ratio or normalized surface drag coefficient, C_{d10}^{*} (small dashes) defined as

$$C_{d10}^{*} = \frac{\left(\frac{u_*}{U_{10}}\right)^2}{2.3 \times 10^{-3}} = \frac{C_{d10}}{C_{dn10}} \quad . \qquad (29)$$

This is the same parameter used in Chapter IV to describe surface layer stability effect.

The final parameter in Figure 42a is the normalized quadratic geostrophic drag coefficient, C_G^{*} (dashed line) defined as

$$C_G^{*} = \frac{\left(\frac{u_*}{U_G}\right)^2}{8.2 \times 10^{-4}} \quad , \qquad (30)$$

where 8.2×10^{-4} is the average measured value during the CEAREX drift. This parameter represents a non-dimensional wind stress.

Because

$$C_G^{*} = C_{d10}^{*} \; C_{UG}^{*} \quad , \qquad (31)$$

the relation between wind stress and the geostrophic forcing is a product of the surface layer effect, C_{d10}^{*}, and an outer layer effect C_{UG}^{*}. This is the normalized version of Equation (6).

Although surface stress measurements were not usually available, there were always continuous measurements of the wind speed ratio, C_{UG}^{*}. They appear in Figure 42b along with a repeat of the model C_{UG}^{*} value plotted in Figure 42a.

to keep up and a downward turbulent heat flux is generated, resulting in a strong surface stability effect.

During the third regime (t > 5 hours) the wind stress changes slightly but remains significantly less than during regime 1. The surface temperature begins to drop at a slower rate allowing the 10 meter and ABL air temperature to catch up and form a less stable internal layer below the new capping inversion. When this occurs, C_{UG}^* starts to level off. The mixed layer and surface layer continue to become less stable, but the entire surface/ABL system is cooling faster than the free atmosphere (Figure 40). The effect on wind stress is that during regime 3, C_{d10}^* will become closer to one (neutral) but C_{UG}^* and hence C_G^* will remain "permanently" lower than average. This is because the ABL during regime 3 is shallower than during regime 1 and the continuously strengthening capping inversion limits further growth or contact with higher momentum air in the free atmosphere.

The measured geostrophic wind speed and direction were based on one hour averages. The resulting measured C_{UG}^* and α for each hour are plotted on Figures 42b and 42c. The measured C_{UG}^* does not agree well with the model results. Although there is a drop in measured C_{UG}^* of about 40% two hours after the clearing event (t = 4 hours), there is also an unexpected increase at t = 2 hours and after t = 13 hours. All the modeled C_{UG}^* values were higher than the observations after the clearing event.

The measured α is also poorly correlated with the model values. The observations show a significant trend toward greater turning angle, which might be expected as the internal stable layer strengthens. However the model predicts only small changes in α.

event, and that the wind stress would be 30% less at $t = t_{max}$ due to the surface layer stability effect.

Wind speed, U_{10}, was kept constant for the Chapter IV standard case. But here it is shown that changes in U_{10} due to cloud events are as important as surface stability effects, thus the need for complete ABL physics model studies. The combined effect of C_{d10}^* and C_{UG}^*, as represented by C_G^* (dashed line) is to reduce the modeled wind stress by 50% one hour after the clearing event and 20% to 30% for the rest of the run. If the model is run without removing the clouds (not shown) the value of C_G^* maintains a constant value of about 1.05; therefore the clearing event has had a large effect on wind stress, according to the model.

The time series of model C_G^*, C_{d10}^* and C_{UG}^* (Figure 42a) reveals three "regimes" which illustrate the effect of boundary layer structure and cloud clearing on wind stress. In the first regime ($0 < t < 2$) there is a a slightly stable surface layer below a mixed layer capped by a cloudy inversion at 300 m (Figure 40, line 1). The lack of heat fluxes or unusual ABL structure results in average wind stress values, i.e. C_G^* is about one. (Here t refers to the time of model run, not time after cloud cover change as in Chapter IV.)

In the next regime ($2 < t < 5$), the wind stress is undergoing rapid changes in response to the clearing event. After a very rapid initial decrease before $t = t_{max}$ the wind stress more gradually returns toward a value of about 75% of the average value at about t = 6 hours. During this time period a strong surface-based inversion has formed (not shown). The effect of the surface-based inversion is to prevent momentum from reaching the surface layer so that C_{UG}^* is reduced. At the same time the surface temperature is dropping so fast that the air temperature is not able

to keep up and a downward turbulent heat flux is generated, resulting in a strong surface stability effect.

During the third regime (t > 5 hours) the wind stress changes slightly but remains significantly less than during regime 1. The surface temperature begins to drop at a slower rate allowing the 10 meter and ABL air temperature to catch up and form a less stable internal layer below the new capping inversion. When this occurs, C_{UG}^{*} starts to level off. The mixed layer and surface layer continue to become less stable, but the entire surface/ABL system is cooling faster than the free atmosphere (Figure 40). The effect on wind stress is that during regime 3, C_{d10}^{*} will become closer to one (neutral) but C_{UG}^{*} and hence C_{G}^{*} will remain "permanently" lower than average. This is because the ABL during regime 3 is shallower than during regime 1 and the continuously strengthening capping inversion limits further growth or contact with higher momentum air in the free atmosphere.

The measured geostrophic wind speed and direction were based on one hour averages. The resulting measured C_{UG}^{*} and α for each hour are plotted on Figures 42b and 42c. The measured C_{UG}^{*} does not agree well with the model results. Although there is a drop in measured C_{UG}^{*} of about 40% two hours after the clearing event (t = 4 hours), there is also an unexpected increase at t = 2 hours and after t = 13 hours. All the modeled C_{UG}^{*} values were higher than the observations after the clearing event.

The measured α is also poorly correlated with the model values. The observations show a significant trend toward greater turning angle, which might be expected as the internal stable layer strengthens. However the model predicts only small changes in α.

In summary, in this case study the model qualitatively simulated the thermodynamics of a Type R event well. The actual cooling was greater because the model did not include the cold advection which occurred in nature, but the general pattern of the surface temperature decrease, negative surface heat fluxes and internal boundary layer formation was comparable. The model generated an ABL depth, h, similar to the measured value after 12 hours. The model predicted a major (50%) short term reduction in wind stress and a longer term significant (20%) reduction. The short term model results were consistent with the results of the simple thermodynamics approach used in Chapter IV. However, the measured wind speed ratio and turning angle showed some large variations which may have been related to the clearing event, but they are not reproduced well by the model.

C. OCT 30 CASE STUDY - CLOUD FORMS ABOVE ABL

This case study investigates the response of the ABL and wind stress to cloud formation just above the ABL. The model is initialized (model t = 0) with the 2300 October 29 rawinsonde profile (Figure 43, line 1). The measured geostrophic wind speed was between 9 and 10 ms^{-1} throughout the period. "Very clear" conditions were observed six hours prior to the study period and for the first four hours of the case study. At t = 5 hours mid-level clouds covered the sky. By t = 7 hours the clouds had lowered to just above the ABL. Associated with the cloud lowering was an increase in the measured downward radiation (Figure 44a). At t = 14.5 hours the clouds were observed to clear, resulting in lower radiation. The clearing event at this time was not modeled.

The model created clouds in a layer 650 to 1000 m above the surface at t = 7 hours, causing a more sudden jump in radiation than measured, but at about the

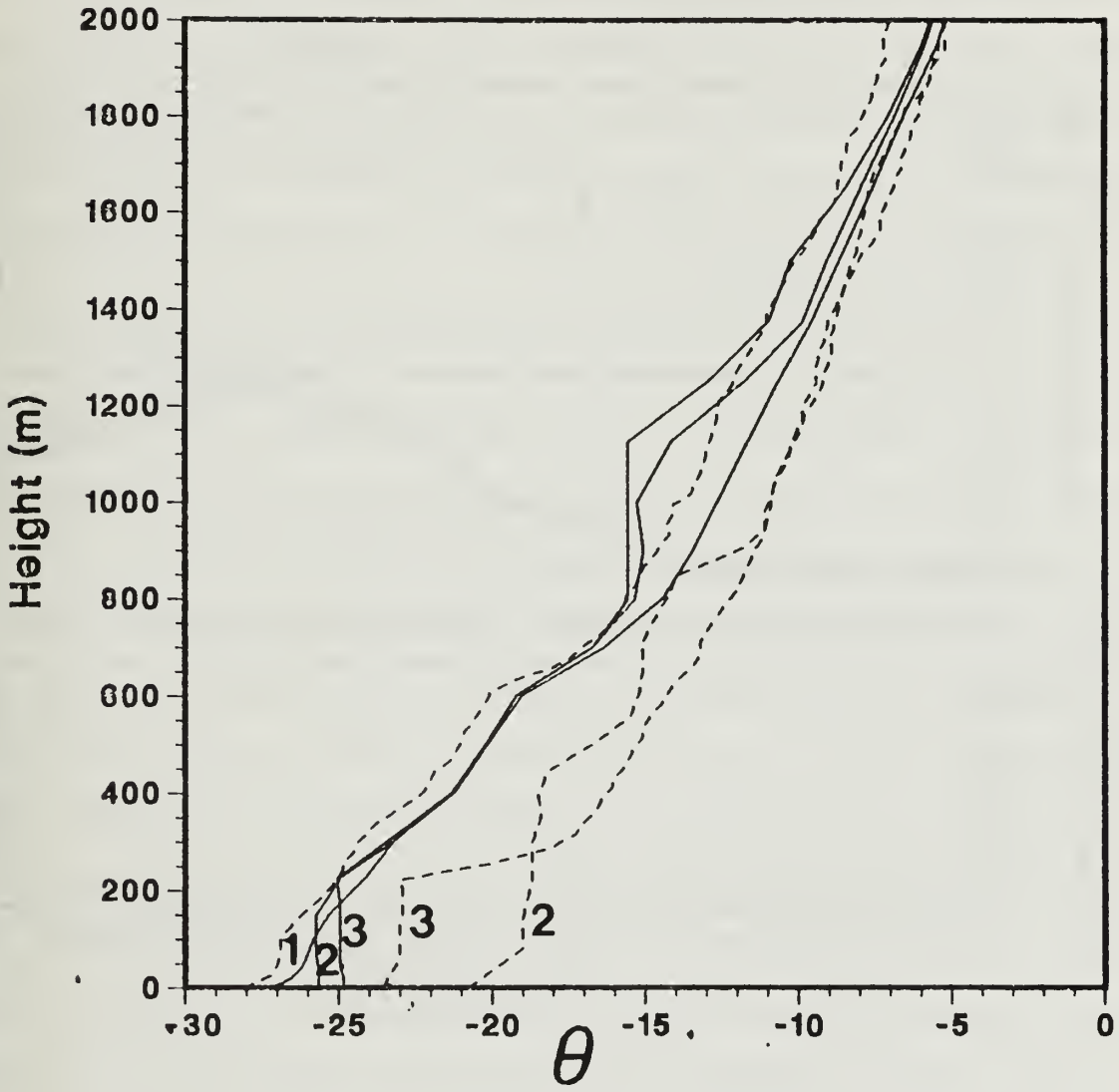

Figure 43 Potential Temperature Profiles for the October 30 Case Study. The model (solid line) and measured (dashed line) initial, 12 hour and 16 hour profiles are labeled "1", "2", and "3".

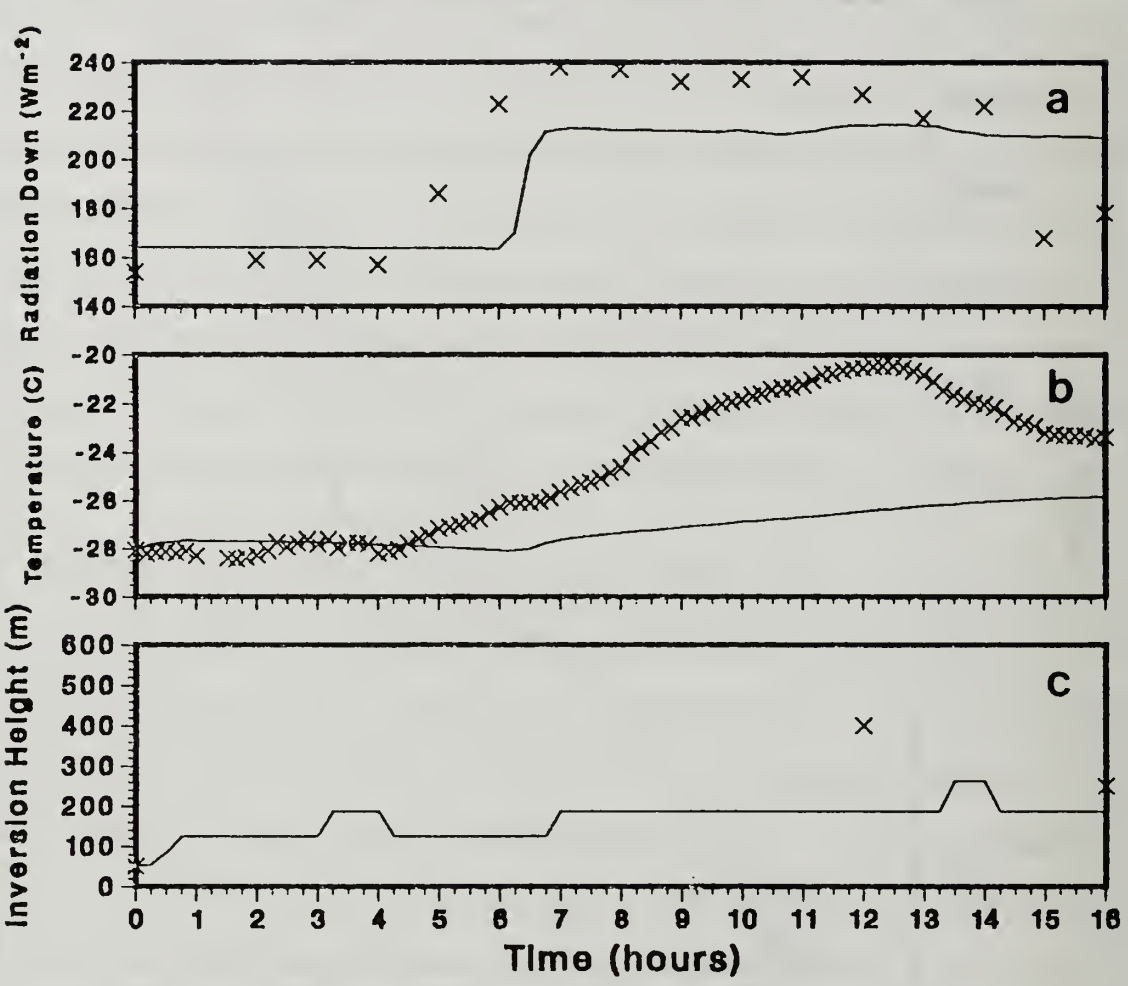

Figure 44 Thermodynamic Variable Times Series for October 30 Case Study. Same point label and line definitions as Figure 41, with some changes in the temperature and radiation Y-axis scales.

correct time (Figure 44a). The measured air temperature increased by 8 C compared to the model 2 C during the eight hour period following the cloud formation (Figure 44b). Toward the end of the run, the measured air temperature decreased 3 C, in association with the clearing event. The model did not have clearing and continued to increase the air temperature. The measured ABL at t = 12 hours was twice as deep as the model simulation (Figure 44b) while another sounding after the clearing at t = 16 hours was just slightly higher than the model value.

The measured potential temperature profiles show a warming at all levels below 1400 m during the first 12 hours (Figure 43). The final (t = 16 hours) measured profile shows that a level of cooler air below 250 m has appeared. Most of these temperature changes must be due to advection, since the surface and radiative heating/cooling are not great enough to explain the measured temperature deviations. The model profiles, which have no advection, show the formation of a mixed layer in the lower 200 m and some cooling of this air. Similar to the previous case study period, the radiational effect of the sky condition change on air temperature is magnified by advection. This is a Type R event in the general sense.

The model normalized wind stress, C_G^*, is below average during the clear period before t = 6 hours (Figure 45a). When the cloud forms, wind stress increases by almost 50% in the one hour and then decreases somewhat. Later at t = 13 hours the wind stress increases due to an increase in the ABL depth. Most of the changes in wind stress are due to changes in wind speed (C_{UG}^*) not changes in surface drag coefficient (C_{U10}^*).

The measured wind speed ratio was near average for the first nine hours (Figure 45b). Between t = 9 hours and t = 13 hours the measured wind speed

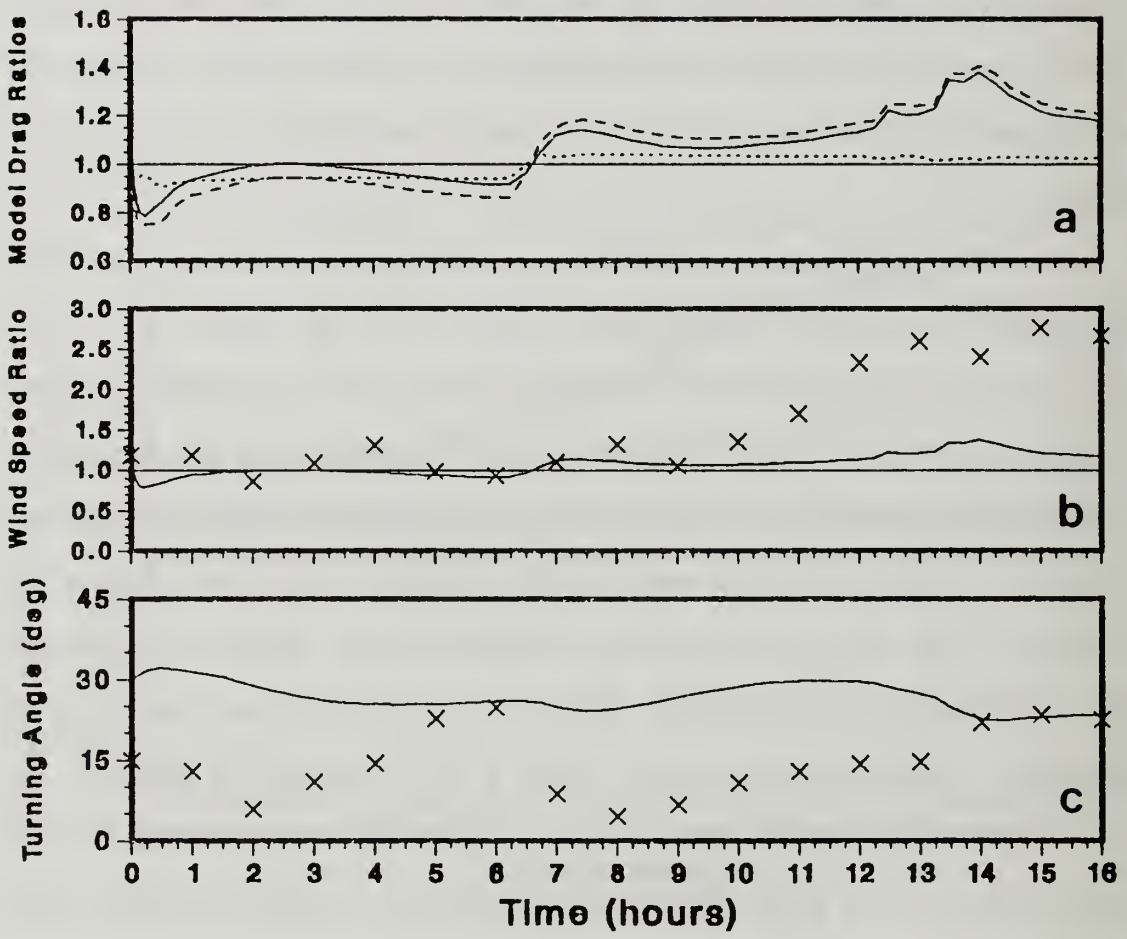

Figure 45 Dynamic Variable Time Series for October 30 Case Study. Same point label and line definitions as Figure 42. Note that unlike Figure 42, the range of the middle plot (b) is larger the range of the top plot (a).

almost doubled while the geostrophic wind remained constant, causing C_{U10}^{*} to increase to 2.5 times the average value. The measured wind speed changes had a similar, but greatly exaggerated pattern compared to the model output.

The measured turning angle, α, sharply decreased after the clouds formed (Figure 45c). The model predicted a slight decrease in α at this time (t = 6 hours). The model α was much more constant throughout the run than the measured values.

In summary, this case study illustrates how upper level clouds can have a large effect on wind stress by destroying the surface inversion or stable layer which is common during clear skies in the Arctic winter. During these moderate (5 - 10 ms^{-1}) winds the surface layer stability effect was small, but the measured and modeled wind stress increased by 50% and 250% respectively due to an increase in wind speed after cloud formation. The large increase in measured wind speed six hour after the initial cloud formation (Figure 45b) may have occurred when a mixed layer underneath the lowering cloud layer first reached the ground. A cloud lowering process was not modeled. The measured profile shows a complicated situation with variable advection at different levels and large changes in wind stress that are not entirely understandable.

D. OCT 21 CASE STUDY - CLOUD FORMATION AND DISSIPATION IN THE ABL

This case study is initialized with the 1100 21 October rawinsonde sounding. The sounding revealed a surface inversion (Figure 46) with surface geostrophic winds of 12.5 ms^{-1} but measured winds of around 6 to 7 ms^{-1} above and below the ABL. The wind just above the ABL is assumed to be geostrophic so there is a strong gradient in the geostrophic wind which could be caused by a sloping inversion. This opposing thermal wind is included in the model for the entire run.

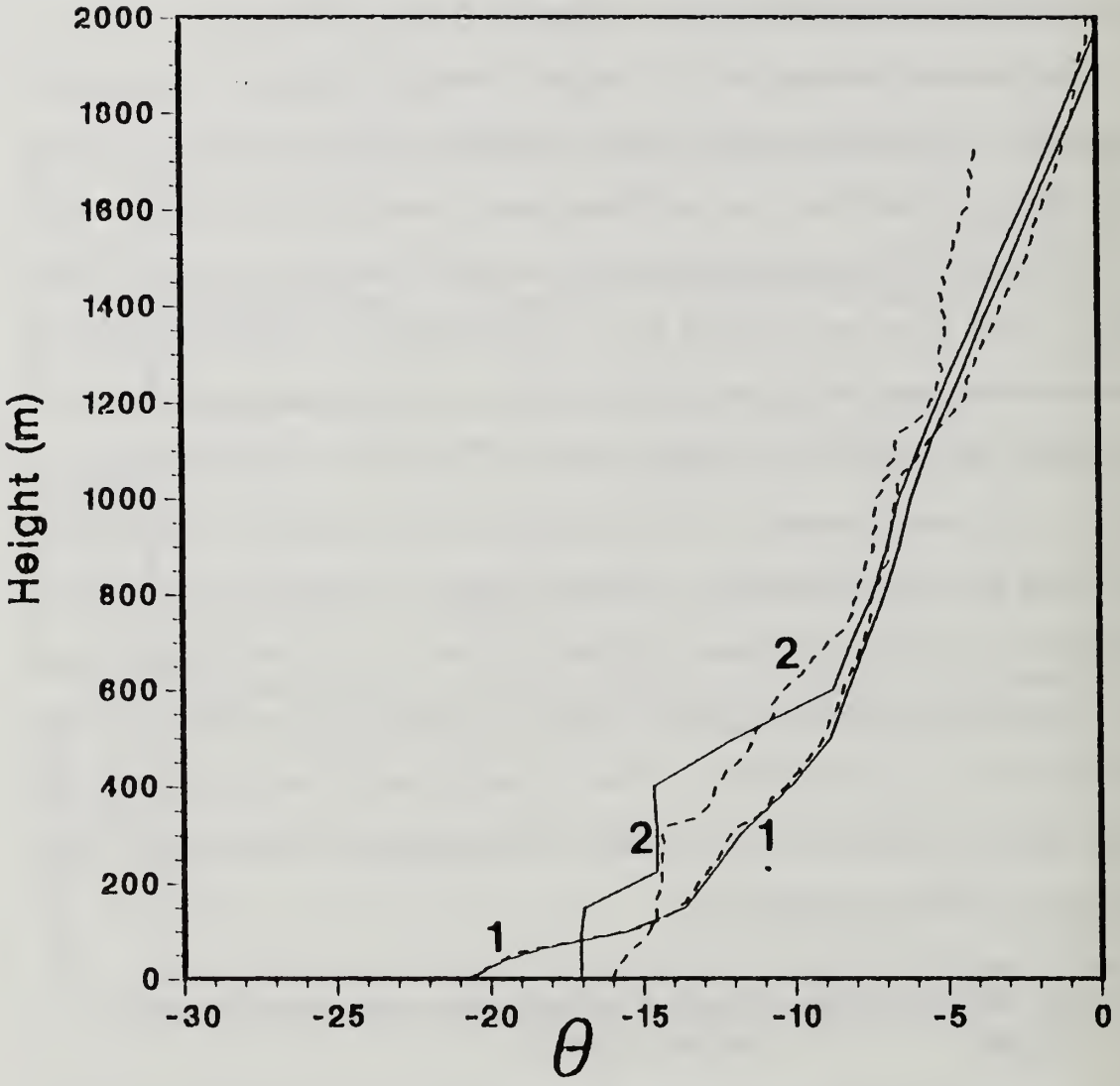

Figure 46 Potential Temperature Profiles for the October 21 Case Study. Same label and line definitions as Figure 40.

Skies were clear until t = 5 hours, at which time the measured and modeled radiation increased sharply as cloud formed at the top of ABL (Figure 47a). At t = 11 hours the clouds were observed to dissipate. Associated with the cloud formation and dissipation was an increase and decrease of measured temperature of 6 C (Figure 47b). The model temperature has the same pattern, but with one third of the amplitude. The measured ABL height after 12 hours was twice the model height (Figure 47c). But the soundings (Figure 46) reveal a similar pattern in the temperature structure between the measurements and the model. Both have an upper level mixed layer capped by an inversion associated with the cloud layer. Below the mixed layer the rawinsonde profile has a stable layer while the model had another inversion/mixed layer combination. In other similar case studies not shown here, any clouds which formed in the ABL tended to separate from the ABL and increase in height. The clouds were kept low in this case study by imposing a negative moisture tendency just above the ABL. Still, layer separation occurred.

The model wind stress was lower than average during the initial five-hour clear period, due equally to low normalized wind speed and drag coefficient (Figure 48a). Immediately after cloud formation the wind stress increased by about 15%, mostly because of the surface layer stability effect. The wind speed, as shown by C_{UG}^{*}, does not increase by much during the first two hours after cloud formation (5 < t < 7 hours) because the upper level air that is being entrained does not have the usual high momentum because of the opposing thermal wind. After t = 8 hours the surface layer stability is nearly neutral but the wind speed is enhanced causing the wind stress to become 20% greater than normal. At t = 13 hours the model clouds are removed and wind stress drops by 40% due to both wind speed (outer layer) and surface layer effects.

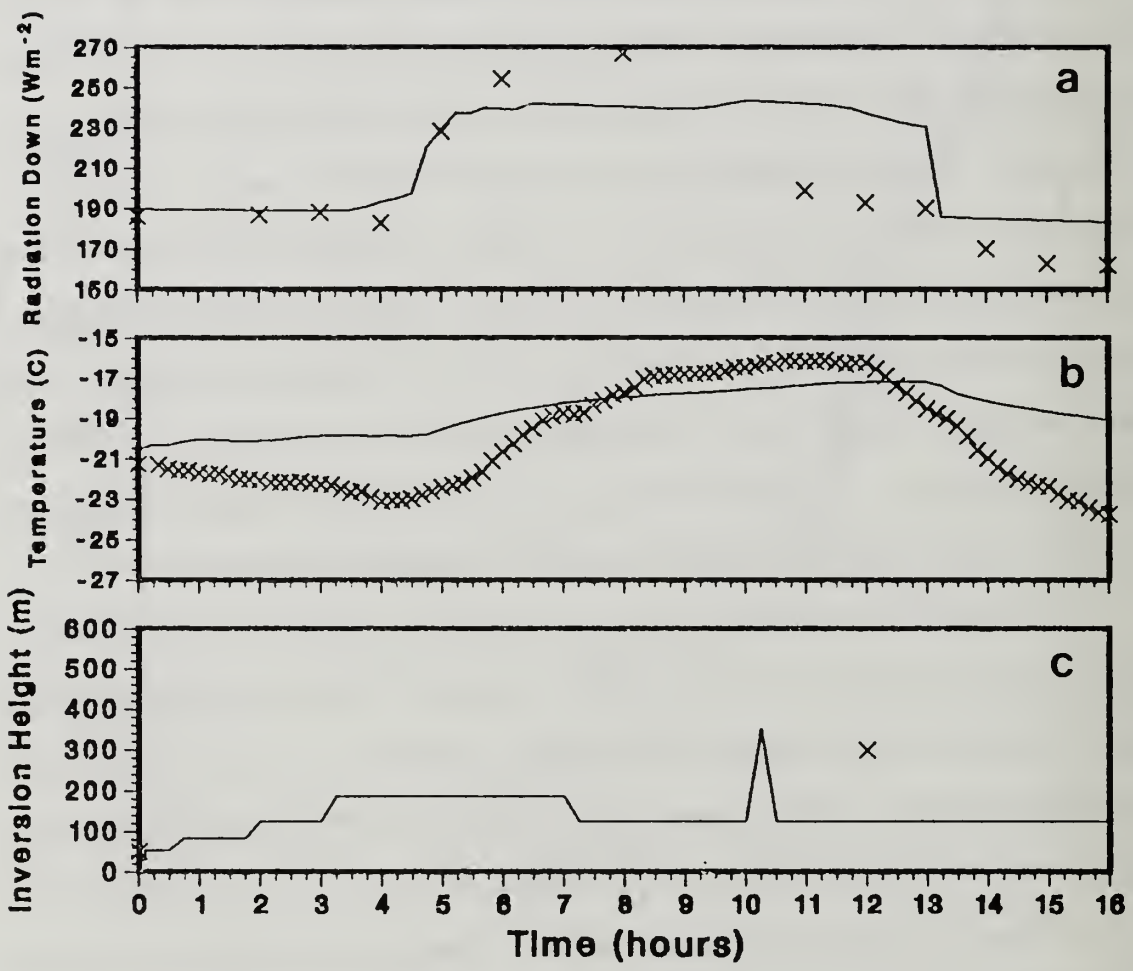

Figure 47 Thermodynamic Variable Times Series for October 21 Case Study. Same point label and line definitions as Figure 41, with some changes in the temperature and radiation Y-axis scales.

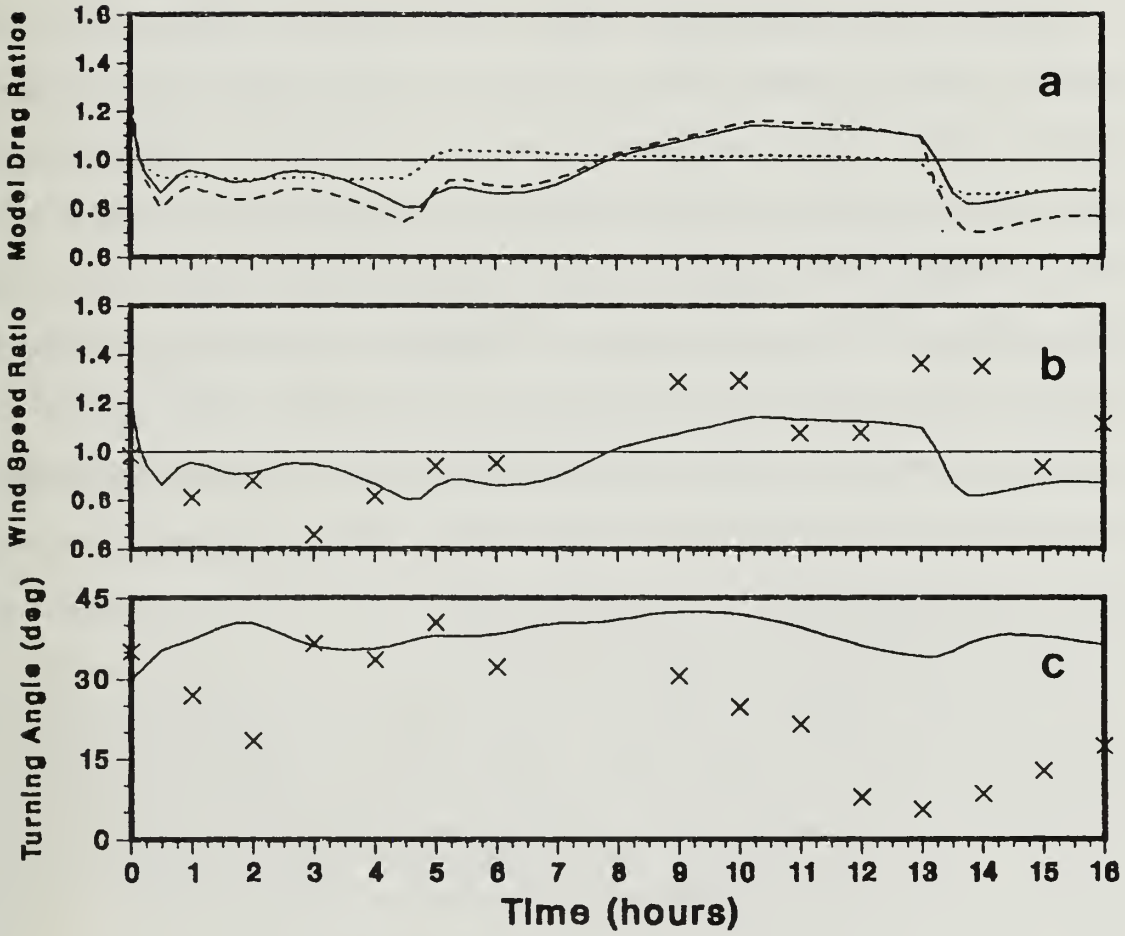

Figure 48 Dynamic Variable Time Series for October 21 Case Study. Same point label and line definitions as Figure 42.

The measured C_{UG}^{*} was lower than normal before the cloud formation (Figure 48b) and increased by about 50% and dropped at the end of the run. This pattern matched the model quite well. The modeled and measured α were quite high, as expected, during the five hour initial clear period (Figure 48c). After the clouds formed, the measured α decreased to a very small value while the model α decreased only a little.

In summary, the surface layer stability in this case study followed the same pattern as the previous case studies and Chapter IV cases, with a rapid deviation immediately after the sky condition change, and then a slow decrease toward neutral. The surface layer stability effect was not great due to the relatively high winds. The major factor causing the modeled changes in wind stress was the wind speed variation. Unlike the earlier cases, the modeled wind speed was not greatly affected by the cloud formation until a few hours later. The model appeared to reproduce the wind stress effects of the cloud formation and clearing quite well. Here, the effect of clouds was significant even during higher wind speeds.

E. OTHER MODEL SIMULATION RESULTS

Many other situations related to cloud effects were simulated with the ABL/Snow/Ice model. Some general results from these simulations will be summarized without showing each case. The response of wind stress to cloud effects depended on the dynamic and thermodynamic structure of the atmosphere, as well as the ice/snow characteristics discussed in Chapter IV.

An important dynamic feature is the thermal wind. The model showed that presence of a thermal wind can counteract or amplify cloud effects depending on the orientation of the thermal wind and whether the ABL is growing or shrinking.

Simulations of strong surface-based inversions, which often form under clear skies during light winds, resulted in the lowest normalized wind stress values. When clouds form during these conditions, the relative change in wind stress is large because the normalized wind stress changes from a very low value to an average or above average value.

The largest effect on wind stress occurred when there was a very low stable ABL with a deep neutral layer above. If cloud formation can warm the cold air and deepen the ABL to the top of the neutral layer, wind stress increases by a factor of two or three.

As a test of long term cloud effects, the model was run for periods of several days. It was hard to draw conclusions with the 1-D model because the long term effects of the clouds were dependent on the specification of temperature and humidity advection. Without any warm advection, a cloud layer near in the lower atmosphere continues to cool to unrealistically low temperatures or dissipate after a few days. The location of the clouds was a crucial factor in determining the long term wind stress effect. In the long term, the effect of the surface fluxes becomes small but the depth of the ABL is an important factor. If the clouds are well above the ABL, their effect on wind will become small after the initial surface flux event. But if there is a cloud layer just above the ABL it may be cool enough to be incorporated into the ABL, thus increasing h and the wind stress.

F. CASE STUDY CONCLUSIONS

The numerical studies show that clouds can have a substantial effect on wind stress by influencing the surface layer wind speed and stratification. With moderate surface winds, a cloud formation/dissipation event will change wind stress by at least

40% temporarily and about 15% permanently. The verification measurements showed amplified temperature responses in some cases, caused by advection. The normalized verification wind stress had large deviations that appeared to be related to the cloud events but did not match the model well in most cases. The deviations in measured turning angles were poorly modeled.

The ABL in the Arctic is rarely in a steady-state situation. Horizontal changes in upwind surface roughness, cloud cover, temperature, geostrophic forcing, etc. change on time scales shorter than the model runs, which assume constant forcing conditions. Therefore verification of the model with the measurements was not expected.

The examination based on measurements and model predictions shows that, all other factors being equal, clouds have a significant effect on wind stress. The surface layer effect is quite straightforward and the complete physics model gives similar results as the Chapter IV thermodynamic model. The outer layer (wind speed ratio) effect is often greater than the surface layer effect, especially during higher winds. This effect depends on a number of factors such as thermal wind, inertial effects, ABL depth, surface fluxes and cloud location.

Verification of the cloud effect is difficult because the measured wind stress has a large amount of unaccounted variability. The model predicts stress values which seem to be reasonable averages of several measurements, but may not compare well with one particular measurement.

VI. STATISTICAL RELATIONSHIPS BETWEEN CLOUDS AND WIND STRESS

The effect of clouds on wind stress was examined for a few short periods in the previous chapter. To quantify average cloud effects, the relationship between clouds and wind stress using all valid geostrophic wind measurements from the CEAREX drift will be studied.

The relationship between ABL structure and clouds was quantified in Chapter III. This chapter continues that line of reasoning to explain the effect of clouds on wind stress by first describing the relationship between wind stress and bulk ABL properties. Then the direct correlation between observed cloud cover or relative humidity and wind stress will be analyzed.

Because the surface heat flux and momentum measurements were usually not available, all geostrophic drag coefficients, $C_G = \frac{u_*}{U_G}$, in this chapter assume a constant surface drag coefficient, C_{d10}. Therefore, variations of C_G are only due to ABL-influenced variations in the ratio of surface wind speed to geostrophic wind speed. The wind vector was determined from buoy array.

A. WIND STRESS AND ABL STRUCTURE

Clouds are expected to affect wind stress by changing the structure of the ABL, which in turn affects the transfer of momentum to the surface. The relationship between ABL structure and clouds was quantified in Chapter III. In this section, the relation between ABL structure and wind stress will be verified for winter Arctic conditions. A study (Guest, 1992) of all factors, not just clouds, affecting C_G will be summarized because ABL, including surface layer, structure

provides the mechanism by which clouds affect wind stress. ABL structure must have an effect on wind stress in order for clouds to affect wind stress.

Using the CEAREX measurements, OD defined a static stability measure based on the temperature difference, $\Delta\theta$, and distance, z_{900}, between the surface and 900 mb level

$$N^2_{900} = \frac{g\,\Delta\theta}{\overline{\theta}\; z_{900}} \quad . \tag{31}$$

The following empirical equation explains 17% of the variation in geostrophic drag coefficient, C_G, assuming constant C_{dn10}.

$$C_G = 0.037 - 0.0083\left(\frac{N_{900}}{0.024}\right)^4 \quad . \tag{32}$$

An expanded CEAREX data set, compared to OG, was created for this study. Data from the entire CEAREX drift period September 17 - November 17 were used except for some obviously spiky geostrophic winds, very low winds and a few outliers. Many different stability parameters were tested for correlation with C_G. The method based on the N_{900} parameter explained 14.3% of the C_G variance using the expanded data set (Figure 49). This was as good or better than any other tested stability parameters.

The best predictor for the turning angle was based on a measure of the strength of the lowest part of the inversion defined as

$$N_{inversion} = \mathrm{Ln}\left(\frac{g\,\Delta\theta}{\overline{\theta}\; 100}\right) \quad , \tag{33}$$

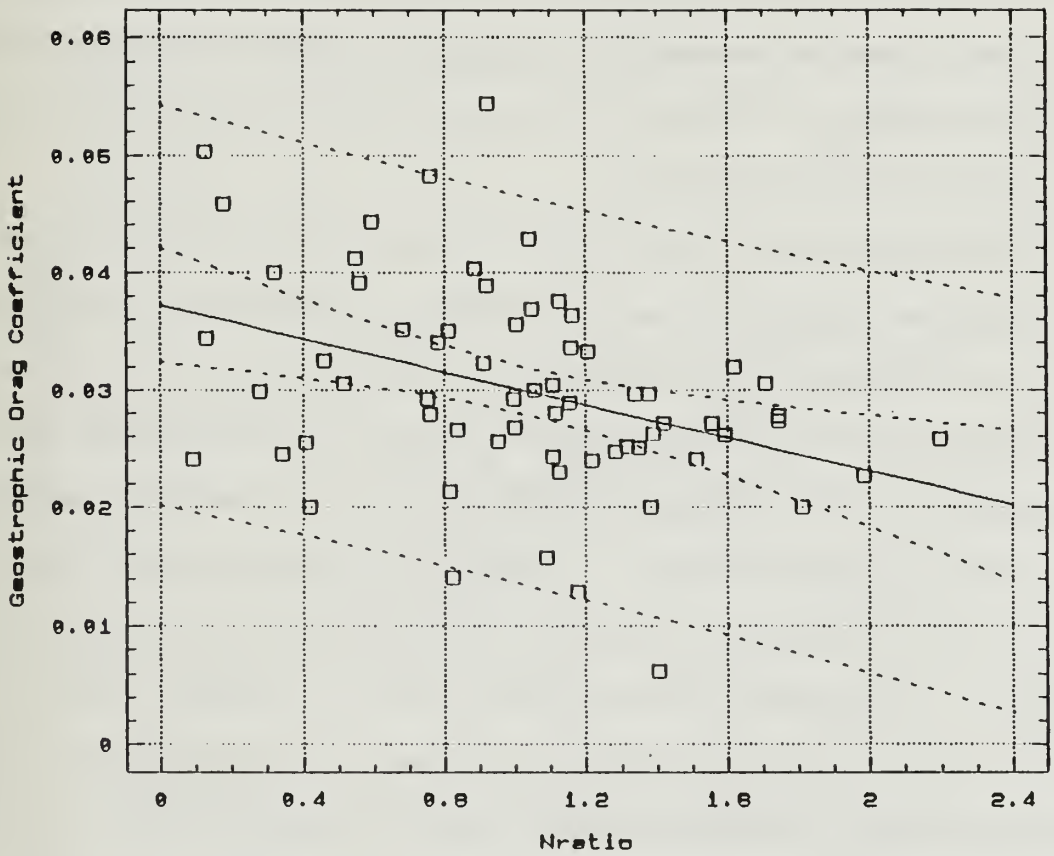

Figure 49 The Effect of $N_{ratio} = (N_{900}/0.24)^4$ on Geostrophic Drag Coefficient During the CEAREX Drift. The solid line is the linear regression fit, the inner dashed lines are the 95% confidence intervals of the regression and the outer dashed lines are the 95% data range limits.

where $\Delta\theta$ is the difference in temperature between the inversion base height, Z_i, and 100 meters higher or Z_i + 100. This parameter accounts for 23.3% of the variance in turning angle (Figure 50). Stronger inversions are associated with greater turning angles.

Inversion base height, Z_i, is also correlated with the wind stress vector because higher inversion bases are associated with increased C_G (Figure 51) and decreased turning angle (Figure 52). The largest C_G and turning angle effects are seen for the surface-based inversions, Z_i = 0, cases.

A statistical test to prove that Z_i is related to wind stress is performed because of the large scatter in Figures 51 and 52. The ABL data with classic inversions are divided into two groups, one group with surface based inversions (Z_i = 0 m) and the other group with elevated inversions (Z_i > 100 m). The surface inversion group has an average C_G and turning angle of 0.0237 and 27.8 degrees, while the elevated inversion group has values of 0.00313 and 21.3 degrees, representing a 40% average difference in scalar wind stress. One-sided t-tests showed that the two groups are different in C_G and turning angle with greater than 95% confidence. While the elevated inversion cases occur during clear and cloudy weather, almost all of the surface inversion cases occur during clear weather. When a surface-based inversion is present, atmospheric stratification has the greatest effect on the measured C_G; the absence of clouds is required for these situations to occur.

B. WIND STRESS AND CLOUDS AND MOISTURE

The previous section demonstrated that a statistical relationship exists between ABL structure and wind stress vector. This section will look at the direct statistical relationship between wind stress and low cloud amount, N_L. For this, the

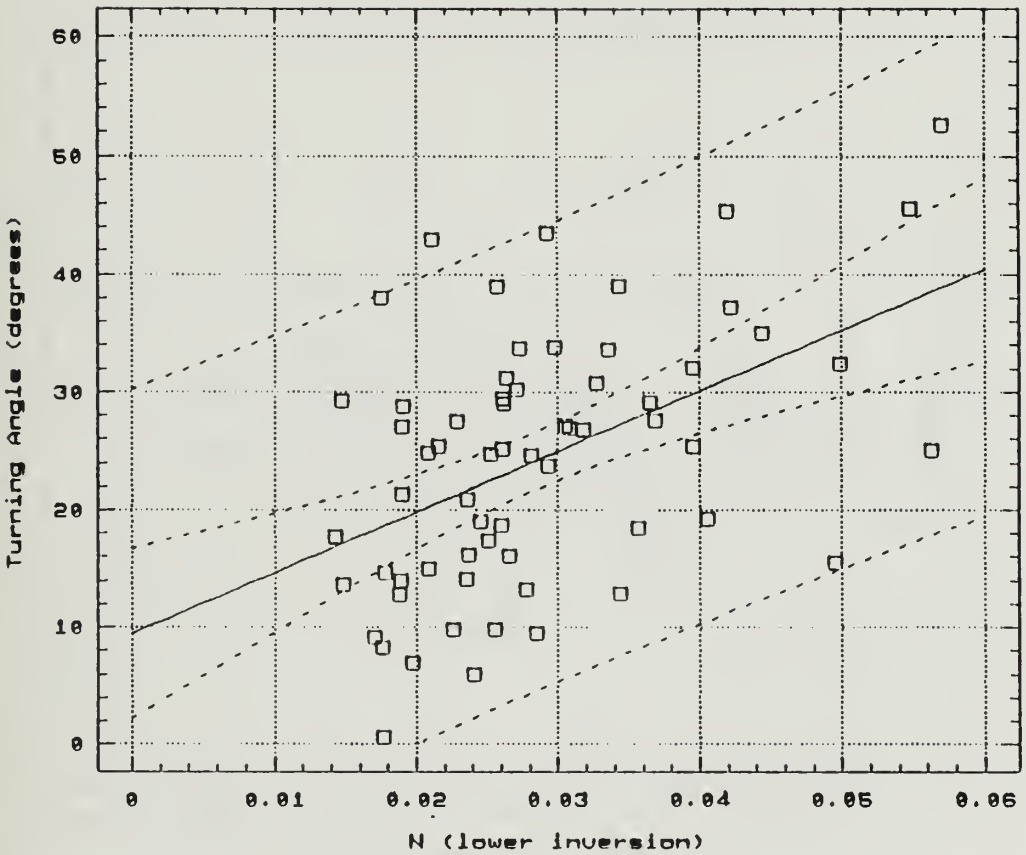

Figure 50 The Effect of $N_{inversion}$ on Turning Angle, α. Same line definitions as Figure 49.

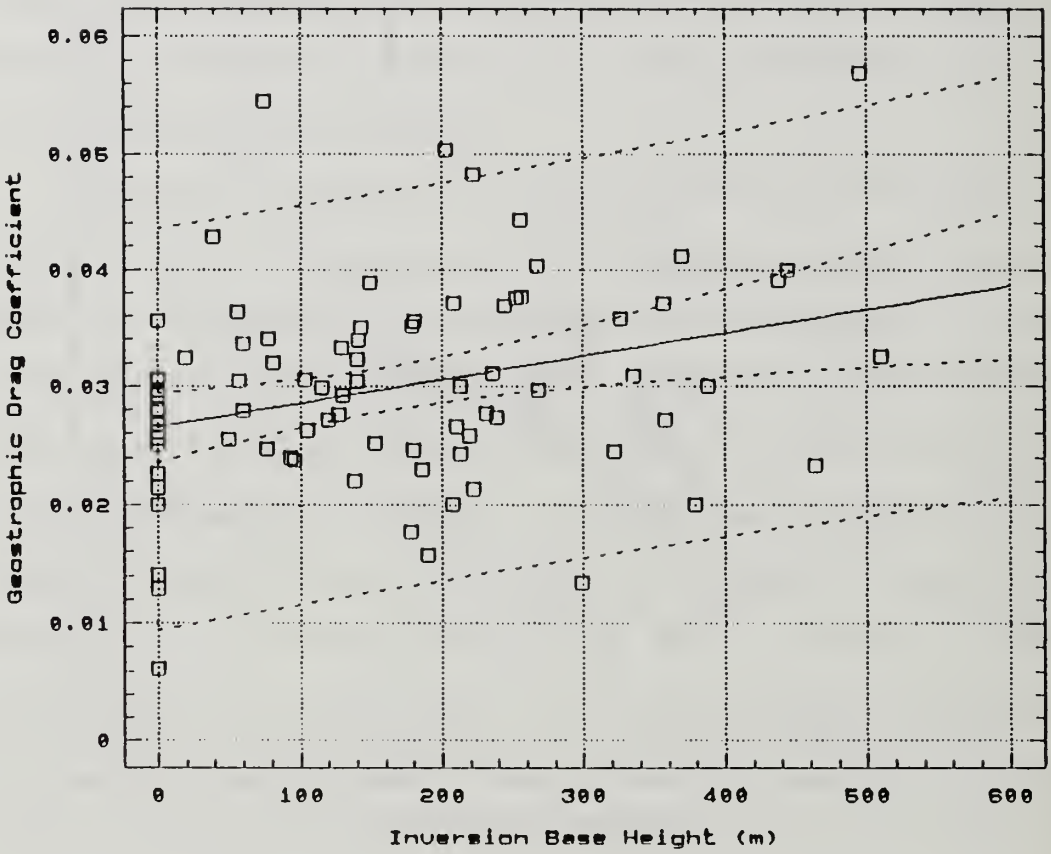

Figure 51 The Relation Between Inversion Base Height, Z_i, and Geostrophic Drag Coefficient, C_G, During the CEAREX Drift. Only classic ABLS (see Chapter IV for definition) are shown.

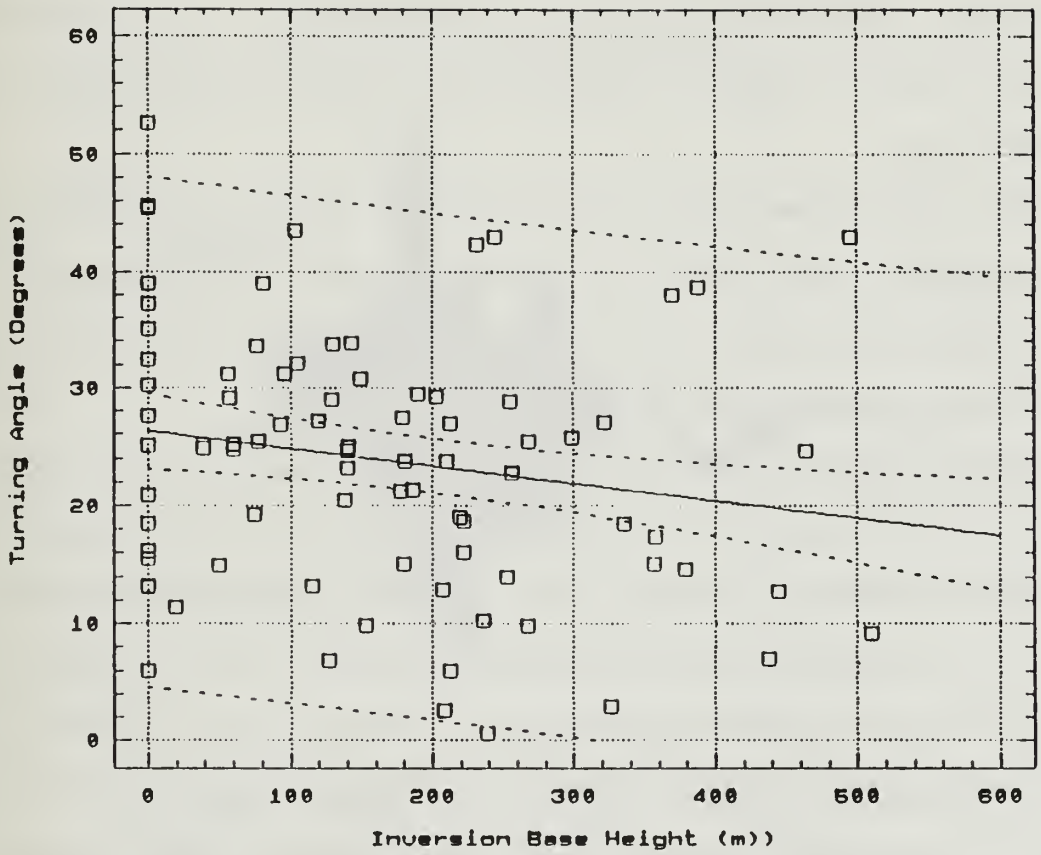

Figure 52 The Relation Between Inversion Base Height, Z_i, and Turning Angle, α, During the CEAREX Drift.

CEAREX data were divided into a group with no low clouds (N_L = 0 octals) and a group with low overcast (N_L = 8 octals).

The frequency histograms of C_G for the two groups reveals that there is not a clear separation in the distributions (Figure 53), but that the overcast group has a higher average C_G than the clear group, a value of 0.0311 vs. 0.0280, respectively, representing a 19% difference in average normalized stress. A one-sided t-test shows that there is a significant difference between the two groups at the 90% confidence level.

The average turning angles for the clear vs. low overcast group are 25.0 and 18.7 respectively. The difference is significant to the 95% confidence level. However, there is considerable scatter shown in Figure 54; therefore virtually any turning angle is possible for any cloud coverage.

Another parameter related to clouds and longwave radiation is the humidity. The relation between relative humidity at several different levels and C_G was tested. The relative humidity at Z_i, $RH(Z_i)$ as the most highly correlated with wind stress (Figure 55). An analysis of the rawinsonde measurements of relative humidity, RH, showed that values of greater than 98% are never measured; this is apparently the limit of the hygrometer on the rawinsondes. If RH was between 93% and 98%, clouds may or may not be present. Clouds are rarely observed if RH is below 90%. Therefore, it is difficult to be sure if a cloud layer exists from a moist (RH > 93%) rawinsonde sounding, but a dry sounding always indicates no cloud is present. For the results of this dissertation, cloud amount was based on human observations, but often a rawinsonde or model output is the only moisture or cloud information available. The points to the left of Figure 55 were mostly from clear periods and have generally low C_G values. The points to the right were from clear and cloudy

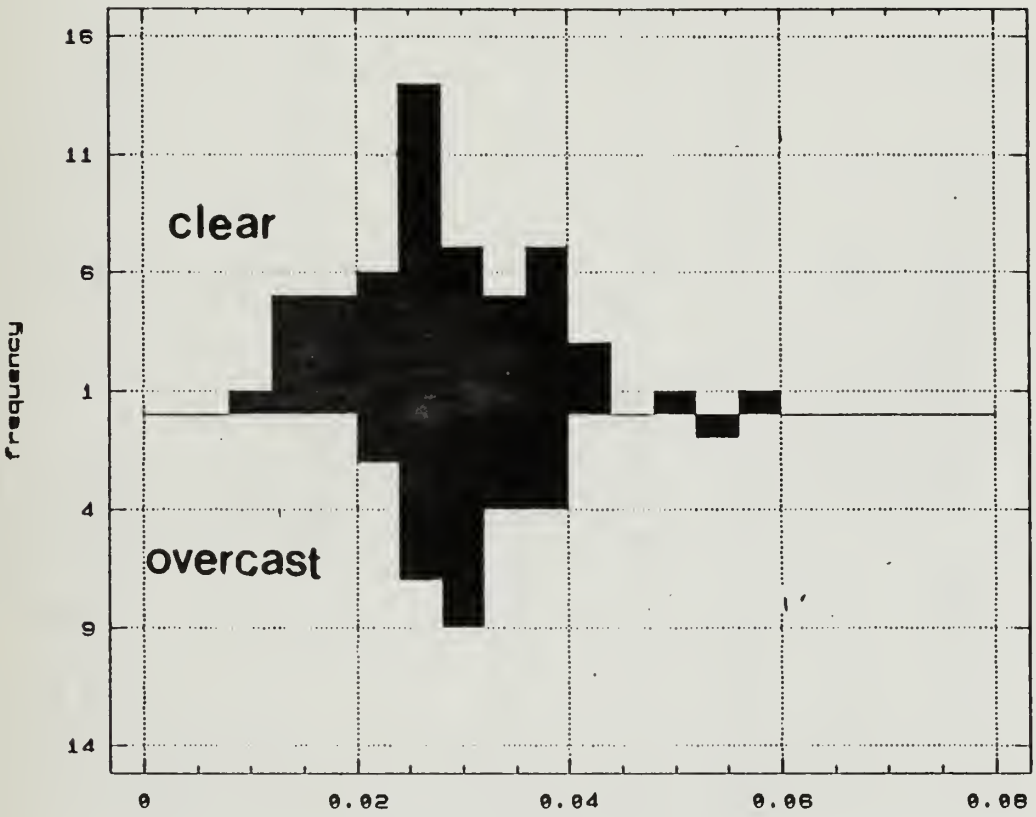

Figure 53 Distribution of C_{ci} for Clear (upper) and Overcast (lower, upside down) Cases. The X-Axis represents different bins of C_{ci} values, while the y-Axis shows the number of occurrences (frequency).

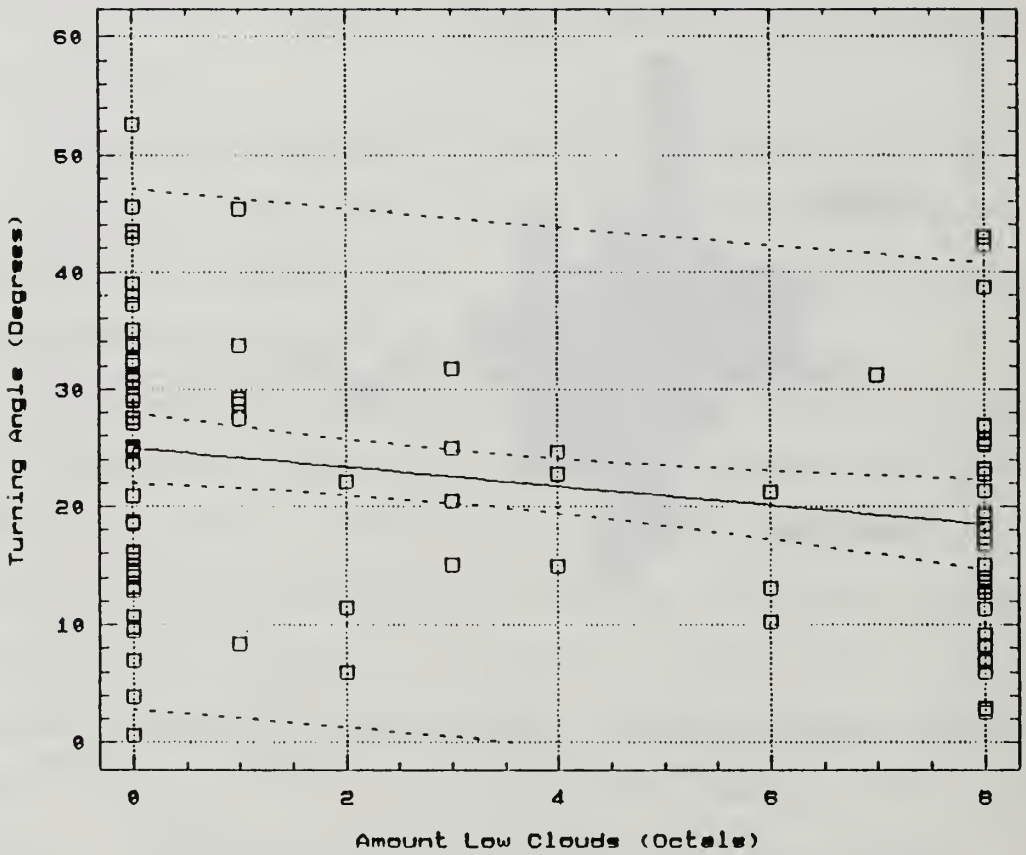

Figure 54 The Relation Between Amount of Low Cloud Coverage and Turning Angle.

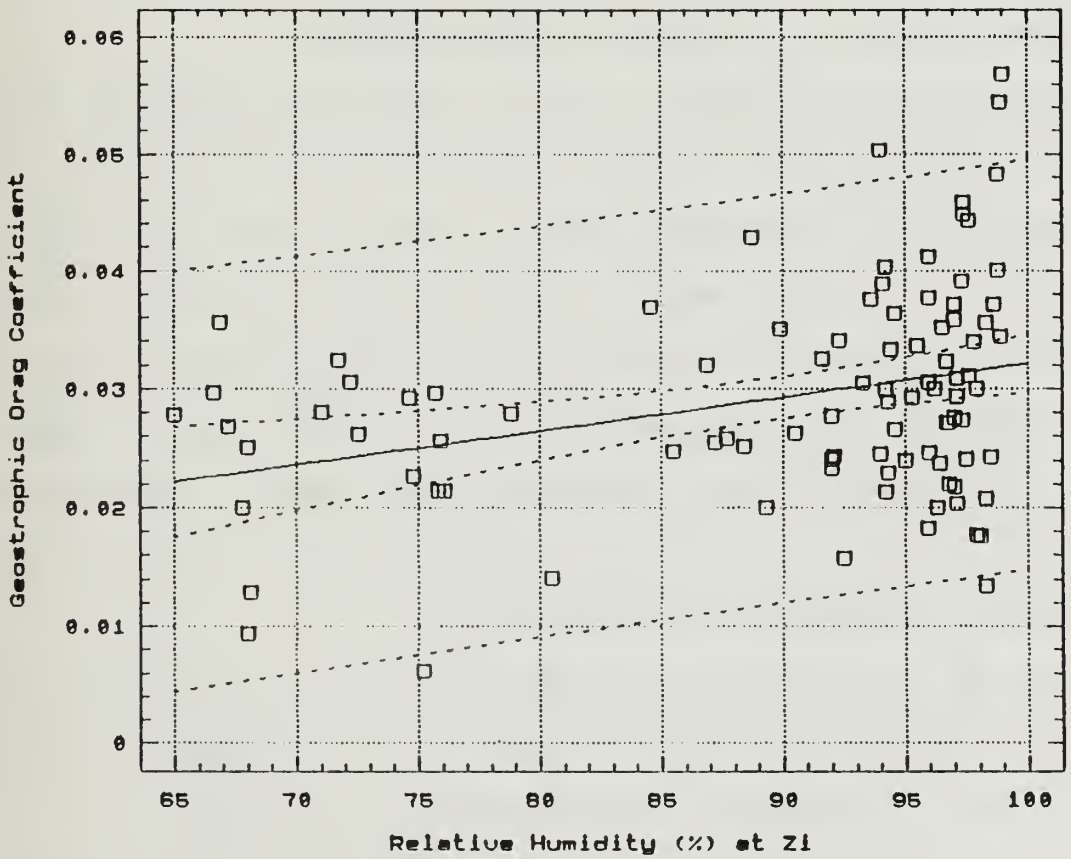

Figure 55 The Relation Between Relative Humidity at the Height of the Inversion Base and Geostrophic Drag Coefficient.

periods and have a large range. Ninety per cent of the greatest C_G values occurs at RH > 93%.

A similar relation between relative humidity and turning angle exists (Figure 56). The average turning angle is smaller for high humidity and the lowest turning angles occur during high humidity periods.

C. CONCLUSIONS ON STATISTICAL RELATIONSHIPS

These results show a statistically significant relationship exists between ABL structure and wind stress, as quantified by the stress parameters C_G and α. The static stability based on temperature difference between the surface and 900 mb, N_{900}, from OD provided the best fit for the C_G values, of the several stability parameters tested. A function based on the strength of the lower inversion, $N_{inversion}$, was the best predictor for turning angle. Surface-based inversions had substantially lower average normalized stress and greater turning angles, α, than elevated inversions. The variations in average stress parameters as a function of Z_i is negligible when considering elevated inversions only.

There was a 19% difference in average normalized stress between clear and overcast conditions but only 6% of the variance in C_G is explained by cloud coverage. These results represent the wind speed (outer layer) effect only. The actual wind stress is also affected by surface layer stability effects. Because surface layer stability effects usually augment the wind speed in affecting wind stress, as shown in Chapter V, the average difference in actual wind stress was larger than 20%.

Correlation does not prove cause and effect; there is the possibility that the value of C_G and/or α is physically affecting the formation of clouds, instead of vice

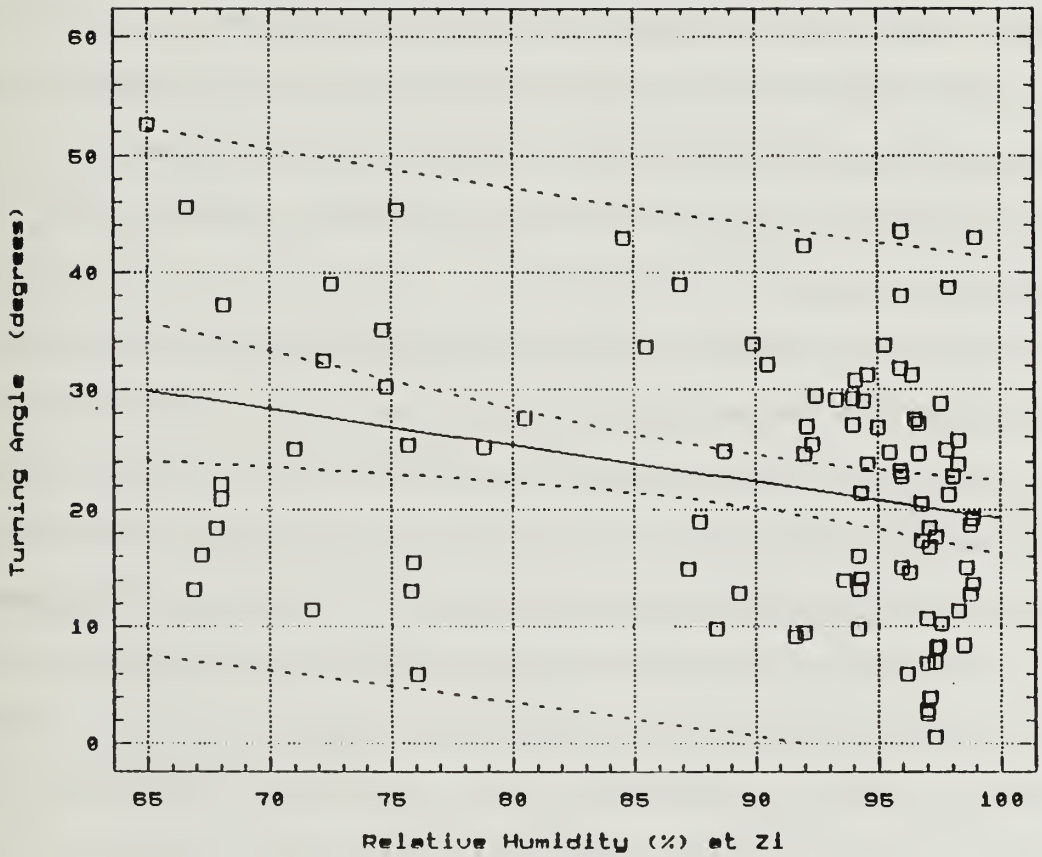

Figure 56 The Relation Between Relative Humidity at the Height of the Inversion Base and Turning Angle.

versa, or that some third factor affects both clouds and wind stress. Cloudiness is a function of moisture, subsidence, surface fluxes and other 4-dimensional factors. Wind stress has no effect on clouds above the ABL and is only a contributing factor for ABL clouds, so there is not a strong physical link by which changes in C_G and/or α can affect cloud formation. The geostrophic wind speed is the most dominant third factor which causes a spurious correlation to exist between clouds and wind stress. An increase in pressure gradient increases wind stress and deepens the ABL, making cloud formation more likely. But by using a normalized wind stress parameter such as C_G, the wind speed effect on wind stress is removed. Other third factors are discussed in the final conclusions.

Surface-based inversions are associated with suppressed wind stress, on the average. The surface base inversions virtually only occur during clear weather. But clear weather does not guarantee the existence of a surface inversion. Therefore, although one can predict wind stress is likely to be suppressed if a surface-based inversion exists, one cannot predict that clear skies will always suppress wind stress.

Another relationship was that virtually all of the most enhanced C_G values occurred when $RH(Z_i)$ was high, but high $RH(Z_i)$ conditions were also associated with normal C_G values. So enhanced C_G can be used to predict high $RH(Z_i)$. But the reverse process is not true; high $RH(Z_i)$ does not guarantee suppressed C_G. In other words, high $RH(Z_i)$ is a necessary but not sufficient condition for large enhancement of C_G and low turning angle.

The enhanced and normal wind stress values which occur when $RH(Z_i)$ is almost 100% can be explained as follows. A larger C_G difference is expected to occur between clear and cloudy conditions than between different RH values. Because some of the high $RH(Z_i)$ values occurred during clear weather, this would

mix low C_G values from the clear periods with the high C_G values from the cloudy periods. On the other hand, the low RH values were virtually all clear sky cases, therefore no large enhanced values occurred when RH was below 90%.

The best fit for average C_G as a function of $RH(Z_i)$ is not linear as shown in Figure 55. Most of the change in average C_G occurs between 93% to 98% relative humidity. An explanation for this could be that much of the variation apparently related to RH is actually related to the amount of cloud cases within each RH bin. The most changes in cloudiness conditions between RH bins occurs above 93%.

Another factor to consider is cloud history. Clear air which has a high humidity may have been cloudy recently and the ABL structure created by the previous cloud could still affect wind stress. Thus, some of the clear cases had a C_G which had earlier been enhanced by clouds. But below 90%, the clear cases probably had been clear for some time, so there are no enhanced C_G cases.

Possibly because humidity is an indicator of cloud history, which may in some cases be more important than current cloud conditions, $RH(Z_i)$ seems to be a better predictor for C_G than current cloud conditions.

VII. CONCLUSIONS

A. SUMMARY OF FINDINGS

This study shows that clouds affect wind and wind stress during the central Arctic dark season. The significance of clouds is supported by measurements and model predictions. However, a lower than expected correlation between cloud coverage and wind stress exists when the entire data set is considered.

Model predictions and observed results show that clouds have a strong effect on ABL structure. They also show that ABL structure is linked to normalized wind stress as represented by C_G. A physical link between clouds and wind stress has been demonstrated.

The effect of clouds on wind stress is a function of time after the last cloud formation or dissipation event. Therefore, existing cloud conditions are not as related to wind stress as the previous cloud changes or cloud history in an air mass. Correlations between relative humidity at the inversion base, $RH(Z_i)$, and wind stress were higher than clouds vs. wind stress correlations. This is further evidence that cloud history is important.

Two regimes of cloud effects on wind stress were identified. The first regime, which lasts for a few hours, consists of a sudden change in downward radiation at the surface due to a cloud formation/dissipation event which changes the surface temperature rapidly, so that surface heat fluxes are generated. This causes surface layer stability effects which change the value of C_{d10} and wind stress. The surface heat flux affects the outer layer (ABL above the surface layer) by causing entrainment and modifying turbulence. This changes surface wind speed and C_{UG}^{*}

on the same order of magnitude as the C_{d10}. The combination of these effects would cause a wind stress change of about 40% maximum. This maximum occurs about one hour after the cloud change for typical Arctic winter conditions. The wind stress changes during the first regime depend primarily on wind speed, thermal wind, ABL depth, magnitude of radiation change, snow age and, sometimes, snow depth.

The second regime begins when heat fluxes become small, typically 4 to 24 hours after a radiation change. Surface heat fluxes are small, but the atmospheric thermodynamic structure has undergone changes which permanently affect wind stress. A typical second regime cloud effect is 15%. This varies depending on whether the cloud layer exists within or above the ABL. If the cloud layer is within the ABL, the cloud layer is dynamically coupled to the surface and the cloud effect is greater than for upper level clouds. The initial lower atmospheric structure is important. Under certain conditions, the initial ABL structure will be radically changed by cloud formation. For example, if a weak surface inversion is capped by a thick mixed layer, clouds may trigger a large deepening event and increase wind stress more than average. A cloud clearing event when the ABL is deep may cause the formation of an internal ABL and suppress wind stress. If the ABL is already shallow before a clearing event or already deep before a clouding event, then the second regime effects of clouds on wind stress will be small.

The wind velocity at the surface is forced not only by surface geostrophic wind but by the ABL integrated geostrophic wind. A thermal wind near the top of the ABL, common with sloping inversions, will affect wind stress depending on whether ABL depth is increasing or decreasing with time and on the orientation and magnitude of the thermal wind, relative to the wind stress vector.

B. SIGNIFICANCE OF RESULTS

Clouds have been shown to have a significant but not dominant effect on wind stress. The most important factor affecting wind stress is the geostrophic wind vector. Cloud effects are second order, with about the same order of magnitude as surface roughness changes and thermal wind effects. Changes in wind stress due to any of these second order effects are significant, as shown by models, but difficult to detect from measurements. For example, model results here and by Brown (1981) show that including thermal wind effects should result in changes in wind stress of 20% or more. However, no thermal wind effect was found using the CEAREX data (it was estimated from the buoy array, which had temperature as well as pressure sensors). This is an example of a proven effect not being readily evident from the measurements. Similarly, the cloud effect is large in model predictions but less obvious in the noisy statistical studies.

The reason for all the "noise", or apparently random variations, in wind stress, even after accounting for geostrophic wind vector and all other known effects (clouds, thermal wind, measurement error, etc.) is probably due to inertial effects. The dynamic forcing in the Arctic is continually changing and the air parcels require some time to reach a force balance. All the model runs assumed constant forcing and therefore did not simulate this continual adjustment process.

Several problems remain in understanding the relation between clouds and air-ice-sea interactions. The model results were usually based on cloud formation or dissipation events which were artificially forced. The physics of cloud formation in the winter is not well understood. The presence of ice crystals will continue to cause problems with verification and initialization of radiation models for Arctic regions.

C. APPLICATIONS OF RESULTS

Wind stress has special importance in Arctic regions because it is the primary driving force for pack ice motion. Ocean/ice features such as leads, polynyas, ice edges, acoustic noise and Ekman pumping are affected by variations in wind stress. Cloud conditions influence these variations. Therefore, studies of these features should consider the effect of clouds on wind stress.

An objective is to provide operational guidance for prediction of wind stress in the Arctic for use as input for dynamic ice and upper ocean models. The problem with achieving this is that C_G varies by 50%. Current cloud state explains a small fraction of the measured variability in C_G, and is therefore an incomplete wind stress predictor. Nevertheless, wind stress forecasts should be improved by an average of about 10% if C_G and α are based on amount of low clouds rather than kept fixed. The following values are recommended for the central Arctic during dark seasons, for totally cloudy and clear situations. (Partly cloudy skies have intermediate values.)

	Cloudy	Clear
C_G	0.0311	0.0280
α	25.0 degrees	18.7 degrees

These values could be used to provide estimates of wind stress as input into dynamic ice and ocean models when the surface horizontal pressure field and cloud amount are known, but no upper level information is available. This is the typical situation in the Arctic Ocean, where buoys provide surface pressure information and satellites reveal clouds, but detailed information on low level stratification is unavailable.

If stratification information is available, then the methods suggested in Chapter V and by OD provide somewhat better predictions than the above values. Because of the lack of routine detailed meteorological measurements in the Arctic Ocean, it is doubtful that 3-dimensional numerical ABL models can provide more accurate wind stress predictions than these simple analytical relationships.

This research has shown that numerical models of radiation and other physical processes must be tuned to Arctic conditions. Phenomena unique to high latitudes, such as low level ice crystals, cause effects which will not be properly modeled if the model formulations are based on mid-latitude verifications.

Climate studies must consider the effect of future changes in cloud coverage on air/ice/sea interactions. The results show that clouds increase surface forcing in marine Arctic regions. This can change ice coverage and may affect global climate.

LIST OF REFERENCES

Anderson, R.J., 1987: Wind stress measurements over rough ice during the 1984 marginal ice zone experiment. *J. Geophys. Res.*, **92**, 6933-6942.

Andreas, E.L. 1987: Comment on "Atmospheric boundary layer modification in the marginal ice zone" by T.J. Bennett, Jr. and K. Hunkins. *J. Geophys. Res.*, **92**, 3965-3968.

Andreas, E.L., W.B. Tucker III, and S.F. Ackley, 1984: Atmospheric boundary-layer modification, drag coefficient, and surface heat flux in the Antarctic marginal ice zone. *J. Geophys. Res.*, **89**, 649-661.

Arya, S.P.S., 1973: Contribution of form drag on pressure ridges to the air stress on Arctic ice. *J. Geophys. Res.*, **78**, 7092-7099.

Arya, S.P.S., 1975: A drag partition theory for determining the large scale roughness parameter and wind stress on the Arctic pack ice. *J. Geophys. Res.*, **80**, 3347-3454.

Baker, M.B., and J. Latham, 1979: The evolution of the droplet spectra and the rate of production of embryonic raindrops in small cumulus clouds. *J. Atmos. Sci.*, **36**, 1612-1615.

Banke, E.G., and S. Smith, 1973: Wind stress on Arctic sea ice. *J. Geophys. Res.*, **78**, 7872-7883.

Banke, E.G., S.D. Smith and R.J. Anderson, 1976: Recent measurements of wind stress on Arctic sea ice. *J. Fish. Res. Board Can.*, **33**, 2307-2317.

Banke, E.G., S.D. Smith, and R.J. Anderson, 1980: Drag coefficients at AIDJEX from sonic anemometer measurements. in *Sea Ice Processes and Models*, edited by R.S. Pritchard, University of Washington Press, 430-442.

Bennett, T.J., and K. Hunkins, 1986: Atmospheric boundary layer modification in the marginal ice zone. *J. Geophys. Res.*, **91**, 13033-13044.

Bennett, T.J., and K. Hunkins, 1987: Reply. *J. Geophys. Res.*, **92**, 3969.

Borisenkov, E.P., L.K. Efimova and B.E. Shneerov, 1985: Numerical modeling of the influence of stratus clouds on the dynamic and thermal regimes of the north polar region. *Soviet Meteorology and Hydrology*, No. 8, 16-23.

Brown, R.A., 1977: NCAR Electra planetary boundary layer flights during AIDJEX. *AIDJEX Bull.*, **36**, 175-185.

Brown, R.A., 1981: Modeling the geostrophic drag coefficient for AIDJEX. *J. Geophys. Res.*, **86**, 1989-1994.

Brown, R.A., 1986: The planetary boundary layer in the marginal ice zone. *MIZEX Bulletin*, **VII**, U.S Army Cold Regions Laboratory, Hanover, NH, 65-78.

Brown, R.A., and W.T. Liu, 1982: An operational large-scale planetary boundary layer model. *J. Appl. Meteor.*, **86**, 261-270.

Burk, S.D., 1977: The moist boundary layer with a higher order turbulence closure model. *J. Atmos. Sci.*, **34**, 629-638.

Burk, S.D., 1980: Refractive index structure parameters: Time-dependent calculations using a numerical boundary layer model. *J. Appl. Meteor.*, **19**, 562-576.

Burk, S.D., and W.T. Thompson, 1982: Operational evaluation of a turbulence closure model forecast system. *Mon. Wea. Rev.*, **110**, 1535-1543.

Burk, S.D., and W.T. Thompson, 1989: A vertically nested regional weather prediction model with second-order closure physics. *Mon. Wea. Rev.*, **117**, 2305-2324.

Campbell, W.J., P. Gloersen, E.G. Josberger, O.M. Johannessen, P.S. Guest, N. Lannelongue and K.L. Davidson, 1987: Mesoscale and large-scale sea ice morphology in MIZEX-84. *J. Geophys. Res.*, **92**, 6805-6824.

Carsey, F.D., 1980: The boundary layer height in air stress measurement, in *Sea Ice Processes and Models*, edited by R.S. Pritchard, University of Washington Press, 443-451.

Chu, P.C, 1986a: An instability theory of ice-air interaction for the migration of the marginal ice zone. Geophys. *J. Roy. Astron. Soc.*, **86**, 863-883.

Chu, P.C, 1986b: An ice-air feedback mechanism for the migration of the marginal ice zone. *MIZEX Bulletin*, **VII**, U.S Army Cold Regions Laboratory, Hanover, NH, 54-64.

Chu, P.C, 1986c: A possible ice-air feedback mechanism for the formation of leads or polynyas. *MIZEX Bulletin*, **VII**, U.S Army Cold Regions Laboratory, Hanover, NH, 79-88.

Chu, P.C, 1988a: Generation of unstable modes of iceward attenuating swell by ice breeze. *J. Phys. Oceanogr.*, **17**, 828-832.

Chu, P.C, 1988b: Ice breeze mechanism for an ice divergence-convergence criterion in the marginal ice zone. *J. Phys. Oceanogr.*, **17**, 1627-1632.

Chu, P.C, 1988c: Instability theory of ice-air interaction for the formation of ice bands. *J. Geophys. Res.*, **92**, 6966-6970.

Chu, P.C., and R.W. Garwood, Jr., 1990: Thermodynamic feedback between clouds and the ocean surface mixed layer. *Advances in Atmospheric Sciences*, **7**, No. 1, 1-10.

Chu, P.C., and R.W. Garwood, Jr., 1991: On the two-phase thermodynamics of the coupled cloud-ocean mixed layer. *J. Geophys. Res.*, **96**, 3425-3436.

Chu, P.C., R.W. Garwood, Jr. and P. Muller, 1990: Unstable and damped modes in coupled ocean mixed layer and cloud models. *Journal of Marine Systems,* **1**, 1-11.

Coon, M.D., 1980: A review of AIDJEX modeling. in *Sea Ice Processes and Models*, edited by R.S. Pritchard, University of Washington Press, 12-27.

Curry, J.A., 1983: On the formation of polar air. *J. Atmos. Sci.*, **40**, 2278-2292.

Curry, J.A., 1986: Interactions among turbulence, radiation and microphysics in Arctic stratus clouds. *J. Atmos. Sci.*, **43**, 90-106.

Curry, J.A., and G.F. Herman, 1985a: Infrared radiative properties of summertime Arctic stratus clouds. *J. Climate Appl. Meteor.,* **24**, 525-538.

Curry, J.A., and G.F. Herman, 1985b: Relationships between large-scale heat and moisture budgets and the occurrence of Arctic stratus clouds. *Mon. Wea. Rev.* **113**, 1441-1457.

Curry, J.A., L.F. Radke, C.A. Brock and E.E. Ebert 1989: Arctic ice-crystal haze, paper presented at Symposium on the Role of Clouds in Atmospheric Chemistry and Global Climate, American Meteorological Society, Anaheim CA.

Davidson, K.L., and G.L. Geernaert, 1984a: R/V Haakon Mosby meteorological measurements/conditions. MIZEX 84 summer experiment PI report, *CRREL Special Report 84-29*, October, 98-100.

Davidson, K.L., and G.L. Geernaert, 1984b: Open water atmospheric boundary layer measurements during MIZEX-84, Fall AGU Meeting, San Francisco, CA; 3 December.

Davidson, K.L., and G.L. Geernaert, 1985: The effect of sea surface temperature gradients on the MIZEX atmospheric boundary layer, Spring AGU Meeting, Baltimore, MD; 27 May.

Davidson, K.L., and P.S. Guest, 1986: Wind stress measurements over the ocean near the East Greenland Sea marginal ice zone, Annual AMS meeting. Miami FL, 13-17 January.

Davidson, K.L., and P.S. Guest, 1987: NPS meteorology studies of the marginal ice zone, *Naval Research Reviews*, **39**, 28-35.

Davidson, K. L., and P. S. Guest, 1988: Wind stress observations in the spring Arctic marginal ice zone, AGU Ocean Sciences Meeting, New Orleans, LA, 18-22 January.

Davidson, K.L., P.S. Guest, D.S. Spiel, C.W. Fairall, R. Markson, R. Lindsay, R. Lind and K. Katsaros, 1984: Preliminary field meteorological data - MIZEX-83, *Naval Postgraduate School Technical Report*, **NPS-63-84-002**, March, 88 pp.

Doronin, Y.P., 1969: Thermal interaction of the atmosphere and the hydrosphere in the Arctic. Report TT70-50091, Arctic and Antarctic Science Research Institute, National Science Foundation, Washington D.C., p. 10.

Dyer, A.J., 1974: A review of flux-profile relationships. *Boundary-Layer Meteorol.*, **7**, 363-372.

Fairall, C.W., and R. Markson, 1987: Mesoscale variations in surface stress, heat fluxes, and the drag coefficient during the 1983 marginal ice zone experiment. *J. Geophys. Res.*, **92**, 6921-6932.

Glendening, J.W., 1992: A model of the atmospheric boundary layer over a marginal ice zone. (in progress).

Guest, P.S., 1985: Forecasting fog in marginal ice zones. unpublished paper for MR 4241, Naval Postgraduate School, Monterey CA, 13 December, 10 pp.

Guest, P.S., 1988: Realistic wind forcing for ice movement models of the marginal ice zone. unpublished paper for MR/OC 4414, Naval Postgraduate School, Monterey CA, 18 March, 27 pp.

Guest, P.S., 1992: Atmospheric boundary layer factors affecting wind stress in the Arctic., (in progress).

Guest, P. S., and K. L. Davidson, 1984a: Drag coefficients obtained during MIZEX-83. AGU Ocean Sciences Meeting, New Orleans, LA, 23-27.

Guest, P. S., and K. L. Davidson, 1984b: The drag coefficient in the marginal ice zone. 10th General Assembly of the European Geophysical Society, Louvain-La-Neuve, Belgium, 31 July - 5 August.

Guest, P.S., and K.L. Davidson, 1984c: R/V Polar Queen atmospheric boundary layer measurements. MIZEX-84 Summer Experiment PI Report, *CRREL Special Report*, **84-29**, October, 98-100.

Guest, P.S., and K.L. Davidson, 1984d: Wind stress as a function of ice characteristics in the marginal ice zone. Fall AGU Meeting, San Francisco, CA, 3-7 Dec.

Guest, P.S., and K.L. Davidson, 1985: Wind/temperature profiles and turbulence on a large flat floe in the East Greenland Sea marginal ice zone. Spring AGU Meeting, Baltimore, MD, 27 May.

Guest, P.S., and K.L. Davidson, 1987a: The effect of observed ice conditions on the drag coefficient in the summer East Greenland Sea marginal ice zone. *J. Geophys. Res.*, **92**, 6943-6954.

Guest, P. S., and K. L. Davidson, 1987b: Factors affecting the atmospheric boundary layer over a summertime marginal ice zone - an observational study. IUGG General Assembly, Vancouver B.C. Canada, August 1987.

Guest, P. S. and K. L. Davidson, 1988: MIZEX 87 Meteorology Atlas. *Naval Postgraduate School Technical Report*, **NPS-63-88-004**, February, 137 pp.

Guest, P.S., and K.L. Davidson, 1991a: The aerodynamic roughness of different types of sea ice. *J. Geophys. Res.*, **96**, 4709-4721.

Guest, P.S., and K.L. Davidson, 1991b: The effect of cloudiness on heat loss from pack ice during dark seasons. AGU 1991 Fall Meeting, Program and Abstracts December 9-13, 1991, a supplement to *EOS*, October 29, p. 237.

Guest, P. S., K.L. Davidson and C.A. Vaucher, 1988: Atmospheric boundary layer features observed in the spring marginal ice zone. *Proceedings Second AMS Conference on Polar Meteorology and Oceanography*, Madison, WI, 29-31 March, 73.

Hakkinen, S., 1986a: Coupled ice-ocean dynamics in the marginal ice zones: upwelling/downwelling and eddy generation. *J. Geophys. Res.*, **91**, 819-832.

Hakkinen, S., 1986b: Ice banding as a response of the coupled ice-ocean system to temporally varying winds. *J. Geophys. Res.*, **91**, 5047-5053.

Hanna, S.R., 1969: The thickness of the planetary boundary layer. *Atmos. Environ.*, **3**, 519-536.

Harshvardhan, R. Davies, D.A. Randall and T.G. Corsetti, 1987: A fast radiation parameterization for atmospheric circulation models. *J. Geophys. Res.*, **92** (D1), 1009-1016.

Herman, G.F., 1977: Solar radiation in summertime Arctic stratus clouds. *J. Atmos. Sci.*, **34**, 1423-1432.

Herman, G.F., 1980: Thermal radiation in Arctic stratus clouds. *Quart. J. Roy. Meteor. Soc.*, **106**, 771-780.

Herman, G.F., and J.A. Curry, 1984: Observational and theoretical studies of solar radiation in Arctic stratus clouds. *J. Climate Appl. Meteor.*, **23**, 5-24.

Herman, G.F., and R. Goody, 1976: Formation and persistence of summertime Arctic stratus clouds. *J. Atmos. Sci.*, **33**, 1049-1062.

Hibler, W.D., 1979: A dynamic thermodynamic sea ice model. *J. Phys. Oceanogr.*, **9**, 815-846.

Jayaweera, K.O.L.F., 1977: Characteristics of Arctic stratus clouds over the Beaufort Sea during AIDJEX. *AIDJEX Bull.*, **37**, 135-151.

Jayaweera, K.O.L.F., and T. Ohtake, 1973: Concentration of ice crystals in Arctic stratus clouds. *J. Res. Atmos.*, **7**, 199-207.

Kantha, L.H., and G.L. Mellor, 1989: A numerical model of the atmospheric boundary layer over a marginal ice zone. *J. Geophys. Res.*, **94**, 4959-4970.

Katz, D.I, 1979: An investigation of the Arctic planetary boundary layer, M.S. Thesis, Dep. of Atmos. Sci., Univ. of Wash.

Katz, D.I, 1980: Air stress measurements from an aircraft, in *Sea Ice Processes and Models*, edited by R.S. Pritchard, University of Washington Press, 442-563.

Kitaigorodskii, S.A., 1988: A note on similarity theory for atmospheric boundary layers in the presence of background stable stratification, *Tellus*, **40A**, 434-438.

Kitaigorodskii, S.A., and S.M. Joffre, 1988: Simple scaling for the height of the stratified atmospheric boundary layer, *Tellus*, **40A**, 419-433.

Kloessel, K.A., B.A. Albrecht and D.P. Wylie, 1988: Fire marine stratocumulus observations -- summary of operations and synoptic conditions. *Fire Technical Report No. 1.*, 171 pp.

Large, W.G., and S. Pond, 1981: Open ocean momentum flux measurements in moderate to strong winds. *J. Phys. Oceanogr.,* **11**, 324-336.

Large, W.G., and S. Pond, 1982: Sensible and latent heat flux measurements over the ocean. *J. Phys. Oceanogr.,* **12**, 464-482.

Leavitt, E., 1980: Surface-based air stress measurements made during AIDJEX, in *Sea Ice Processes and Models*, edited by R.S. Pritchard, University of Washington Press, 419-429.

Lewellen, W.S., D.A. Oliver, M.E. Teske and G.G. Williamson, 1976: Status report on low-level atmospheric turbulence model for marine environment. *A.R.A.P. Report No. 289.* [Available from ARAP, P.O. Box 2229, 50 Washington Road, Princeton, NJ 08543.]

Lilly, D.K., 1968: Models of cloud top mixing under a strong inversion. *Quart. J. Roy. Meteor. Soc.*, **94**, 292-302.

Lindsay, R.W., 1985: MIZEX 84 Integrated Surface Meteorological Data Set and Meteorological Atlas, Second Edition, Polar Science Center, Univ. of Washington, 1 Nov.

Ling, C., and N. Untersteiner, 1974: On the calculation of the roughness parameter of sea ice. *J. Geophy. Res.*, **79**, 4112-4114.

McPhee, M.G., G.A. Maykut and J.H. Morison, 1987: Dynamics and thermodynamics of the ice/upper ocean system in the marginal ice zone of the Greenland Sea. *J. Geophys. Res.*, **92**, 7016-7031.

Maykut, G.A., 1982: Large-scale heat exchange and ice production in the central Arctic, *J. Geophys. Res.*, **87**, 7971-7984.

Mellor, G.L. and T. Yamada, 1974: A hierarchy of turbulence closure models for planetary boundary layers. *J. Atmos. Sci.,* **31**, 1791-1806.

MIZEX Group, 1986. MIZEX East 83/84: the summer marginal ice zone program in the Fram Strait/Greenland Sea. *EOS*, **27**, No. 33, June.

MIZEX '87 Group, 1989. MIZEX East 1987 - Winter marginal ice zone program in the Fram Strait and the Greenland Sea. *EOS*, **70**, No. 17, April 25, 545-555.

Moritz, R.E., 1985: Accuracy of surface geostrophic wind forecasts in the central Arctic. *Mon. Wea. Rev.*, **111**, 1746-1758.

Nansen, F., 1902: Norwegian North Polar Expedition 1893-1896. Scientific Results, Vol 3, *The Oceanography of the North Polar Basin*, Longmans, 427 pp.

Neralla, V.R., W.S. Liu, S. Venkatesh and M.B. Danard, 1980: Techniques for predicting sea ice motion, in *Sea Ice Processes and Models*, edited by R.S. Pritchard, University of Washington Press, 197-206.

Oliver, D. A., W. S. Lewellen and G.G. Williamson, 1978: The interaction between turbulent and radiative transport in the development of fog and low-level stratus. *J. Atmos. Sci.*, **35**, 301-316.

Overland, J.E., 1985: Atmospheric boundary layer structure and drag coefficients over sea ice. *J. Geophys. Res.*, **90**, 9029-9049.

Overland, J.E., 1988: A model of the atmospheric boundary layer over sea ice during winter. *Preprints from The Second Conference on Polar and Meteorology and Oceanography*, A.M.S., Madison, WI, March 29-31, 1987, 69-72.

Overland, J.E., and K.L. Davidson, 1992: Geostrophic drag coefficients over sea ice. *Tellus,* **44A**, 54-66.

Overland, J.E., and P.A. Guest, 1991: The Arctic snow and air temperature budget over sea ice during winter, *J. Geophys. Res.*, **96**, 4651-4662.

Overland, J.E., M. Reynolds and C. Pease, 1983: A model of the atmospheric planetary boundary layer over the marginal ice zone. *J. Geophys. Res*, **88**, 2836-2840.

Panofsky, H.A., and J.A.Dutton, 1984: *Atmospheric turbulence models and methods for engineering applications*, John Wiley & Sons, 397 pp.

Reynolds, M., 1984: On the local meteorology at the marginal ice zone of the Bering Sea. *J. Geophys. Res*, **89**, 6515-6524.

Roed, L., 1983: Sensitivity studies with a coupled ice-ocean model of the marginal ice zone. *J. Geophys. Res.*, **88**, 6039-6042.

Roed, L., and J. O'Brien, 1983: A coupled ice-ocean model of upwelling in the marginal ice zone. *J. Geophys. Res*, **88**, 2863-2872.

Semtner, A.J., Jr., 1976: A model for the thermodynamic growth of sea ice in numerical investigations of climate. *J. Phys. Ocean.*, **6**, 379-389.

Shuleikin, V.V., 1938: The drift of ice fields. *C. R. Dokl. Acad. Sci. URSS*, Engl. Trans, **19**, 589-594.

Smith, S.D., 1988: Coefficients for sea surface wind stress, heat flux, and wind profiles as a function of wind speed and temperature, *J. Geophys. Res.,* **93**, 15,467-15,472.

Smith, S.D., E.G. Banke and O.M. Johannessen, 1970: Wind stress and turbulence over ice in the Gulf of St. Lawrence, *J. Geophys. Res.*, **75**, 2803-2812.

Smith, D.C.,IV, A.A. Bird and W.P. Budgell 1988: A numerical study of mesoscale ocean eddy interaction with a marginal ice zone. *J. Geophys. Res*, **93**, 12461-12473.

Sommeria, G., and J.W. Deardorff, 1977: Subgrid-scale condensation in models of nonprecipitating clouds. *J. Atmos. Sci.,* **34**, 344-355.

Stull, R.B., 1988: *An Introduction to Boundary Layer Meteorology*, Kluwer Academic Publishers, 666 pp.

Sverdrup, H.U., 1933: *The Norwegian North Polar Expedition with the "Maud", Vol II, Meteorology*, Geophysical Institute, Bergen, 331 pp.

Thompson, W.T., and S.D. Burk, 1991: Simulation of Arctic frontogenesis with a vertically nested regional model, *Mon. Wea. Rev.,* **119**, 233-243.

Thorndike, A.S. and R. Colony, 1982: Sea ice motion in response to geostrophic winds, *J. Geophys. Res.*, **87**, 5845-5852

Tsay S.C., and K. Jayaweera, 1983: Dependence of radiative properties of Arctic stratus clouds on cloud microstructure. *Geophys. Res. Lett.*, **10**, 1188-1191.

Tsay S.C., and K. Jayaweera, 1984: Physical characteristics of Arctic stratus clouds. *J. Climate Appl. Meteor.*, **23**, 584-596.

Untersteiner N., and F.I. Badgley, 1965: The roughness parameter of sea ice. *J. Geophys. Res.*, **70**, 4573-4577.

Vowinckel, E., and S. Orvig, 1970: The climate of the north polar basin. in *Climates of Polar Regions*, S. Orvig, Ed., Elsevier, 370 pp.

Wettlaufer, J.S., 1991: Heat flux at the ice-ocean interface, *J. Geophys. Res.*, **70**, 7215-7236.

Wetzel, P.J. 1982: Toward parameterization of the stable boundary layer, *J. Appl. Meteor.*, **21**, 7-13.

Zilitinkevich, S.S, 1972: On the determination of the height of the Ekman boundary layer, *Boundary-Layer Meteorol.*, **3**, 11, 141-145.

Zilitinkevich, S.S, 1974: Resistance laws and prediction equations for the depth of the planetary boundary layer, *J. Atmos. Sci.*, **32**, 741-752.

INITIAL DISTRIBUTION LIST

		No. Copies
1.	Defense Technical Information Center Cameron Station Alexandria, VA 22304-6145	2
2.	Library, Code 0142 Naval Postgraduate School Monterey, CA 93943-5002	2
3.	Dr. K.L. Davidson (Code Mr/Ds) Department of Meteorology Naval Postgraduate School Monterey, CA 93943-5000	2
4.	Dr. R. L. Haney (Code MR/Hy) Department of Meteorology Naval Postgraduate School Monterey, CA 93943-5000	1
5.	Dr. Robert J. Renard (Code MR/Rd) Department of Meteorology Naval Postgraduate School Monterey, CA 93943-5000	1
6.	Dr. Teddy R. Holt (Code MR/Ht) Department of Meteorology Naval Postgraduate School Monterey, CA 93943-5000	1
7.	Dr. Pecheng Chu (OC/Cu) Department of Oceanography Naval Postgraduate School Monterey, CA 93943-5000	1

8. Dr. Gordon Schacher (Code 07) 1
Naval Postgraduate School
Monterey, CA 93943-5000

9. Dr. Peter S. Guest (Code MR/Gs) 3
Department of Meteorology
Naval Postgraduate School
Monterey, CA 93943-5000